

Geometry of Moving Space Curves Associated with Integrable Equations: Connections and Applications



A THESIS IN PHYSICS

Submitted to the University of Madras in Partial Fulfilment
of the Requirements for the Degree of Doctor of Philosophy

by

S. Murugesh

The Institute of Mathematical Sciences
Chennai-600113, India.

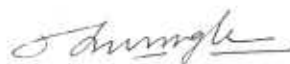
UNIVERSITY OF MADRAS
CHENNAI - 600 005.

July 2002

DECLARATION

I declare that the thesis entitled **GEOMETRY OF MOVING CURVES ASSOCIATED WITH INTEGRABLE EQUATIONS: CONNECTIONS AND APPLICATIONS** submitted by me for the Degree of Doctor of Philosophy is the record of my work carried out by me during the period from June 1997 to June 2002 under the guidance of Prof. Radha Balakrishnan and has not formed the basis for the award of any degree, diploma, associateship, fellowship or other titles in this or any other University or other similar Institution of higher learning.

Signature of the Candidate



S. Muruges

THE INSTITUTE OF MATHEMATICAL SCIENCES

C I T CAMPUS, CHENNAI 600 113, INDIA

Phone: (044)254 1856, (044)254 2588

(044)254 2397, (044)254 2398

Fax: (044)254 1586; Grams: MATSCIENCE

Telex: 041 8960 PCO IN PP WDT 20

E-mail: radha@imsc.ernet.in

Radha Balakrishnan
Professor

CERTIFICATE

This is to certify that the Ph. D. thesis titled *Geometry of Moving Space Curves Associated with Integrable Equations: Connections and Applications* submitted by **S. Muruges**h to the University of Madras is a record of bonafide research work done under my guidance and supervision. The research work presented in this thesis has not formed the basis for the award to the candidate of any Degree, Diploma, Associateship, Fellowship or other similar titles. It is further certified that the thesis represents independent work done by the candidate and collaboration was necessitated by the nature and scope of the problems dealt with.



Radha Balakrishnan

Thesis Supervisor

July 2002

Abstract

In this thesis, we have formulated a unified approach to study possible connections between the geometry of moving space curves in three dimensional space and integrable nonlinear evolution equations in (1+1) dimensions. Existing literature shows that each solution of such an evolution equation can be associated with *one* moving curve. Our unified formalism leads to the interesting result that the same solution can be associated with two more distinct moving space curves in addition to the existing one mentioned above. Applications of the formalism to two nonlinear evolution equations, namely, the nonlinear Schrödinger (NLS) equation and the Lamb equation, are presented in detail. Our main results are summarized below.

Lamb has given a procedure which helps identify a certain moving space curve with a given solution of an integrable equation. Examples such as the NLS equation, the sine-Gordon equation and the modified Korteweg-de Vries equation have been considered by him. A space curve is described in terms of the usual Frenet-Serret equations for the unit orthonormal triad of vectors consisting of the tangent \mathbf{t} , the normal \mathbf{n} and the binormal \mathbf{b} to the curve. Central to the Lamb formulation is the introduction of a particular complex function, namely the Hasimoto function $\psi = \kappa \exp[i \int^s \tau ds']$, where $\kappa(s, u)$ and $\tau(s, u)$ are the curvature and torsion of the moving curve. Here s is the arc length of the curve and u , the time. It is this function that satisfies various integrable equations in Lamb's work. By comparing the functional form of ψ with a soliton solution of a given integrable equation for ψ , one can identify κ and τ , and hence obtain the associated moving curve parameters that correspond to a certain integrable, shape-preserving curve motion. In other words, corresponding to any given $\psi(s, u)$, we have a curve in space, moving in time, thereby generating a surface. This in turn unravels a certain special geometric structure of the given soliton-bearing equation.

We first present a unified analysis to show that in addition to ψ , two other complex functions, defined as $\Phi = \tau \exp[i \int^s \kappa ds']$ and $\chi = \kappa + i\tau$, also arise from the basic curve evolution equations, just as naturally as the Hasimoto function ψ does. We demonstrate that these can also satisfy various soliton equations. This in turn leads to the interesting result that each such integrable equation is associated with not just one, but *three* distinct classes of space curve motion, and therefore has a much *richer* geometric structure than hitherto envisaged.

We then proceed to apply our formalism to the NLS equation, $iq_u + q_{ss} + \frac{1}{2}|q|^2q = 0$. This is an integrable nonlinear partial differential equation (NLPDE). We first show that any given solution of the NLS gets associated with three distinct space

curve evolutions. The tangent vector \mathbf{t}_1 of the first of these curves, the binormal vector \mathbf{b}_2 of the second and the normal vector \mathbf{n}_3 of the third, are all shown to satisfy the same integrable Landau-Lifshitz (LL) equation, $\mathbf{S}_u = \mathbf{S} \times \mathbf{S}_{ss}$. This equation is well known to be the spin (\mathbf{S}) evolution equation of a classical Heisenberg ferromagnetic chain, in the continuum limit: Of the above three connections, the first is just the converse of Lakshmanan's mapping where, starting with the LL equation, and identifying \mathbf{S} with the tangent to a moving curve, it becomes possible to obtain the NLS for ψ . The other two are shown to represent new geometries connected with the NLS. Furthermore, the converses of these two are also seen to hold good, i.e., starting with the LL equation, and identifying \mathbf{S} with \mathbf{b} and \mathbf{n} successively, we can show that the NLS for Φ and χ are obtained, respectively. These are two analogs of Lakshmanan's mapping. The LL equation is known to be completely integrable. Its exact solutions can be found. We provide a method to derive expressions for $\mathbf{r}_1(s, u)$, $\mathbf{r}_2(s, u)$ and $\mathbf{r}_3(s, u)$, the position vectors generating the three moving curves underlying the NLS, in terms of an exact solution \mathbf{S} of the LL equation. As an example, the three surfaces swept-out by the moving curves associated with a stationary envelope soliton solution of the NLS are explicitly derived and displayed.

Next, we focus on the intrinsic kinematics of the three moving curves associated with the NLS. We obtain three sets of coupled evolution equations for the evolution of the curvature and torsion, one set for each curve. The first set is given by the usual Da Rios-Betchov (DB) equations. The other two new sets are certain analogs of the DB equations. We show that each of the three moving curves is in general endowed with an infinite set of geometric invariants.

We also show that the velocities (at every point) of the two new moving curves underlying the general NLS evolution are certain *nonlocal* functions of the curve variables, quite in contrast to the *local* expression for the velocity of the usual moving curve that has thus far been associated with the NLS. We suggest possible application of our results to vortex filament motion in fluids. We also obtain the three moving curves for a non-stationary envelope soliton solution of the NLS and compare their behaviors.

Finally, we consider the application of our formalism to an *integro-differential equation*, namely, the Lamb equation, given by $iq_u + q_s + q \int^s |q|^2 ds' = 0$. This equation can also be written in the form of coupled NLPDEs. This equation can be mapped to the elliptic Liouville equation. The general solution of the elliptic Liouville equation being known, the mapping implies the so called C-integrability of

the Lamb equation. We then demonstrate that the Lamb equation can be associated with three moving curves. The tangent of the first curve, the binormal of the second and normal of the third all satisfy the Belavin-Polyakov equation, $\mathbf{m}_u = \mathbf{m} \times \mathbf{m}_s$, with $\mathbf{m}^2 = 1$. This equation appears in a variety of physical contexts, including the description of low energy excitations of classical Heisenberg antiferromagnets, static configurations of two dimensional ferromagnets and the $O(3)$ nonlinear sigma model. It is also known to possess interesting exact solutions such as ‘twists’ and ‘instantons’. We then demonstrate that these correspond to an “envelope-soliton” $q^{(S)}$ and an “envelope-instanton” $q^{(I)}$, respectively, of the Lamb equation. The three moving curves associated with the Lamb equation are obtained in terms of an exact solution \mathbf{m} of the BP equation, using an analog of the method we developed for obtaining the geometry of the NLS. The explicit expressions for the three surfaces corresponding to the above soliton solution and the three surfaces associated with the instanton solution are derived and displayed pictorially. We conclude the thesis with a summary of our results and a brief discussion of related open problems.

This thesis is based on the following publications and preprint:

Publications

- *New connections between moving curves and soliton equations.*
S. Murugesh and Radha Balakrishnan, Phys. Lett. A. **290**, 81 (2001).
- *New geometries associated with the nonlinear Schrödinger equation*
S. Murugesh and Radha Balakrishnan, nlin.PS/0111052. To appear in Euro. Phys. Jour. B (2002).
- *Kinematics of three moving space curves associated with the nonlinear Schrödinger equation.*
Radha Balakrishnan and S. Murugesh, nlin.SI/0111048. To appear in Theor. and Math. Phys. (2002).

Preprint

- *Geometric characterizations of the Lamb equation.*
S. Murugesh and Radha Balakrishnan, IMSc/2002/07/15.

ACKNOWLEDGEMENTS

I wish to thank my supervisor Prof. Radha Balakrishnan for suggesting the problem for the thesis, constant encouragement, discussions and her patience in bearing with my frequent digressions. I have benefited through discussions with and suggestions from Profs. R. Parthasarathy, R. Sridhar and H. S. Sharatchandra and all other faculty members and students of Institute.

I also wish to thank all my friends in the hostel for making my stay in the Institute over the years a pleasant one.

I am greatly indebted to my everloving family for having stood by me at all times.

Contents

1	Introduction	1
2	New connections between moving curves and soliton equations	7
2.1	Introduction	7
2.2	Moving space curves	8
2.3	Lamb's connection: Formulation(I) using the Hasimoto function ψ . .	9
2.4	Two new connections: Formulations (II) and (III)	13
2.5	Summary and discussion	16
3	Application to the nonlinear Schrödinger equation	18
3.1	Introduction	18
3.2	Curvature, torsion and time evolution parameters of the three moving curves	19
3.3	Construction of three moving curves for the NLS using the Landau- Lifshitz equation	23
3.4	Swept out surfaces associated with a stationary envelope NLS soliton	28
3.5	The NLS and two analogs of the Da Rios-Betchov equations	31
3.6	Stroboscopic plots of space curve evolutions associated with a moving envelope NLS soliton	33
3.7	Three curve velocities associated with NLS evolution	36
3.8	Summary and discussion	37
4	Application to the Lamb equation	45
4.1	Introduction	45
4.2	Mapping of Lamb equation to the Belavin-Polyakov equation and the elliptic Liouville equation	47
4.3	Appearance of the BP equation in Low dimensional Heisenberg fer- romagnets and antiferromagnets	52

4.4	Construction of the three moving curves for the Lamb equation . . .	56
4.5	Instantons, Twists and associated geometries of the Lamb equation .	58
4.6	Summary and discussion	67
5	Summary of results and future directions	78
A	One-soliton solution for the nonlinear Schrödinger equation	84
B	One-soliton solution of the Landau-Lifshitz equation	86
C	Determination of functions $C_1(u)$ and $C_2(u)$	89
D	The local induction approximation	93
	Bibliography	95

Chapter 1

Introduction

Systems governed by integrable [1] nonlinear evolution equations are important, for they allow one to make global statements about their behavior, in contrast to chaotic systems [2] which have a sensitive dependence on the initial conditions. Some of the general features exhibited by these equations include (i) an associated Lax pair [3], (ii) exact solvability by the inverse scattering transform method [4], (iii) an infinite number of integrals of motion in pairwise involution [5], and (iv) interesting solutions, such as solitons. A soliton [6] is a solitary traveling wave solution, which retains its identity (i.e., shape and velocity) even after a collision with another soliton. This particle-like feature makes it a particularly interesting special solution to look for. Although the concept of a soliton first arose in hydrodynamics [7, 8], it is now widely used to explain certain nonlinear phenomena in various other areas such as nonlinear optics [9, 10], condensed matter physics and plasma physics, as well as certain field theories [11, 12, 13].

The study of possible connections between the geometry of moving space curves and integrable evolution equations deserves attention, especially because many problems in physics can be modeled in terms of space curves. A vortex filament in a fluid [14], and in a superfluid [15], an interface between two phases of matter [16], scroll waves in chemical dynamics [17, 18, 19], a polymer chain [20] and a biomolecular strand such as DNA [21], are obvious examples of a space curve in three dimensions. A more subtle example is that of a magnetic moment vector of a magnetic spin chain in the continuum limit: Here a spin vector may be regarded as the unit tangent vector to some space curve [22, 23]. The mathematical tools of classical differential geometry prove to be ideal in finding the links between moving curves and integrable equations.

We begin by briefly outlining some of the basic features of the space curve formalism. Consider a *static* space curve $\mathbf{r}(s)$ in three dimensions. Here, s stands for the arc length of the curve. Its unit tangent vector $\mathbf{t}(s) \equiv \partial \mathbf{r} / \partial s$, along with the unit normal, $\mathbf{n}(s)$, and unit binormal $\mathbf{b}(s) = \mathbf{t} \times \mathbf{n}$, form an orthonormal triad at any point on the curve, and obey the Frenet-Serret (FS) equations [24],

$$\mathbf{t}_s = \kappa \mathbf{n}; \quad \mathbf{n}_s = -\kappa \mathbf{t} + \tau \mathbf{b}; \quad \mathbf{b}_s = -\tau \mathbf{n}, \quad (1.1)$$

where κ is the *curvature* and τ , the *torsion*. Here, the subscript s stands for differentiation with respect to the arclength s . From Eqs. (1.1), it is easily verified that $\kappa^2 = \mathbf{t}_s^2$ and $\tau = \mathbf{t} \cdot \mathbf{t}_s \times \mathbf{t}_{ss} / \mathbf{t}_s^2$. While the curvature describes how locally the curve deviates from linearity, torsion is a measure of its local deviation from planarity. A planar curve, for instance would have zero torsion. The functions κ and τ uniquely determine a curve except for its orientation and origin in space.

Clearly, a *moving* curve is described by $\mathbf{r}(s, u)$, where u denotes time. The connection between moving curves and solitons is a topic with a fascinating history [25], going back almost a hundred years. Using the so-called local induction approximation in fluid dynamics, Da Rios [26] showed that the velocity $\mathbf{v}(s, u) = \mathbf{r}_u$, at each point s of a vortex filament regarded as a moving space curve, is given by the following local induction equation [27]:

$$\mathbf{v} = \mathbf{r}_u = -\kappa \mathbf{b}. \quad (1.2)$$

Here, the subscript u stands for differentiation with respect to time u . For non-stretching curves, using compatibility conditions $\mathbf{r}_{us} = \mathbf{r}_{su} = \mathbf{t}_u = \kappa_s \mathbf{b} - \kappa \tau \mathbf{n}$, along with similar compatibility conditions for the unit vectors \mathbf{t} and \mathbf{n} leads to [26]

$$\kappa_u = -(\kappa \tau)_s - \kappa_s \tau; \quad \tau_u = [(\kappa_{ss} / \kappa) - \tau^2]_s + \kappa \kappa_s. \quad (1.3)$$

Subsequently, the above coupled equations for κ and τ were also derived independently by Betchov [28], and hence Eqs. (1.3) are referred to as the Da Rios-Betchov (DB) equations.

Hasimoto [14] was the first to unravel the connection between the moving curve equations and solitons. He showed that by defining the complex function

$$\psi = \kappa \exp[i \int^s \tau ds], \quad (1.4)$$

the two equations in (1.3) can in fact be combined to give the nonlinear Schrödinger equation (NLS),

$$i\psi_u + \psi_{ss} + \frac{1}{2}|\psi|^2\psi = 0. \quad (1.5)$$

The NLS is an integrable nonlinear partial differential equation (NLPDE), whose initial value problem can be solved through the inverse scattering technique [29] and possesses soliton solutions [5, 30]. A shape-preserving filament motion in a fluid, corresponding to the soliton solutions of the NLS were hence suggested by Hasimoto [14], and were subsequently experimentally observed [31].

Motivated by this result, Lamb [32, 33] gave a procedure which helps identify a certain space curve evolution with a given integrable equation. In addition to the NLS, other soliton supporting equations such as the sine-Gordon and the modified Korteweg-de Vries (mKdV) equation were considered by him. Here it is important to note that, central to Lamb's formulation is the use of the complex function ψ defined in Eq. (1.4). This function will be referred to as the Hasimoto function. It is this function that satisfies several integrable evolution equations in Lamb's work, and is used frequently in the study of various aspects of curve-dynamics [34]. Further, it is clear that by comparing the functional form of ψ (Eq. (1.4)) with a soliton solution of a given integrable equation for ψ , one can identify κ and τ , and hence obtain the associated moving curve parameters that correspond to a certain integrable, shape-preserving curve motion. Thus, corresponding to any given solution $\psi(s, u)$ of the evolution equation, there exists a certain curve in space, moving in time, thereby sweeping out a surface. This in turn yields a corresponding geometric realization of the evolution equation satisfied by ψ . However, as is well recognized, finding the explicit solution of the position vector $\mathbf{r}(s, u)$ of a moving curve, given the parameters κ and τ , is a nontrivial task in general.

In this thesis, we take a deeper look into the structure of the basic curve evolution equations, namely the FS equations and their temporal counterparts (which will be explained in the next chapter) to present a unified formalism and find new connections between moving curves and integrable equations. As is well known by now, integrable equations can be broadly divided into two categories [35]: (i) S-integrable equations, for which it is possible to obtain an exact solution through the inverse *scattering* technique and (ii) C-integrable equations for which it is possible to find a suitable *change* of variables to another equation with known general solutions (Hence the letters 'S' and 'C' to distinguish them). Clearly, NLS, sine-Gordon, etc., are S-integrable. A well known example of C-integrability is the Burgers equation, which can be transformed into the linear diffusion equation, with known solutions, via the Hopf-Cole transformation [7, 8]. We shall apply our formalism to two physically interesting systems, one of which is S-integrable and other, C-integrable. We then study them in detail to unravel the geometric structures associated with each

of them.

In Chapter 2, we formulate a unified analysis [36], to show that in addition to the Hasimoto function ψ , defined in Eq. (1.4), two other complex functions, defined by $\Phi = \tau \exp[i \int^s \kappa ds']$ and $\chi = (\kappa + i\tau)$, arise from the basic curve evolution equations in a natural fashion. We then demonstrate that all the three functions ψ , Φ and χ satisfy the *same* nonlinear evolution equation such as the NLS. This leads to the result that each integrable equation is associated with not just one, but *three* distinct space curve evolutions, and therefore has a *much richer geometric structure than hitherto envisaged*.

In Chapter 3, we illustrate this by applying the two new methods to the example of the NLS [37]. We first show that any given solution of the NLS gets associated with three distinct space curve evolutions, by demonstrating that the curve evolution parameters are distinct for the three curves. Next, the tangent vector of the first of these curves, the binormal vector of the second and the normal vector of the third, are shown to satisfy the integrable Landau-Lifshitz (LL) equation. This equation is well known to be the evolution equation for the spin S of a classical Heisenberg ferromagnetic chain, in the continuum limit:

$$S_u = S \times S_{ss} ; \quad S^2 = 1. \quad (1.6)$$

Of the above mentioned three results for the NLS, the first is just the *converse* of Lakshmanan's mapping [22] where, starting with the LL equation, and identifying S with the tangent to a moving curve, it becomes possible to obtain the NLS for ψ . The other two moving curves clearly represent new geometries connected with the NLS.

As is well known, the LL equation is completely integrable [38] and its exact solutions can be found [22, 38, 39]. We provide a method to derive general expressions for the position vectors r_1 , r_2 and r_3 , which generate the three moving curves that induce the NLS, in terms of any given exact solution S of the LL equation. As an example, the three surfaces swept-out by the moving curves associated with a *stationary* envelope soliton solution of the NLS are explicitly derived analytically and displayed.

Next, we focus on the intrinsic kinematics of the three moving curves associated with the NLS [40]. We obtain three sets of coupled evolution equations for the evolution of the curvature and torsion, one set for each curve. The first set is given by the usual DB [26, 28] equations, Eq. (1.3). The other two new sets are certain analogs of the DB equations. We show that each of the three moving curves is in general endowed with an infinite set of geometric invariants.

We then show that the velocities (at every point) of the two new moving curves underlying the general NLS evolution are certain *nonlocal* functions of the curve variables, quite in contrast to the *local* expression for the velocity of the usual moving curve that has thus far been associated with the NLS. We also obtain the three moving curves for a *non-stationary* envelope soliton solution of the NLS, display them graphically and compare their behaviors. Interestingly, shape preserving vortex filament motion has been observed experimentally in fluids [31]. We suggest a possible application of our theoretical results to vortex filament motion in fluids.

In Chapter 4, we consider the application of our formalism to the Lamb equation [32]. This is a *nonlinear integro-differential equation*

$$iq_u + q_s + q \int^s |q|^2 ds' = 0. \quad (1.7)$$

We shall refer to Eq. (1.7) as the Lamb equation, since (to our knowledge) it was first introduced by Lamb in connection with moving curves (see Eq. (3.24) in [32]), although the soliton nature of *other* integral equations of this type had been considered earlier [41, 42]. Note that by defining $\tilde{Q} = \int^s |q|^2 ds'$, Eq. (1.7) can be written in the form of *coupled* NLPDEs for q and Q .

C-integrability of the Lamb equation has been shown in [43], essentially by mapping it to the following elliptic Liouville equation:

$$f_{uu} + f_{ss} = -e^{2f}. \quad (1.8)$$

(It can be verified from Eq. (1.7) that $|q| = \exp(f)$ and $\arg(q) = -\int^s f_u ds'$). The exact general solution of Eq. (1.8) is well known and will be elaborated further in chapter 4.

Using the three distinct formulations obtained in Chapter 2, we first show that any given solution $q(s, u)$ of Eq. (1.7) can be associated with three corresponding moving space curves such that the tangent vector of the first curve, the binormal of the second curve and the normal of the third all satisfy the Belavin-Polyakov(BP) equation

$$\mathbf{m}_u = \mathbf{m} \times \mathbf{m}_s ; \quad \mathbf{m}^2 = 1. \quad (1.9)$$

This equation first appeared [44] in the context of the nonlinear sigma model field theory, and in the static two-dimensional classical Heisenberg ferromagnet in the continuum limit [11]. More recently, this equation has been shown [45] to describe very low-energy dynamics of a classical Heisenberg antiferromagnetic chain in the continuum limit.

The instanton solution of Eq. (1.9) is well known [44]. This is a solution localized in both space and time. In addition, the BP equation also supports a domain wall-like twist solution [45], which is a special kind of a traveling wave. (The nature of this solution will be explained in Chapter. 4). As illustrative examples, we consider two specific solutions of the Lamb equation (1.7), which correspond to the above two physically interesting solutions of the BP equation. One is an 'instanton-type' solution that corresponds to the BP instanton. The other is a 'soliton-type' solution connected with the BP twist. The expressions for the three surfaces (swept out by the three moving curves), corresponding to each of the above two solutions are derived and displayed pictorially.

Chapter 5 contains a short summary of our results and a brief discussion of related open problems. Details of the derivations of certain salient results used in the text, as well as the technical details of some intermediate steps of our formalism, are contained in Appendices A to D.

Chapter 2

New connections between moving curves and soliton equations

2.1 Introduction

Over two decades ago, Lamb [32, 33] presented a formalism which showed that certain completely integrable, soliton-supporting [1] nonlinear partial differential equations (NLPDE), such as the NLS, the sine-Gordon equation, the modified Korteweg-de Vries equation, the Hirota equation, etc., can each be associated with a certain corresponding moving curve. Consequently the corresponding curve evolution can also be termed integrable. Lamb's formulation arose as an extension of Hasimoto's earlier work [14], which had established a connection between the NLS and the so called "local-induction" equation of motion of a vortex filament [27] regarded as a moving space curve. Since all soliton equations [1] possess similar characteristics such as Lax pair [3], solvability by the inverse scattering transform (IST) method and an infinite number of constants of motion in pairwise involution, Hasimoto's procedure for the NLS motivated Lamb to provide a certain formulation to obtain the curve evolution that gets associated with each of the above mentioned example of soliton supporting equations.

In particular, using Lamb's formulation, one can identify a certain *specific* moving curve with each *solution* of a given integrable equation. This raises the question as to whether, in addition to that curve, other distinct moving curves can also be associated with *that* solution. In this chapter, we show that the answer to this

is in the affirmative: There are indeed two other distinct moving curves that get identified with each solution of the integrable equation in a natural fashion. With these two new connections, we see that a given integrable equation gets associated with, not just one but three (classes of) moving curves. As we shall demonstrate, this happens essentially because of the following reason we outline below.

In Lamb's formulation the complex Hasimoto function ψ , defined as

$$\psi = \kappa \exp[i \int^s \tau ds'] \quad (2.1)$$

appears and is shown to satisfy various integrable equations. In this chapter, by starting with general curve evolution equations, and combining them appropriately, we shall demonstrate that two other complex functions, $\Phi = \tau \exp[i \int^s \kappa ds']$ and $\chi = (\kappa + i\tau)$ appear *just as naturally* as ψ does. In addition, these also can satisfy various integrable equations as ψ did. Hence, by comparing a solution of the integrable equation concerned, with ψ , Φ and χ respectively, we can identify *three* distinct pairs of curvature and torsion functions for that solution. In other words, there are three distinct moving curves associated with the same solution.

We shall begin with the basic evolution equations of moving curves. First we briefly review the formulation proposed by Lamb [32, 33] and then present our two additional new formulations [36] that lead to the emergence of new geometries for a given integrable equation.

2.2 Moving space curves

A moving space curve embedded in three dimension may be described in parametric form by a position vector $\mathbf{r}(s, u)$, where s is the arclength and u , time. Let $\mathbf{t} = \partial \mathbf{r} / \partial s$ be the unit tangent vector along the curve. As mentioned in Chapter 1, an orthonormal triad $(\mathbf{t}, \mathbf{n}, \mathbf{b})$, can be defined at every point s on the curve. At a *given instant* of time, these vectors satisfy the following Frenet-Serret(FS) equations [46]

$$\mathbf{t}_s = \kappa \mathbf{n}, \quad (2.2a)$$

$$\mathbf{n}_s = -\kappa \mathbf{t} + \tau \mathbf{b}, \quad (2.2b)$$

$$\mathbf{b}_s = -\tau \mathbf{n}, \quad (2.2c)$$

where κ and τ denote, respectively, the curvature and torsion of the (moving) curve and the subscript s denotes $\partial / \partial s$. As before, Eqs. (2.2) lead to

$$\kappa^2 = (\mathbf{t}_s)^2, \quad (2.3)$$

$$\tau = \frac{(\mathbf{t} \cdot \mathbf{t}_s \times \mathbf{t}_{ss})}{\kappa^2}, \quad (2.4)$$

Note that in the case of a moving curve, κ and τ are functions of *both* s and u .

We write the temporal evolution of the triad at any point s in the general form [47],

$$\mathbf{t}_u = g\mathbf{n} + h\mathbf{b}, \quad (2.5a)$$

$$\mathbf{n}_u = -g\mathbf{t} + \tau_o\mathbf{b}, \quad (2.5b)$$

$$\mathbf{b}_u = -h\mathbf{t} - \tau_o\mathbf{n}, \quad (2.5c)$$

the subscript u denoting $\partial/\partial u$. Clearly, for a moving curve, the parameters g, h, τ_o (appearing in Eq. (2.5)) are also functions of both s and u .

On requiring the compatibility conditions $\mathbf{t}_{su} = \mathbf{t}_{us}$ and $\mathbf{n}_{su} = \mathbf{n}_{us}$, which together imply $\mathbf{b}_{su} = \mathbf{b}_{us}$ (since $(\mathbf{t}, \mathbf{n}, \mathbf{b})$ form a orthonormal triad), a short calculation using Eqs. (2.2) and (2.5) leads to the following equations for the scalar parameters $\kappa, \tau, g, h, \tau_o$:

$$\kappa_u = g_s - \tau h, \quad (2.6)$$

$$\tau_u = \tau_{os} + \kappa h, \quad (2.7)$$

$$h_s = \kappa\tau_o - \tau g, \quad (2.8)$$

In the next section, we briefly describe Lamb's formulation, which shows how the connection between the moving curve equations (Eqs. (2.2) and (2.5)) and an integrable equation, can possibly arise.

2.3 Lamb's connection: Formulation(I) using the Hasimoto function ψ

In this section, we review Lamb's formulation [33], which will be referred to hereafter as formulation (I). In this formulation, the second and third equations of the FS set (2.2) are combined to yield

$$(\mathbf{n} + i\mathbf{b})_s + i\tau(\mathbf{n} + i\mathbf{b}) = -\kappa\mathbf{t}. \quad (2.9)$$

This immediately suggests the definition of a certain complex vector

$$\mathbf{N} = (\mathbf{n} + i\mathbf{b}) \exp \left[i \int^s \tau ds' \right]. \quad (2.10)$$

Differentiating Eq. (2.10) with respect to s and using Eq. (2.9), we get

$$N_s = -\kappa \exp[i \int^s \tau ds'] t. \quad (2.11)$$

Thus the Hasimoto function ψ (Eq. (2.1)) appears in a natural fashion in the above equation, and we may write

$$N_s = -\psi t. \quad (2.12)$$

Using the definitions of N and ψ given in Eqs. (2.10) and (2.1) respectively, the first equation in the FS set (2.2), takes on the form

$$t_s = \frac{1}{2}(\psi^* N + \psi N^*), \quad (2.13)$$

where the asterisk denotes complex conjugation. It is convenient to use the vectors (t, N, N^*) instead of (t, n, b) . These satisfy the relations, $t \cdot N = t \cdot N^* = N \cdot N = 0$ and $N \cdot N^* = 2$. Differentiating Eq. (2.10) with respect to u and using second and third of Eqs. (2.5), a short calculation yields,

$$N_u - i R_1 N = \gamma_1 t, \quad (2.14)$$

where

$$\gamma_1 = -(g + ih) \exp[i \int^s \tau ds'], \quad (2.15)$$

$$R_1 = \int^s \tau_u ds' - \tau_0 = \int^s \kappa h ds'. \quad (2.16)$$

Here, the second compatibility condition Eq. (2.7), has been used in writing the last equality. We also have, on using

$$n = \frac{1}{2}(N \exp[-i \int^s \tau ds'] + N^* \exp[i \int^s \tau ds']) \quad (2.17)$$

and

$$b = \frac{-i}{2}(N \exp[-i \int^s \tau ds'] - N^* \exp[i \int^s \tau ds']), \quad (2.18)$$

in the first equation of the set (2.5), along with γ_1 and R_1 from Eqs. (2.15) and (2.16),

$$t_u = -\frac{1}{2}(\gamma_1^* N + \gamma_1 N^*). \quad (2.19)$$

We use the subscript '1' here, to denote formulation(1). It may be noted that although equations with the same structure (and notation) as Eqs. (2.14) and (2.19) were written down by Lamb, the dependence of γ_1 and R_1 on the curve parameters g, h, τ_0, κ and τ could not be unraveled since Eq. (2.5) was not explicitly introduced

by him. We shall see subsequently that the explicit introduction of these curve parameters in Eq. (2.5), proves to be very useful in identifying the curve geometry associated with a given integrable equation such as the NLS.

From Eqs. (2.12) and (2.14), setting $N_{su} = N_{us}$ and equating the coefficients of t and N , respectively, we get

$$\psi_u + \gamma_{1s} - iR_1\psi = 0 \quad (2.20)$$

and

$$R_{1s} = \frac{i}{2}(\gamma_1\psi^* - \gamma_1^*\psi). \quad (2.21)$$

Note that the condition $t_{su} = t_{us}$ gives the same equations, (2.20) and (2.21) as expected, due to the orthogonality conditions. On combining Eqs. (2.20) and (2.21), we obtain,

$$\psi_u + \gamma_{1s} + \frac{\psi}{2} \int^s (\gamma_1\psi^* - \gamma_1^*\psi) ds' = 0. \quad (2.22)$$

Using Eqs. (2.1) and (2.15), it is easily verified that Eq. (2.21) is consistent with Eq. (2.16).

Interestingly, as noted by Lamb [32], the structure of Eqs. (2.20) and (2.21) which arose from compatibility conditions on curve evolution, suggests a possible relationship with soliton-bearing equations, via the Ablowitz-Kaup-Newell-Segur (AKNS) formalism [41, 42]. This is seen as follows: It is well known that for a class of soliton-bearing equations, with a function $q(s, u)$ as the dependent variable, the Lax pair L and M in the AKNS formalism are given by:

$$L y = \begin{pmatrix} i\frac{\partial}{\partial s} & -iq \\ -iq^* & -i\frac{\partial}{\partial s} \end{pmatrix} y = \zeta y \quad (2.23)$$

$$\frac{\partial y}{\partial u} = \begin{pmatrix} A(s, u, \zeta) & B(s, u, \zeta) \\ -B^*(s, u, \zeta) & -A(s, u, \zeta) \end{pmatrix} y = M y \quad (2.24)$$

Here, the eigenfunction y is the column vector $(y_1 \ y_2)^T$ and ζ is the eigenvalue parameter. Requiring $y_{su} = y_{us}$, Eqs. (2.23) and (2.24) lead to the following AKNS compatibility conditions [1]:

$$q_u = 2Aq + B_s + 2i\zeta B \quad (2.25)$$

$$A_s = (Bq^* - B^*q) \quad (2.26)$$

Equations (2.25) and (2.26) are identical in form to Eqs. (2.20) and (2.21) provided we make the following identifications:

$$q = \psi/2; \quad A = iR_1/2; \quad B = -\gamma_1/2; \quad \zeta = 0. \quad (2.27)$$

Thus the curve evolution Eqs. (2.2) and (2.5) imply AKNS equations, but with $\zeta = 0$.

Now, let us return to γ_1 and R_1 given in Eqs. (2.15) and (2.16) respectively. It was shown by Lamb [32] that for appropriate choices of γ_1 as a function of ψ and its derivatives, R_1 can be found from Eq. (2.21) and substituted in Eq. (2.20) to yield evolution equations for ψ . In case the choice of γ_1 is such that the function R_{1s} in Eq. (2.21) could be integrated in a closed form, one obtains a *nonlinear partial differential equation* (NLPDE) for ψ . On the other hand if, with a certain choice of γ_1 , an exact integration of the function R_1 is not possible, then the evolution equation for ψ is a *nonlinear integro-differential equation* instead of an NLPDE. In the subsequent chapters we shall consider one example of each of these categories to illustrate this.

Going back to the Lax pair connection, we note another alternative. Once the quantities γ_1 and R_1 are identified so that Eqs. (2.20) to (2.21) take on the form of an integrable evolution equations for ψ , it is possible to find the corresponding Lax pair, by working directly with equations (2.12) and (2.13) for N_s and t_s , along with equations (2.14) and (2.19) for N_u and t_u . This is done [32] by considering the constraint $t_l^2 + n_l^2 + b_l^2 = 1$, where the subscript $l = 1, 2, 3$ is used to represent the three components of the vectors concerned. One then defines a complex function

$$f_l^{(1)} = (n_l + ib_l)/(1 - t_l) = (1 + t_l)/(n_l - ib_l), \quad (2.28)$$

along with its two other counterparts $f_l^{(2)}$ and $f_l^{(3)}$, obtained by cyclically changing t_l , n_l and b_l in Eq. (2.28). It can then be shown that all the three functions $f_l^{(\alpha)}$, $\alpha = 1, 2, 3$ satisfy appropriate Riccati equations [48, 49]. The corresponding Lax pair in each case can then be obtained by setting $f^{(\alpha)} = y_2^{(\alpha)}/y_1^{(\alpha)}$, and identifying the corresponding eigenfunction to be the column vector $(y_1^{(\alpha)} \ y_2^{(\alpha)})^T$. A short calculation shows that only one of the Lax pairs thus obtained has the AKNS form of Eqs. (2.23) and (2.24), with the identifications (2.27).

In the next section, we show that in addition to the Hasimoto function ψ , there exist two other complex functions Φ and χ which can also satisfy integrable equations. However, this happens for some *other* choices of γ and R . (Hence the use of subscript 1 on these quantities in this section). These will be seen to correspond to two other classes of curve motion, different from that obtained using ψ . Thus we shall see that there is not just one, but three distinct curve evolutions that all can be associated with the same integrable equation.

2.4 Two new connections: Formulations (II) and (III) using Φ and χ

As seen in the last section, in Lamb's formulation or formulation (I), one proceeds by first combining the second and third equations of the FS set, Eqs. (2.2), to yield Eq. (2.9). This procedure subsequently leads to the appearance of the Hasimoto function ψ in Eq. (2.12), which can satisfy integrable equations for certain choices of curve evolutions. In this section, we consider two other possibilities: Formulation (II), that combines the first and second equations of the set (2.2), and formulation (III) that combines its first and third equations. As we shall see, these formulations lead to the appearance of two other complex functions Φ and χ respectively.

Formulation (II)

In the FS equations (2.2), combining first and second, we get

$$(\mathbf{n} - i\mathbf{t})_s + i\kappa(\mathbf{n} - i\mathbf{t}) = \tau\mathbf{b}. \quad (2.29)$$

This suggests the definition of a *second* complex vector

$$\mathbf{M} = (\mathbf{n} - i\mathbf{t}) \exp[i \int^s \kappa ds']. \quad (2.30)$$

Differentiating Eq. (2.30) with respect to s and using Eq. (2.29), we get

$$\mathbf{M}_s = \tau \exp[i \int^s \kappa ds'] \mathbf{b}. \quad (2.31)$$

Thus a corresponding *second* complex function

$$\Phi(s, u) = \tau \exp[i \int^s \kappa ds'], \quad (2.32)$$

appears in a natural fashion in this case, just as ψ did in Lamb's formulation. In this formulation, we expand all vectors in terms of the linearly independent vectors, \mathbf{b} , \mathbf{M} and \mathbf{M}^* , which satisfy $\mathbf{b} \cdot \mathbf{M} = \mathbf{b} \cdot \mathbf{M}^* = \mathbf{M} \cdot \mathbf{M} = 0$, $\mathbf{M} \cdot \mathbf{M}^* = 2$. Then, using the definitions of \mathbf{M} and Φ given in Eqs. (2.30) and (2.32) with the basic equations (2.2) and (2.5), we obtain, after some algebra, the following counterparts of Eqs. (2.12) to (2.16):

$$\mathbf{M}_s = \Phi \mathbf{b}, \quad (2.33)$$

$$\mathbf{b}_s = -\frac{1}{2}(\Phi^* \mathbf{M} + \Phi \mathbf{M}^*), \quad (2.34)$$

$$\mathbf{M}_u - iR_2 \mathbf{M} = -\gamma_2 \mathbf{b} \quad (2.35)$$

and

$$\mathbf{b}_u = \frac{1}{2}(\gamma_2^* \mathbf{M} + \gamma_2 \mathbf{M}^*), \quad (2.36)$$

where

$$\gamma_2 = -(\tau_0 - ih) \exp[i \int^s \kappa ds'] \quad (2.37)$$

and

$$R_2 = \int^s \kappa_u ds' - g = - \int^s \tau h ds'. \quad (2.38)$$

Here, we have used the first equation of the compatibility conditions, Eq. (2.6), to write the last equality. The subscript 2 is used on γ and R to indicate that these correspond to formulation (II). From Eqs. (2.33) and (2.35), setting $\mathbf{M}_{su} = \mathbf{M}_{us}$, and equating the coefficients of \mathbf{b} and \mathbf{M} , respectively, we get

$$\Phi_u + \gamma_{2s} - iR_2\Phi = 0 \quad (2.39)$$

and

$$R_{2s} = \frac{i}{2}(\gamma_2\Phi^* - \gamma_2^*\Phi), \quad (2.40)$$

$$\Phi_u + \gamma_{2s} + \frac{\Phi}{2} \int^s (\gamma_2\Phi^* - \gamma_2^*\Phi) ds' = 0. \quad (2.41)$$

The structure of Eqs. (2.39) and (2.40) is the same as that obtained in Lamb's formulation (see Eqs. (2.20) and (2.21)). Thus, these can also be cast in the form of AKNS compatibility conditions Eqs. (2.25) and (2.26), with the following *new* identifications:

$$q = \Phi/2; \quad A = iR_2/2; \quad B = -\gamma_2/2; \quad \zeta = 0. \quad (2.42)$$

This shows that, just as one does in Lamb's formalism, here also we could take choices of γ_2 , as an appropriate function of Φ and its derivatives, find R_2 from Eq. (2.40), and substitute these expressions in Eq. (2.39) to obtain some of the well known integrable equations.

Formulation (III)

Here, we combine the first and third of the FS equations, (2.2), to get

$$(\mathbf{t} - i\mathbf{b})_s = (\kappa + i\tau)\mathbf{n}. \quad (2.43)$$

This suggests the definition of a *third* complex vector

$$\mathbf{P} = (\mathbf{t} - i\mathbf{b}). \quad (2.44)$$

Differentiating Eq. (2.44) with respect to s and using Eq. (2.43), we get

$$\mathbf{P}_s = (\kappa + i\tau)\mathbf{n}. \quad (2.45)$$

Thus a corresponding *third* complex function

$$\chi(s, u) = (\kappa + i\tau), \quad (2.46)$$

appears in this case. As is clear, here we express all vectors in terms of \mathbf{n} , \mathbf{P} and \mathbf{P}^* , which satisfy $\mathbf{n} \cdot \mathbf{P} = \mathbf{n} \cdot \mathbf{P}^* = \mathbf{P} \cdot \mathbf{P} = 0$ and $\mathbf{P} \cdot \mathbf{P}^* = 2$. Using the definitions of \mathbf{P} and χ given in Eqs. (2.44) and (2.46) in the basic equations (2.2) and (2.5), we proceed the same way as in the previous two formulations, to obtain, after some algebra,

$$\mathbf{P}_s = \chi \mathbf{n}, \quad (2.47)$$

$$\mathbf{n}_s = -\frac{1}{2}(\chi^* \mathbf{P} + \chi \mathbf{P}^*), \quad (2.48)$$

$$\mathbf{P}_u - iR_3 \mathbf{P} = -\gamma_3 \mathbf{n} \quad (2.49)$$

and

$$\mathbf{n}_u = \frac{1}{2}(\gamma_3^* \mathbf{P} + \gamma_3 \mathbf{P}^*), \quad (2.50)$$

where

$$\gamma_3 = -(g + i\tau_0) \quad (2.51)$$

and

$$R_3 = -h = -\int^s (\kappa\tau_0 - \tau g) ds'. \quad (2.52)$$

Here, we have used the last of the compatibility conditions, Eq. (2.8), to write the last equality, and the subscript 3 is used to denote formulation (III). From Eqs. (2.47) and (2.49), setting $\mathbf{P}_{su} = \mathbf{P}_{us}$, and equating the coefficients of \mathbf{n} and \mathbf{P} , respectively, we get

$$\chi_u + \gamma_{3s} - iR_3 \chi = 0 \quad (2.53)$$

and

$$R_{3s} = \frac{i}{2}(\gamma_3 \chi^* - \gamma_3^* \chi), \quad (2.54)$$

which can be shown to be consistent with Eq. (2.52). Combining the above two equations, we have

$$\chi_u + \gamma_{3s} + \frac{\chi}{2} \int^s (\gamma_3 \chi^* - \gamma_3^* \chi) ds' = 0. \quad (2.55)$$

Once again, Eqs. (2.53) and (2.54) have the same form as Lamb's result (Eqs. (2.20) and (2.21)), as well as the AKNS compatibility conditions (2.25) and (2.26). Here, the identifications are

$$q = \chi/2; \quad A = iR_3/2; \quad B = -\gamma_3/2; \quad \zeta = 0. \quad (2.56)$$

Thus using the same reasoning as before, for suitable choices of γ_3 as functions of χ and its derivatives, Eq. (2.53) for χ can take the form of known integrable equations.

2.5 Summary and discussion

Starting with the general description of a moving curve, we have presented a unified formalism comprising three formulations, to show that three distinct moving space curves can be identified with (a solution of) a given integrable equation: It is clearly seen from Eq. (2.15), (2.37) and (2.51), the parameters $\gamma_n, n = 1, 2, 3$, that arise in three formulations, correspond to three complex functions involving *different* combinations of the curve evolution parameters g, h and τ_o . Further, the corresponding complex functions ψ, ϕ and χ that appear in the formulations are also *different* functions of κ and τ (see Eqs. (2.1), (2.32) and (2.46) respectively). Thus it is clear that the three formulations describe three *distinct* curve motions.

It would be instructive to apply our results to find the three associated geometric structures explicitly for some integrable examples. We shall consider these in the next two chapters.

Given the curvature κ and torsion τ of a curve, though the existence of the curve is guaranteed in principle [46], obtaining the explicit expressions for these curves is, in general, a nontrivial task. Primarily, this requires solving the three coupled vector FS equations, (2.2), or the nine scalar equations

$$t_{is} = \kappa n_i, \quad (2.57a)$$

$$n_{is} = -\kappa t_i + \tau b_i, \quad i = 1, 2, 3 \quad (2.57b)$$

$$b_{is} = -\tau n_i, \quad (2.57c)$$

where (t_i, n_i, b_i) are the components of the unit vectors $(\mathbf{t}, \mathbf{n}, \mathbf{b})$. These components can be easily seen to satisfy the conditions,

$$t_i^2 + n_i^2 + b_i^2 = 1. \quad (2.58)$$

It can be shown that [49] the complex functions,

$$\Pi_i = \frac{t_i + in_i}{1 - b_i}, \quad (2.59)$$

obey certain Riccati equations directly due to the FS equations (2.57), satisfied by the components and the conditions in Eq. (2.58). Thus the components (t_i, n_i, b_i) are obtained through the solutions of these Riccati equations. However, this still remains a complicated process for obtaining the explicit expression for the tangent vector \mathbf{t} and hence \mathbf{r} . We find that a simple procedure can be given for finding \mathbf{r} , if the equations satisfied by ψ, Φ and χ can be mapped to a dynamical equation for a

unit vector. Such a procedure will be adapted in Chapters 3 and 4, in applying the results obtained in this chapter.

In Chapter 3, we obtain the three moving curves (and the associated surfaces swept out by them) in the case of the NLS and show that they are indeed different from each other explicitly. Some other ramifications of the new geometries will also be presented there. A nonlinear integro-differential equation, equivalent to the Belavin-Polyakov equation and mappable to the elliptic Liouville equation, will be considered in Chapter 4.

Chapter 3

Application to the NLS:

Emergence of two new geometric realizations

3.1 Introduction

In the last chapter, we presented a unified formalism to show how an integrable evolution equation gets associated with three moving space curves. Of these three, the first is obtainable from Lamb's well known formulation [32, 33]. As we have shown, the other two curves are new geometrical realizations that the integrable equation concerned is endowed with.

It is of interest to apply our extended formalism to specific examples of integrable equations. In this chapter, the application to the NLS equation

$$iq_u + q_{ss} + \frac{1}{2}|q|^2q = 0, \quad (3.1)$$

will be discussed, as an illustrative example and all the three moving curves associated with it will be obtained explicitly.

The complete integrability of NLS was shown by Zakharov and Shabat [30], three decades ago. They constructed its Lax pair and obtained strict soliton solutions using the inverse scattering transform (IST) method developed by Gardner, Greene, Kruskal and Miura [4]. Further, they also showed analytically, the stability of these solitons in a pairwise collision process and the existence of an infinite

number of integrals of motion for the system. A Hamiltonian approach to the NLS, and the pairwise involution of the integrals of motion are well known [5]. Integrability through the IST can be regarded as the infinite dimensional counterpart of the well known Liouville-Arnold definition of integrable Hamiltonian systems with finite number of degrees of freedom, via the construction of action angle variables. The IST method can also be seen as the nonlinear analog of the Fourier transform method for solving a linear partial differential equation [41].

The choice of the NLS is appropriate, not only because it was one of the first integrable equations to appear in the context of curve motion [14], but also because it has applications in various other fields such as vortex filament motion, optical fibers [9, 10], magnetic chain dynamics [22, 50], etc.

To find the moving curves associated with the NLS, we return to Sections (2.3) and (2.4) of the last chapter. It can be easily verified that the respective choices

$$\gamma_1 = -i\psi_s ; \quad \gamma_2 = -i\Phi_s ; \quad \gamma_3 = -i\chi_s, \quad (3.2)$$

when used in Eqs. (2.22), (2.41) and (2.55) lead to the NLS given in Eq. (3.1), with $q = \psi, \Phi$ and χ , respectively. The complex functions $\gamma_i, i = 1, 2, 3$ depend on some of the curve *evolution* parameters g, h and τ_0 (see Eqs. (2.15), (2.37) and (2.51) respectively), whereas ψ, Φ and χ depend on κ and τ (see Eqs. (2.1), (2.32) and (2.46) respectively). Thus Eq. (3.2) essentially determines how the parameters g, h and τ_0 must depend on κ, τ and their derivatives, in order to be associated with the NLS. Besides, κ and τ in each case can be determined from any given solution of the NLS, by using Eqs. (2.1), (2.32) and (2.46) respectively. Thus *three* sets of parameters $(\kappa, \tau, g, h, \tau_0)$ appearing in Eqs. (2.2) and (2.5) can be found for a given solution.

3.2 Curvature, torsion and time evolution parameters of the three moving curves

Let us consider a known general solution q of the NLS, Eq. (3.1). Let it be written in the form

$$q = \rho(s, u) \exp(i\alpha(s, u)), \quad (3.3)$$

where ρ and α are real (known) functions. By identifying q given in Eq. (3.3), with the complex functions ψ, Φ and χ , defined in Eqs. (2.1), (2.32) and (2.46) in the

three formulations (I) to (III) respectively, the curvature and torsion of the three corresponding moving space curves are seen to be

$$(I) \quad q = \psi = \kappa_1 \exp[i \int^s \tau_1 ds] ; \quad \kappa_1 = \rho, \tau_1 = \alpha_s \quad (3.4)$$

$$(II) \quad q = \Phi = \tau_2 \exp[i \int^s \kappa_2 ds] ; \quad \kappa_2 = \alpha_s, \tau_2 = \rho \quad (3.5)$$

$$(III) \quad q = \chi = \kappa_3 + i\tau_3 ; \quad \kappa_3 = \rho \cos \alpha, \tau_3 = \rho \sin \alpha \quad (3.6)$$

Here we have used the subscripts 1, 2 and 3 corresponding to formulations (I), (II) and (III). These are clearly three distinct space curves, each with a different curvature and torsion, for any known solution of the NLS. For the complete description of the moving curve, we also need to find the 'temporal parameters' g, h and τ_o that appear in Eqs. (2.5), in the three formulations. We find them as follows. The expression for γ_1, γ_2 and γ_3 for a *general* moving curve are given in Eqs. (2.15), (2.37) and (2.51). For convenience, we rewrite them below, with the appropriate subscripts for the three formulations affixed:

$$\gamma_1 = -(g_1 + ih_1) \exp[i \int^s \tau_1 ds] \quad (3.7)$$

$$\gamma_2 = -(\tau_{o2} - ih_2) \exp[i \int^s \kappa_2 ds] \quad (3.8)$$

$$\gamma_3 = -(g_3 + i\tau_{o3}) \quad (3.9)$$

The three moving curves that correspond to the NLS are found by using Eq. (3.2), as follows.

(I) From Eqs. (3.2) and (3.4)

$$\gamma_1 = -i\psi_s = (-i\kappa_{1s} + \kappa_1\tau_1) \exp[i \int^s \tau_1 ds] \quad (3.10)$$

Equating Eq. (3.10) and Eq. (3.7), we get

$$g_1 = -\kappa_1\tau_1 ; \quad h_1 = \kappa_{1s}. \quad (3.11)$$

Substituting Eq. (3.11) in Eq. (2.8), we get

$$\tau_{o1} = (\kappa_{1ss}/\kappa_1) - \tau_1^2. \quad (3.12)$$

(II) From Eqs. (3.2) and (3.5)

$$\gamma_2 = -i\Phi_s = (-i\tau_{2s} + \kappa_2\tau_2) \exp[i \int^s \kappa_2 ds] \quad (3.13)$$

Comparing Eq. (3.13) with Eq. (3.8), we get

$$\tau_{o2} = -\kappa_2\tau_2 ; \quad h_2 = -\tau_{2s}. \quad (3.14)$$

Substituting these in Eq. (2.8),

$$g_2 = \tau_{2ss}/\tau_2 - \kappa_2^2. \quad (3.15)$$

(III) Similarly, from Eqs. (3.2) and (3.6)

$$\gamma_3 = -i\chi_s = -i\kappa_{3s} + \tau_{3s}. \quad (3.16)$$

Comparing Eq. (3.16) with Eq. (3.9) gives

$$g_3 = -\tau_{3s} ; \quad \tau_{o3} = \kappa_{3s}. \quad (3.17)$$

Again, substituting these in Eq. (2.8) gives,

$$h_3 = \frac{1}{2}(\kappa_3^2 + \tau_3^2). \quad (3.18)$$

It is interesting to note that of the three compatibility conditions Eqs. (2.6) to (2.8) which should be satisfied by any moving curve, the last one plays a special role in that it is the only one that connects *all* the five curve parameters, κ, τ, g, h and τ_o . In every formulation, Eq. (2.8) has been repeatedly used in obtaining one or the other of the three time evolution parameters g, h and τ_o appearing in Eqs. (2.5), in terms of the basic curvature and torsion functions κ and τ appearing in Eqs. (2.2).

To demonstrate explicitly that the three formulations lead to three distinct space curve evolutions, each with a different set κ, τ, g, h and τ_o , we consider the simple example of a one-soliton solution q of the NLS equation:

$$q = a_0 \text{sech}\left(\frac{a_0}{2}\xi\right) \exp(iV_e(s - V_c u)/2). \quad (3.19)$$

Here V_e and V_c denote, respectively, the envelope velocity and carrier velocity of the soliton. The amplitude $a_0 = [V_e(V_e - 2V_c)]^{\frac{1}{2}}$ and $\xi = (s - V_e u)$. Also, $V_e(V_e - 2V_c) \geq 0$. Note that any two of the three parameters a_0, V_e and V_c can be taken to be independent, the most convenient being V_e and V_c .

In Appendix A, we present a derivation of this solution Eq. (3.19), and the condition of inequality involving V_e and V_c mentioned above, using the method of quadratures, for ready reference. This solution (and the N-soliton solutions of the NLS) can also be obtained using the inverse scattering technique [30], but the derivation given in the appendix suffices for our purpose.

We have taken the case $V_c = 0$ for illustration, and obtained the expressions for κ and τ for this solution in the three formulations, by using ψ , Φ and χ defined in Eqs. (2.1), (2.32) and (2.46) respectively. These have been entered in Table 3.1. Using these, the corresponding time-evolution parameters g_i , h_i and τ_{0i} for the three formulations are computed from Eqs. (3.11) and (3.12), (3.14) and (3.15), (3.17) and (3.18) respectively. These are given in Table 3.2.

Formulation	Solution of NLS	κ	τ
I	ψ	$V_e \text{sech} \frac{V_e}{2} \xi$	$V_e/2$
II	Φ	$V_e/2$	$V_e \text{sech} \frac{V_e}{2} \xi$
III	χ	$V_e \text{sech} \frac{V_e}{2} \xi \cos V_e s$	$V_e \text{sech} \frac{V_e}{2} \xi \sin V_e s$

Table 3.1: Example: The curvature κ and torsion τ for the special soliton solution (Eq. (3.19)) of the NLS for ψ , Φ and χ in the respective formulations (I), (II) and (III). This soliton has a vanishing carrier velocity ($V_c = 0$) and a non-vanishing envelope velocity V_e .

Formulation	g	τ_0	h
I	$(-V_e^2/2) \text{sech} \frac{V_e}{2} \xi$	$(-V_e^2/2) \text{sech}^2 \frac{V_e}{2} \xi$	$(-V_e^2/2) \text{sech} \frac{V_e}{2} \xi \times \tanh \frac{V_e}{2} \xi$
II	$(-V_e^2/2) \text{sech}^2 \frac{V_e}{2} \xi$	$(-V_e^2/2) \text{sech} \frac{V_e}{2} \xi$	$(V_e^2/2) \text{sech} \frac{V_e}{2} \xi \times \tanh \frac{V_e}{2} \xi$
III	$(V_e^2/2) \text{sech} \frac{V_e}{2} \xi \times (\tanh \frac{V_e}{2} \xi \sin V_e s - 2 \cos V_e s)$	$(-V_e^2/2) \text{sech} \frac{V_e}{2} \xi \times (\tanh \frac{V_e}{2} \xi \cos V_e s + 2 \sin V_e s)$	$(V_e^2/2) \text{sech}^2 \frac{V_e}{2} \xi$

Table 3.2: The corresponding time evolution parameters g , τ_0 and h in the three formulations for the example considered in Table 3.1.

According to the fundamental theorem of curves [46], smooth functions $\kappa(> 0)$ and τ , define a curve $\mathbf{r}(s, u)$ uniquely, modulo orientation in space at every instant of time u . Now, from the expressions for κ and τ given in Table 3.1, we

see that formulation (I) yields a moving space curve with constant torsion τ but a space-time varying curvature κ . On the other hand, the moving curve obtained using formulation (II) has a constant κ but varying τ . In formulation (III), both κ and τ are space-time dependent. Since the three moving curves have different (κ, τ) parameters, our results explicitly illustrate that they are indeed *geometrically distinct*. Further, since they all arise from the NLS, they correspond to integrable curve evolution.

However, as mentioned in Chapter 1, finding the position vector of the moving curve $\mathbf{r}(s, u)$ explicitly by integrating the FS equations (2.2), given its curvature κ and torsion τ , is a nontrivial task in general. (In addition, here we have to find three curves). We get around this difficulty by using the relationship of the NLS to a certain unit vector evolution equation, namely, the Landau-Lifshitz (LL) equation (Eq. (1.6)), and present a procedure to find the three curves for the NLS in terms of any exact solution \mathbf{S} of the LL equation. This will be discussed in detail in the next section.

3.3 Construction of three moving curves for the NLS using the Landau-Lifshitz equation

In the last section we showed how, given a solution q of the NLS, all the parameters $\kappa_i, \tau_i, g_i, h_i$ and τ_{oi} , ($i = 1, 2, 3$), for the three curves can be explicitly found (see the example in Tables (3.1) and (3.2)). However, as we explained in Section (2.5), even if these are known explicitly, to obtain the tangent vector, $\mathbf{t}(s, u)$ of the corresponding moving curve, in order to construct its position vector, $\mathbf{r}_i(s, u) = \int^s \mathbf{t}_i ds'$ that describes the (moving) curve at the instant u , is non-trivial in general. In the present context, we shall show that a certain connection of the underlying curve evolutions of the NLS with the following Landau-Lifshitz equation [51]

$$\mathbf{S}_u = \mathbf{S} \times \mathbf{S}_{ss}; \quad \mathbf{S}^2 = 1, \quad (3.20)$$

via three distinct mappings, suggests a slightly easier procedure to construct these curves explicitly. First we show how these mappings arise in the three formulations as follows:

(I) Here $q = \psi = \kappa_1 \exp[i \int^s \tau_1 ds']$ satisfies the NLS (see Eq. (3.4)). Substituting

the parameters g_1 and h_1 from Eq. (3.11) in the equation for \mathbf{t}_{1u} , Eq. (2.5), we get

$$\mathbf{t}_{1u} = g_1 \mathbf{n}_1 + h_1 \mathbf{b}_1 = -\kappa_1 \tau_1 \mathbf{n}_1 + \kappa_{1s} \mathbf{b}_1. \quad (3.21)$$

On the other hand, from the FS equations (2.2), we find

$$(\mathbf{t}_1 \times \mathbf{t}_{1ss}) = \mathbf{t}_1 \times (\kappa_1 \mathbf{n}_1)_s = -\kappa_1 \tau_1 \mathbf{n}_1 + \kappa_{1s} \mathbf{b}_1. \quad (3.22)$$

Thus from Eqs. (3.21) and (3.22)

$$\mathbf{t}_{1u} = (\mathbf{t}_1 \times \mathbf{t}_{1ss}), \quad (3.23)$$

which is just the LL equation (3.20) for \mathbf{t}_1 .

(II) Here, $q = \Phi = \tau_2 \exp[i \int^s \kappa_2 ds']$ satisfies the NLS. In this case, let us consider the equation for \mathbf{b}_{2u} given in Eq. (2.5). This involves h_2 and τ_{o2} , whose expressions are given in Eq. (3.14). Thus Eqs. (2.5) becomes,

$$\mathbf{b}_{2u} = -h_2 \mathbf{t}_2 - \tau_{o2} \mathbf{n}_2 = \kappa_2 \tau_2 \mathbf{n}_2 + \tau_{2s} \mathbf{t}_2. \quad (3.24)$$

Next, from the FS equations (2.2), we compute

$$(\mathbf{b}_2 \times \mathbf{b}_{2ss}) = \mathbf{b}_2 \times (-\tau_2 \mathbf{n}_2)_s = \kappa_2 \tau_2 \mathbf{n}_2 + \tau_{2s} \mathbf{t}_2. \quad (3.25)$$

Thus Eq. (3.24) and (3.25) yield

$$\mathbf{b}_{2u} = (\mathbf{b}_2 \times \mathbf{b}_{2ss}). \quad (3.26)$$

Thus, in the second formulation, \mathbf{b}_2 satisfies the LL equation (3.20).

(III) Here $q = \chi = \kappa_3 + i\tau_3$. On substituting for the parameters g_3 and τ_{o3} from Eq. (3.17) into the equation for \mathbf{n}_{3u} in (2.5), we get

$$\mathbf{n}_{3u} = -g_3 \mathbf{t}_3 + \tau_{o3} \mathbf{b}_2 = \kappa_{3s} \mathbf{b}_3 + \tau_{3s} \mathbf{t}_3. \quad (3.27)$$

On the other hand, from the FS equations (2.2), we get

$$(\mathbf{n}_3 \times \mathbf{n}_{3ss}) = \mathbf{n}_3 \times (-\kappa_3 \mathbf{t}_3 + \tau_3 \mathbf{b}_3)_s = \kappa_{3s} \mathbf{b}_3 + \tau_{3s} \mathbf{t}_3. \quad (3.28)$$

Hence,

$$\mathbf{n}_{3u} = (\mathbf{n}_3 \times \mathbf{n}_{3ss}), \quad (3.29)$$

which is just the LL equation (3.20) for \mathbf{n}_3 , the normal to the curve in the third formulation. We remark that this equation for \mathbf{n} , with its correspondence to the

NLS, has been used in a different context [52] to show that Eq. (3.1) (with q replaced by χ) and Eq. (3.29), both reduce to the same bilinear form.

Collecting our results, Eqs. (3.23), (3.26) and (3.29) show that the LL equation (3.20) is satisfied by the *tangent* \mathbf{t}_1 of the moving space curve in the first formulation, by the *binormal* \mathbf{b}_2 of the curve in the second, and the *normal* \mathbf{n}_3 to the curve in the third formulation [53]. Of the above, the first may be regarded as the *converse* of Lakshmanan's mapping [50], where, *starting with* the LL equation, and identifying \mathbf{S} with the tangent to a moving curve, one obtained the DB equations, (1.3), and from them, the NLS for ψ . As we shall show in Section (3.5), our other two formulations will yield two *analogs* of the DB equations, and will clearly correspond to new geometries connected with the NLS.

Before we proceed further, it is instructive to recall briefly how the LL equation arises in the context of magnetism. It describes the spin evolution of the classical Heisenberg ferromagnetic chain given by the Hamiltonian

$$H = -J \sum_i \mathbf{S}_i \cdot \mathbf{S}_{i+1}; \quad \mathbf{S}_i^2 = 1, \quad J > 0, \quad (3.30)$$

in the continuum limit. Adjacent spins tend to be parallel to each other for low energies, and hence nearby spins differ only by a small angle. Eq. (3.20) is easily seen to be the continuum limit of the dynamical equation

$$\frac{d}{dt} \mathbf{S}_i = J \mathbf{S}_i \times (\mathbf{S}_{i+1} + \mathbf{S}_{i-1}). \quad (3.31)$$

Eq. (3.31) can be derived from the Hamiltonian, Eq. (3.30), by using the equation

$$\frac{d}{dt} \mathbf{S}_i = \{H, \mathbf{S}_i\}, \quad (3.32)$$

where the Poisson bracket $\{, \}$, is computed using the relation $\{\mathbf{S}_i^a, \mathbf{S}_j^b\} = \epsilon_{abc} \mathbf{S}_i^c \delta_{ij}$. Taking the continuum limit of Eq. (3.31), by setting $\mathbf{S}_i(t) \rightarrow \mathbf{S}(x, t)$, $\mathbf{S}_{i\pm 1}(t) \rightarrow \mathbf{S}(x \pm a, t)$, where a is the nearest neighbor distance, and using Taylor expansion, leads to the LL equation (3.20), on appropriately rescaling time and space variables.

As stated in Chapter 1, the LL equation has been shown to be completely integrable through the IST [38] and is gauge equivalent to the NLS [50, 54]. Its exact solutions can be found [22, 38, 39]. A derivation of its one-soliton solution is given in Appendix B, since we will be using this solution in our applications.

At this stage, let us pause and state the problem we intend to address. Our objective is to find $\mathbf{r}_1(s, u)$, $\mathbf{r}_2(s, u)$ and $\mathbf{r}_3(s, u)$, which are the position vectors generating the three moving curves associated with the NLS, given the unit vectors

$\mathbf{t}_1, \mathbf{b}_2$ and \mathbf{n}_3 respectively, of the above three curves. Further, as we have shown $\mathbf{t}_1, \mathbf{b}_2$ and \mathbf{n}_3 vectors are given by $\mathbf{S}(s, u)$, a known solution of the LL equation, Eq. (3.20). We now proceed to find $\mathbf{r}_i, i = 1, 2, 3$, for any solution $\mathbf{S}(s, u)$ as follows:

(I) Let \mathbf{t}_1 be the tangent to a certain moving curve created by a position vector $\mathbf{r}_1(s, u)$. Thus we set $\mathbf{t}_1 = \mathbf{r}_{1s} = \mathbf{S}$, a solution of the LL equation. Now, the corresponding triad $(\mathbf{t}_1, \mathbf{n}_1, \mathbf{b}_1)$ of this curve satisfies the FS equations (2.2) with curvature κ_1 and torsion τ_1 . In terms of \mathbf{t}_1 (and hence \mathbf{S}), these are given by the usual expressions

$$\kappa_1 = |\mathbf{t}_{1s}| = |\mathbf{S}_s| \quad (3.33)$$

and

$$\tau_1 = \frac{\mathbf{t}_1 \cdot (\mathbf{t}_{1s} \times \mathbf{t}_{1ss})}{t_{1s}^2} = \frac{\mathbf{S} \cdot (\mathbf{S}_s \times \mathbf{S}_{ss})}{S_s^2}. \quad (3.34)$$

Then the underlying moving curve $\mathbf{r}_1(s, u)$, in this formulation, is simply given in terms of the solution \mathbf{S} directly by,

$$\mathbf{r}_1(s, u) = \int^s \mathbf{t}_1 ds = \int^s \mathbf{S}(s, u) ds' \quad (3.35)$$

The above expression for \mathbf{r}_1 is indeed the surface that one obtains using the Sym's method of soliton surfaces [55].

(II) Let the binormal of some moving curve $\mathbf{r}_2(s, u)$ be denoted by \mathbf{b}_2 . For this case, since \mathbf{b}_2 satisfies the LL equation, $\mathbf{b}_2 = \mathbf{S}$, a known quantity. Here, the tangent $\mathbf{t}_2 = \mathbf{r}_{2s}$. The triad $(\mathbf{t}_2, \mathbf{n}_2, \mathbf{b}_2)$ satisfies Eq. (2.2) with curvature κ_2 and torsion τ_2 . We wish to find all relevant quantities \mathbf{t}_2, κ_2 and τ_2 in terms of \mathbf{b}_2 and its derivatives. It can be verified that the curvature

$$\kappa_2 = \mathbf{b}_2 \cdot (\mathbf{b}_{2s} \times \mathbf{b}_{2ss}) / |\mathbf{b}_{2s}|^2 = \mathbf{S} \cdot (\mathbf{S}_s \times \mathbf{S}_{ss}) / |\mathbf{S}_s|^2 = \tau_1, \quad (3.36)$$

on using Eq. (3.34). The torsion is given by

$$\tau_2 = |\mathbf{b}_{2s}| = |\mathbf{S}_s| = \kappa_1, \quad (3.37)$$

where Eq. (3.33) has been used. Next, \mathbf{t}_2 can be expressed in terms of \mathbf{b}_2 and its derivatives as

$$\mathbf{t}_2 = \mathbf{n}_2 \times \mathbf{b}_2 = \mathbf{b}_2 \times \mathbf{b}_{2s} / |\mathbf{b}_{2s}| = \mathbf{S} \times \mathbf{S}_s / |\mathbf{S}_s|. \quad (3.38)$$

In the second equality above, $\mathbf{n}_2 = -\mathbf{b}_{2s} / |\mathbf{b}_{2s}|$ (arising from FS equations (2.2)) has been used. From Eq. (3.38), the position vector $\mathbf{r}_2(s, u)$ generating the second moving curve is found to be

$$\mathbf{r}_2(s, u) = \int^s \mathbf{t}_2 ds' = \int^s \mathbf{S} \times \frac{\mathbf{S}_s}{|\mathbf{S}_s|} ds'. \quad (3.39)$$

(III) Finally, let the normal of yet another moving curve $\mathbf{r}_3(s, u)$ be denoted by \mathbf{n}_3 . So we have $\mathbf{n}_3 = \mathbf{S}$, the solution to the LL equation. The tangent of this curve is $\mathbf{t}_3 = \mathbf{r}_{3s}$, and the triad $(\mathbf{t}_3, \mathbf{n}_3, \mathbf{b}_3)$ satisfies Eq. (2.2) with curvature κ_3 and torsion τ_3 . Here, clearly, we need the expressions for \mathbf{t}_3 , κ_3 and τ_3 , in terms of \mathbf{n}_3 and its derivatives.

From Eq. (2.2) for this case,

$$\mathbf{n}_{3s} = -\kappa_3 \mathbf{t}_3 + \tau_3 \mathbf{b}_3. \quad (3.40)$$

Hence

$$\mathbf{n}_3 \times \mathbf{n}_{3s} = \kappa_3 \mathbf{b}_3 + \tau_3 \mathbf{t}_3. \quad (3.41)$$

Multiplying Eq. (3.41) by τ_3 and Eq. (3.40) by κ_3 and subtracting the latter from the former, we get

$$(\kappa_3^2 + \tau_3^2) \mathbf{t}_3 = \tau_3 (\mathbf{n}_3 \times \mathbf{n}_{3s}) - \kappa_3 \mathbf{n}_{3s}. \quad (3.42)$$

Thus

$$\mathbf{t}_3 = \frac{\tau_3 (\mathbf{n}_3 \times \mathbf{n}_{3s}) - \kappa_3 \mathbf{n}_{3s}}{(\kappa_3^2 + \tau_3^2)}. \quad (3.43)$$

Next, we find κ_3 and τ_3 in terms of \mathbf{n}_3 . From Eq. (3.40) above, $(\mathbf{n}_{3s})^2 = (\kappa_3^2 + \tau_3^2)$. But from Eq. (3.33), $|\mathbf{n}_{3s}| = |\mathbf{S}_s| = \kappa_1$. Hence,

$$(\mathbf{n}_{3s})^2 = (\kappa_3^2 + \tau_3^2) = \kappa_1^2. \quad (3.44)$$

From Eq. (3.41), it can be verified that

$$(\mathbf{n}_{3ss} \times \mathbf{n}_3) = (\mathbf{n}_{3s} \times \mathbf{n}_3)_s = -\kappa_{3s} \mathbf{b}_3 - \tau_{3s} \mathbf{t}_3. \quad (3.45)$$

Hence on taking the scalar product of Eq. (3.40) with Eq. (3.45),

$$\frac{\mathbf{n}_{3s} \cdot (\mathbf{n}_{3ss} \times \mathbf{n}_3)}{|\mathbf{n}_{3s}|^2} = \frac{\kappa_3 \tau_{3s} - \kappa_{3s} \tau_3}{(\kappa_3^2 + \tau_3^2)} = \frac{\partial}{\partial s} \tan^{-1} \left(\frac{\tau_3}{\kappa_3} \right). \quad (3.46)$$

But since $\mathbf{n}_3 = \mathbf{S}$, the left hand side is just τ_1 (see Eq. (3.34)), i.e.,

$$\tau_1 = \frac{\partial}{\partial s} \tan^{-1} \left(\frac{\tau_3}{\kappa_3} \right). \quad (3.47)$$

In Eq. (3.44), on parameterizing

$$\kappa_3 = \kappa_1 \cos \alpha; \quad \tau_3 = \kappa_1 \sin \alpha, \quad (3.48)$$

and substituting these in Eq. (3.47) gives $\tau_1 = \partial \alpha / \partial s$. Thus α is determined as

$$\alpha = \int^s \tau_1 ds' + C_1(u). \quad (3.49)$$

Here, $C_1(u)$ is an arbitrary function of time u at this stage, which can be determined in terms of κ_1 and τ_1 using the appropriate compatibility conditions Eqs. (2.6) and (2.7) for κ_{3u} and τ_{3u} . These details will be given in Appendix C.

Substituting for κ_3 and τ_3 in terms of κ_1 and α from Eq. (3.48) and setting $\mathbf{n}_3 = \mathbf{S}$ in Eq. (3.43), the position vector $\mathbf{r}_3(s, u)$ creating the third moving space curve can be found to be

$$\mathbf{r}_3(s, u) = \int^s \mathbf{t}_3 ds = \int^s \frac{[(\mathbf{S} \times \mathbf{S}_s) \sin \alpha - \mathbf{S}_s \cos \alpha]}{\kappa_1} ds', \quad (3.50)$$

where α is given in Eq. (3.49). Note that the expressions for \mathbf{r}_i , $i = 1, 2, 3$, obtained in this section are valid for *any* general exact solution of the LL equation (3.20) and equivalently, correspond to *any* solution q of the NLS. In the next section we specialize to soliton solutions. All figures pertaining to this chapter will be given at the end of this chapter.

3.4 Swept out surfaces associated with a stationary envelope NLS soliton

The one-soliton solution of the LL equation (3.20) is given in Cartesian coordinates by

$$\mathbf{S}(s, u) = \left\{ \mu \text{sech}(\nu \xi) (\nu \tanh(\nu \xi) \cos \eta + \lambda \sin \eta), \right. \\ \left. \mu \text{sech}(\nu \xi) (\nu \tanh(\nu \xi) \sin \eta - \lambda \cos \eta), 1 - \mu \nu \text{sech}^2(\nu \xi) \right\}, \quad (3.51)$$

where

$$\xi = (s - 2\lambda u), \quad (3.52a)$$

$$\eta = (\lambda s + (\nu^2 - \lambda^2)u), \quad (3.52b)$$

$$\mu = 2\nu/(\nu^2 + \lambda^2). \quad (3.52c)$$

In the above, ν and λ are arbitrary constant parameters (the solution (3.51) has been derived in Appendix B). Using Eq. (3.51) and our results of the previous section, the three moving curves that correspond to the soliton solution of the NLS

$$q = \rho \exp i\alpha = 2\nu \text{sech}(\nu \xi) \exp i\eta \quad (3.53)$$

of the NLS (Eq. (3.1)) will be found by substituting Eq. (3.51) in Eqs. (3.35), (3.39) and (3.50), respectively. It is instructive to compare Eq. (3.53) with the NLS

soliton given in Eq. (3.19). We see that the relation between the parameters are $\lambda = V_e/2$ and $\nu = \frac{1}{2}(V_e(V_e - 2V_c))^{1/2}$.

For the sake of illustration, let us first consider the special case $\lambda = 0$, which corresponds to $V_e = 0$, a vanishing envelope velocity of the NLS soliton. We obtain the following three surfaces swept out by the three moving curves as follows:

In every case, let us express the position vector of the moving curve in Cartesian coordinate in parametric form as

$$\mathbf{r}_i = \{x_i(s, u), y_i(s, u), z_i(s, u)\} ; \quad i = 1, 2, 3. \quad (3.54)$$

Setting $\lambda = 0$ in Eq. (3.51), we get the expression for \mathbf{S} as

$$\mathbf{S}(s, u, \lambda = 0) = \{(1 - 2\text{sech}^2 \nu s), 2\text{sech} \nu s \tanh \nu s \cos \nu^2 u, 2\text{sech} \nu s \tanh \nu s \sin \nu^2 u\}. \quad (3.55)$$

From Eq. (3.55), we find

$$\begin{aligned} \mathbf{S}_s = 2\nu \text{sech} \nu s \{ & 2\text{sech} \nu s \tanh \nu s, \\ & (2\text{sech}^2 \nu s - 1) \cos \nu^2 u, (2\text{sech}^2 \nu s - 1) \sin \nu^2 u \} \end{aligned} \quad (3.56)$$

and

$$\mathbf{S} \times \mathbf{S}_s = 2\nu \text{sech} \nu s \{ 0, \sin^2 \nu u, -\cos^2 \nu u \}. \quad (3.57)$$

Equations (3.56) and (3.57) will be used in (II) and (III) below. Let us find the three curves as follows:

(I) Here $\mathbf{t}_1 = \mathbf{S}$. This expression can be explicitly integrated to yield the expression for the position vector as $\mathbf{r}_1 = \int^s \mathbf{S} ds'$. Thus

$$\mathbf{r}_1(s, u) = \{s - (2/\nu) \tanh \nu s, (-2/\nu) \text{sech} \nu s \cos \nu^2 u, (-2/\nu) \text{sech} \nu s \sin \nu^2 u\} \quad (3.58)$$

Substituting Eq. (3.55) in Eqs. (3.33) and (3.34), we find $\kappa_1 = 2\nu \text{sech}(\nu s)$ and $\tau_1 = 0$. It is easily seen that the Cartesian components obey the relation,

$$y_1^2 + z_1^2 = (4/\nu^2) \text{sech}^2 \nu s. \quad (3.59)$$

The y and z components thus form a circle, whose radius has a maximum at $s = 0$ and vanishes asymptotically for $s \rightarrow \infty$. Besides, from Eq. (3.58), $\mathbf{r}_1 \rightarrow (s, 0, 0)$ as $s \rightarrow \pm\infty$. This behavior is clearly seen in the surface given in Fig.(3.1). This figure is a plot of the analytic expression (3.58) using *Mathematica* [56].

(II) Substituting Eq. (3.57) in Eq. (3.38) immediately yields

$$\mathbf{t}_2 = \{ 0, \sin \nu^2 u, -\cos \nu^2 u \}. \quad (3.60)$$

Integrating Eq. (3.60), we get

$$\mathbf{r}_2(s, u) = s \{ 0, \sin \nu^2 u, -\cos \nu^2 u \}. \quad (3.61)$$

Here, $\kappa_2 = 0$ and $\tau_2 = 2\nu \operatorname{sech}(\nu s)$, since $\kappa_2 = \tau_1$ and $\tau_2 = \kappa_1$. Evidently, the components satisfy the condition $y_2^2 + z_2^2 = s^2$, for all times. For the sake of completeness, we display this planar surface in Fig.(3.2).

(III) Here $\mathbf{n}_3 = \mathbf{S}$. Upon substituting Eqs. (3.56) and (3.57) in Eq. (3.43) and using $\kappa_3 = 2\nu \operatorname{sech} \nu s \cos \nu^2 u$ and $\tau_3 = 2\nu \operatorname{sech} \nu s \sin \nu^2 u$, we get

$$\mathbf{t}_3 = \{-2 \operatorname{sech} \nu s \tanh \nu s \cos \nu^2 u, 1 - 2 \operatorname{sech}^2 \nu s \cos^2 \nu^2 u, -2 \operatorname{sech}^2 \nu s \cos \nu^2 u \sin \nu^2 u\}, \quad (3.62)$$

where, since $\tau_1 = 0$ when $\lambda = 0$, Eq. (3.49) gives $\alpha = \nu^2 u = C_1(u)$ (see Appendix C for determination of $C_1(u)$). Eq. (3.62) can be easily integrated to yield

$$\mathbf{r}_3(s, u) = \{(2/\nu) \operatorname{sech} \nu s \cos \nu^2 u, (s - (2/\nu) \tanh \nu s \cos^2 \nu^2 u), - (2/\nu) \tanh \nu s \cos \nu^2 u \sin \nu^2 u\}. \quad (3.63)$$

An expression relating the Cartesian components for this case, however, is more complicated than the previous cases. However, from Eq. (3.63), we see that x_3 and z_3 are bounded functions for all s and u . As $s \rightarrow \pm\infty$, $y_3 \rightarrow \pm\infty$, $x_3 \rightarrow 0$ and $z_3 \rightarrow \mp(1/\nu) \sin 2\nu^2 u$. This depicts an oscillation of the z component, with a finite amplitude $(1/\nu)$. As $s \rightarrow 0$, y_3 and z_3 vanish and $x_3 \rightarrow (2/\nu) \cos \nu^2 u$. This describes oscillation of the x component with a finite amplitude $(2/\nu)$. These limiting behaviors can be seen clearly in the swept-out surface described by Eq. (3.63) which has been plotted using *Mathematica* in Fig. (3.3).

For the case $\lambda \neq 0$, the envelope of the NLS soliton moves. Geometrically, this motion can be shown to correspond to the "twisting out" of the surface in Fig.(3.1) around its symmetry axis, and "stacking up" of more such surfaces in a helical fashion along this axis. This will lead to corresponding changes in Figs.(3.2) and (3.3) as well. This case will be discussed in Section (3.6).

Before we conclude this section, we mention that the geometry underlying the NLS can also be studied by working with the complex conjugates of the complex vectors and functions that we used in the three formulations. These can be shown to lead to a mapping to the LL equation for $-\mathbf{t}$, $-\mathbf{n}$ and $-\mathbf{b}$ respectively. It can be verified that these merely yield swept out surfaces which are created by the negative of the position vectors $\mathbf{r}_i, i = 1, 2, 3$, which we found in Section (3.3), so that essentially no new surfaces result from these. We remark that while in the first

formulation, it can be easily verified that the curve velocity \mathbf{r}_{1u} satisfies the local induction equation [26] $\mathbf{r}_{1u} = \kappa_1 \mathbf{b}_1$, the velocities \mathbf{r}_{2u} and \mathbf{r}_{3u} appearing in the other two formulations can be shown to satisfy more complicated equations [36]. This will be discussed in Section (3.7).

Next, we focus on the intrinsic geometries and kinematics of the three space curves associated with *general* NLS evolution.

3.5 The NLS and two analogs of the Da Rios-Betchov equations

As described in Chapter 1, the topic of possible connection between geometry of curve motion and integrable equations started with the (coupled) DB equations,

$$\kappa_u = -(\kappa\tau)_s - \kappa_s\tau, \quad (3.64)$$

$$\tau_u = [(\kappa_{ss}/\kappa) - \tau^2]_s + \kappa\kappa_s, \quad (3.65)$$

which could be combined to yield the NLS equation (3.1), with q replaced by $\psi = \kappa \exp[i \int^s \tau ds]$. Since the NLS is a completely integrable equation [1], it possesses an infinite set of conserved quantities I_k , $k = 1, 2, \dots, \infty$, which are in involution pairwise. The first three of these invariants are given by [57]

$$I_1 = \int |q|^2 ds, \quad (3.66a)$$

$$I_2 = (1/2i) \int (q_s q^* - q_s^* q) ds, \quad (3.66b)$$

$$I_3 = \int [|q_s|^2 - \frac{1}{4}|q|^4] ds; \dots \quad (3.66c)$$

(I) Setting $q = \psi$ in Eqs. (3.66) above, the invariants now appear as *geometric* constraints [58] involving the curvature κ and torsion τ .

$$I_1 = \int \kappa^2 ds, \quad (3.67a)$$

$$I_2 = \int \kappa^2 \tau ds, \quad (3.67b)$$

$$I_3 = \int [\kappa_s^2 + \kappa^2 \tau^2 - \frac{1}{4}\kappa^4] ds; \dots \quad (3.67c)$$

Thus the DB equations (3.64) and (3.65) are seen to be endowed with the above geometric constraints. Further, Eq. (3.65) can be written as

$$\tau_u = [(\kappa_{ss}/\kappa) - \tau^2 + \frac{1}{2}\kappa^2]_s, \quad (3.68)$$

which is of the form of a continuity equation, showing that the *total torsion* $I_0 = \int \tau ds$ is also conserved. This additional geometric constraint obtained from the DB equations, has no counterpart among the invariants obtained in terms of ψ , given in Eq. (3.66).

From formulations (II) and (III) in Chapter 2, we saw that the functions $q = \Phi$ and $q = \chi$, also arose in a natural fashion, by starting with general moving curve evolution equations. We consider these next.

(II) Here, we set $q = \Phi$ in (3.1), to yield the coupled equations

$$\kappa_u = [(\tau_{ss}/\tau) - \kappa^2]_s + \tau\tau_s, \quad (3.69)$$

$$\tau_u = -(\kappa\tau)_s - \tau_s\kappa. \quad (3.70)$$

This is the *first* analog of the DB equations (3.64) and (3.65). As is obvious from comparing ψ in Eq. (2.1) and Φ in Eq. (2.32), this analog may be found by simply interchanging κ and τ in Eqs. (3.64) and (3.65). Thus the associated infinite number of geometric constraints can also be found using this interchange in Eqs. (3.67):

$$I_1 = \int \tau^2 ds, \quad (3.71a)$$

$$I_2 = \int \tau^2 \kappa ds, \quad (3.71b)$$

$$I_3 = \int [\tau_s^2 + \tau^2 \kappa^2 - \frac{1}{4} \tau^4] ds; \dots \quad (3.71c)$$

Here, as is obvious from Eq. (3.69), the total *curvature* $I_0 = \int \kappa ds$ is *also* conserved. This has no counterpart among the conserved densities (3.66) of the NLS equation.

(III) Finally, setting $q = \chi$ in (3.1) yields the following *second* analog of the DB equations:

$$\kappa_u = -\tau_{ss} - \frac{1}{2}(\kappa^2 + \tau^2)\tau, \quad (3.72)$$

$$\tau_u = \kappa_{ss} + \frac{1}{2}(\kappa^2 + \tau^2)\kappa. \quad (3.73)$$

Again, setting $q = \chi$ in Eq. (3.66), we get the third set of infinite geometric constraints:

$$I_1 = \int (\kappa^2 + \tau^2) ds, \quad (3.74a)$$

$$I_2 = \int (\kappa_s \tau - \kappa \tau_s) ds, \quad (3.74b)$$

$$I_3 = \int [\kappa_s^2 + \tau_s^2 - \frac{1}{4}(\kappa^2 + \tau^2)^2] ds; \dots \quad (3.74c)$$

It is interesting to note that multiplying Eq. (3.72) by κ and Eq. (3.73) by τ and adding, we get

$$\frac{1}{2}(\kappa^2 + \tau^2)_u - (\kappa_s \tau - \kappa \tau_s) = 0. \quad (3.75)$$

From this continuity equation, we see that $\int^s (\kappa^2 + \tau^2) ds'$ is conserved. This is the first integral I_1 in the set Eq. (3.74) and not an additional constraint unlike the earlier two cases.

The results obtained in this section are *general* and applicable to all solutions of the NLS. We end this section with the remark that the total length of the curve, $L = \int ds$ is also conserved in *all three* formulations, since the curves are non-stretching.

3.6 Stroboscopic plots of space curve evolutions associated with a moving envelope NLS soliton

In Section (3.3), the general expressions for $\mathbf{r}_1, \mathbf{r}_2$ and \mathbf{r}_3 , in the three formulations were determined for any solution of the NLS, using the corresponding solution of the LL equation. In Section (3.4) their expressions corresponding to *stationary* envelope soliton solution, Eq. (3.53), of the NLS with $\lambda = V_e = 0$, was considered. The three swept out surfaces were also plotted in Figs. (3.1) to (3.3). In this section we consider the moving envelope case, $\lambda \neq 0$.

A remark is in order here. As mentioned at the end of Section (3.4), for $\lambda \neq 0$, the surface that is swept out by the moving curve gets twisted out due to the motion of the soliton along the curve and hence gets more complicated to visualize. For this reason, in this section we display the *stroboscopic plots* for the three moving curves, rather than the surfaces swept out. Besides, it is interesting to ask whether such a solitonic propagation along a vortex filament can be experimentally observed in a real fluid. In such an experiment one could observe the filament at regular time intervals [31] and look for 'compact' distortion or a 'soliton' propagating along the filament. Thus stroboscopic plots are more useful in this context. From the one-soliton solution Eq. (3.51), for the LL equation (which corresponds to the one-soliton solution Eq. (3.53) of the NLS), we derive,

$$S_s = \mu \operatorname{sech} \nu \xi \left\{ 2\nu^2 \operatorname{sech} \nu \xi \tanh \nu \xi, \right.$$

$$\begin{aligned} & -2\lambda\nu \tanh \nu\xi \sin \eta + 2\nu^2 \operatorname{sech}^2 \nu\xi \cos \eta + (\lambda^2 - \nu^2) \cos \eta, \\ & 2\lambda\nu \tanh \nu\xi \cos \eta + 2\nu^2 \operatorname{sech}^2 \nu\xi \sin \eta + (\lambda^2 - \nu^2) \sin \eta \}. \end{aligned} \quad (3.76)$$

After some algebra, we obtain from Eqs. (3.51) and (3.76),

$$\begin{aligned} \mathbf{S} \times \mathbf{S}_s = \mu \operatorname{sech} \nu\xi \{ & 2\nu\lambda \operatorname{sech} \nu\xi, \\ & -2\lambda\nu \tanh \nu\xi \cos \eta - (\lambda^2 - \nu^2) \sin \eta, \\ & -2\lambda\nu \tanh \nu\xi \sin \eta + (\lambda^2 - \nu^2) \cos \eta \}, \end{aligned} \quad (3.77)$$

where η and ξ are defined in Eqs. (3.52) (Eqs. (3.76) and (3.77) will be used in formulations (II) and (III) discussed below). Now we find the explicit expression for the moving curve in the three formulations, corresponding to the one-soliton solution Eq. (3.53) of the NLS, using the general results of Section (3.3).

(I) Here $\mathbf{t}_1 = \mathbf{S}$. Substituting Eq. (3.51) in Eqs. (3.33) and (3.34), a short calculation yields

$$\kappa_1 = 2\nu \operatorname{sech}(\nu\xi) ; \quad \tau_1 = \lambda. \quad (3.78)$$

Eq. (3.51) can be integrated *exactly* to give the explicit expression for the position vector \mathbf{r}_1 of the moving curve,

$$\mathbf{r}_1 = \left\{ s - \mu \tanh(\nu\xi), -\mu \operatorname{sech}(\nu\xi) \cos \eta, -\mu \operatorname{sech}(\nu\xi) \sin \eta \right\}. \quad (3.79)$$

This is seen to agree with the result obtained in [59] using Sym's [55] procedure. In Fig.(3.4), we have presented a *stroboscopic* plot of the moving curve, (3.79), at different instants of time. This describes the propagation of the well known Hasimoto "loop" soliton along the curve. In the intermediate periods, the loop changes its size and also rotates about the axial direction. In this figure, these intermediate times have been omitted for the sake of clarity. The loop regains its form at regular intervals, as seen from the figure.

(II) In this formulation, the binormal $\mathbf{b}_2 = \mathbf{S}$. Here, we get

$$\kappa_2 = \lambda ; \quad \tau_2 = 2\nu \operatorname{sech}(\nu\xi), \quad (3.80)$$

since, as shown in Eqs. (3.36) and (3.37), $\kappa_2 = \tau_1$ and $\tau_2 = \kappa_1$. Substituting Eqs. (3.76) and (3.77) in Eq. (3.39), the moving curve \mathbf{r}_2 is found to be

$$\begin{aligned} \mathbf{r}_2 = \int^s [& \mu\lambda \operatorname{sech}(\nu\xi) \hat{\mathbf{i}} - (\mu\lambda \tanh(\nu\xi) \cos \eta + \frac{(\lambda^2 - \nu^2)}{(\lambda^2 + \nu^2)} \sin \eta) \hat{\mathbf{j}} \\ & - (\mu\lambda \tanh(\nu\xi) \sin \eta - \frac{(\lambda^2 - \nu^2)}{(\lambda^2 + \nu^2)} \cos \eta) \hat{\mathbf{k}}] ds' \end{aligned} \quad (3.81)$$

In this case, since the curvature κ_2 is constant and the torsion τ_2 vanishes as $s \rightarrow \pm\infty$ for all finite times, the curve is bounded by two planar circles at both ends. Since $\xi = (s - 2\lambda u)$, maximum torsion τ_2 , i.e., maximum non-planarity of the curve occurs at $s = 2\lambda u$. A stroboscopic plot of Eq. (3.81) (using *Mathematica*) given in Fig.(3.5). This curve is clearly seen to rotate and propagate as time progresses, and regains its shape after some time, as seen in Fig (3.5).

(III) In this case $\mathbf{n}_3 = \mathbf{S}$. We find on using Eq. (3.78) in Eq. (3.48)

$$\kappa_3 = 2\nu \operatorname{sech}(\nu\xi) \cos \alpha ; \quad \tau_3 = 2\nu \operatorname{sech}(\nu\xi) \sin \alpha. \quad (3.82)$$

From Eqs. (3.49) and (3.78), $\alpha = \lambda s + C_1(u)$. But from Appendix C, Eq. (C.18), $C_1(u) = (\nu^2 - \lambda^2)u$. Hence

$$\alpha = \eta, \quad (3.83)$$

where η is given in the second equation of the set Eqs. (3.52). Next, Eqs. (3.76) and (3.77) are substituted in Eq. (3.50), with $\alpha = \eta$. A long but straightforward calculation yields

$$\begin{aligned} \mathbf{r}_3 = & \int^s \left[\mu \operatorname{sech}(\nu\xi) (\lambda \sin \eta - \nu \tanh(\nu\xi) \cos \eta) \hat{\mathbf{i}} \right. \\ & - \left(\frac{(\lambda^2 - \nu^2)}{(\lambda^2 + \nu^2)} \sin^2 \eta + (1 - \mu\nu \tanh^2(\nu\xi)) \cos^2 \eta \right) \hat{\mathbf{j}} \\ & \left. + \left[\left(\frac{(\lambda^2 - \nu^2)}{(\lambda^2 + \nu^2)} - (1 - \mu\nu \tanh^2(\nu\xi)) \right) \sin \eta \cos \eta - \mu\lambda \tanh(\nu\xi) \hat{\mathbf{k}} \right] ds' \right] \quad (3.84) \end{aligned}$$

A stroboscopic plot of the moving curve \mathbf{r}_3 (Eq. (3.84)) at different instants of time is given in Fig. (3.6). This depicts the propagation of a "loop" soliton *distinct* from the Hasimoto soliton in the sense that it also *oscillates* with time along the curve, as is clear from the figure. Furthermore, at intermediate times, the loop rotates about the asymptotic direction, decreasing its loop size, and almost straightens out periodically, after which it starts looping again.

Such intermediate plots have not been presented in any of the three figures (3.4) to (3.6), since our stress here is in noting the property of shape preservation of the distinct curves in all the three formulations (I) to (III). For the same reason, the values of the parameters (ν and λ) are also appropriately chosen in order to see the 'loops' clearly in these plots.

3.7 Three curve velocities associated with NLS evolution

Returning to our general results of Section (3.3), the three position vectors \mathbf{r}_i , $i = 1, 2$ and 3 , which are associated with the NLS evolution, can be found from Eqs. (3.35), (3.39) and (3.50) respectively, using an exact solution \mathbf{S} (Eq. (3.51)) of the LL equation. The corresponding curve velocities $\mathbf{v}_i = \mathbf{r}_{iu}$ at each point s , can therefore be found from these equations by direct differentiation with respect to time, u . However, to compare and contrast the intrinsic geometries of the three space curves, it is instructive to express these velocities in terms of the vectors of the corresponding Frenet triads and the curve parameters as follows.

Since all the three curves are *non-stretching*, we have $\mathbf{v}_{is} = \mathbf{r}_{ius} = \mathbf{r}_{isu} = \mathbf{t}_{iu}$. On the other hand, from the first equation of Eqs. (2.5), we have, $\mathbf{t}_{iu} = g_i \mathbf{n}_i + h_i \mathbf{b}_i$. Here, the quantities g_i and h_i for the three curves of the NLS are given in Eqs. (3.11), (3.14) and (3.17), respectively. Using these in $\mathbf{v}_i(s, u) = \int^s \mathbf{t}_{iu} ds'$, we get

$$(I) \quad \mathbf{v}_1 = \int^s (-\kappa_1 \tau_1 \mathbf{n}_1 + \kappa_{1s'} \mathbf{b}_1) ds' = \kappa_1 \mathbf{b}_1. \quad (3.85)$$

$$(II) \quad \mathbf{v}_2 = \int^s [(\tau_{2s's'}/\tau_2 - \kappa_2^2) \mathbf{n}_2 - \kappa_{2s'} \mathbf{b}_2] ds'. \quad (3.86)$$

$$(III) \quad \mathbf{v}_3 = \int^s [-\tau_{3s'} \mathbf{n}_3 + \frac{1}{2}(\kappa_3^2 + \tau_3^2) \mathbf{b}_3] ds'. \quad (3.87)$$

Not surprisingly, \mathbf{v}_1 coincides with the vortex filament velocity Eq. (1.2) derived by Da Rios in fluid mechanics. This derivation of \mathbf{v}_1 , in the local induction approximation (for Formulation (I) of the NLS) is given in Appendix D for ready reference. It is a *local* expression in the curve variables: The velocity \mathbf{v}_1 at a point s depends on the curvature and binormal at that point only. In contrast, \mathbf{v}_2 and \mathbf{v}_3 are seen to be *nonlocal* in the curve variables: If we partially integrate the right hand sides of Eqs. (3.86) and (3.87), and use the FS equations (Eqs. (2.2)) repeatedly in the resulting expressions, both these velocities take on the form $\mathbf{v}_i = A_i \mathbf{t}_i + B_i \mathbf{n}_i + C_i \mathbf{b}_i$, $i = 2, 3$, where the components A_i, B_i and $C_i, i = 2, 3$ can be written in terms of an infinite sum of *integrals* of certain functions involving the curvature, the torsion, their higher derivatives and their various products. It is indeed interesting that in spite of such a complicated behavior of these velocities, their corresponding curve evolutions are also endowed with an infinite number of constants of motion. This essentially stems from their connection with the NLS. More specifically, this is be-

cause, as we have shown in Section(3.3), the binormal \mathbf{b}_2 of the second curve and the normal \mathbf{n}_3 of the third, satisfy the integrable LL equation.

3.8 Summary and discussion

In this chapter, we have discussed the application of the three formulations presented in Chapter 2 to the NLS. This has been done exploiting the connection between the NLS and the LL equations for the tangent, normal and binormal vectors. In particular we have obtained the expression for the position vectors $\mathbf{r}_i(s, u)$, $i = 1, 2, 3$, of the three non-stretching moving space curves in terms of the unit vectors, \mathbf{t}_1 , \mathbf{b}_2 and \mathbf{n}_3 , which satisfy the LL equations in the three cases. As an example, we considered the geometries associated with the one soliton solution of the NLS (Appendix A), and found the three moving curves explicitly. The swept out surfaces corresponding to a soliton with vanishing envelope velocity have been displayed in Figs. (3.1) to (3.3). For the general case of the moving envelope soliton, stroboscopic plots of the moving curve in the three cases, are shown in Figs. (3.4) to (3.6).

We conclude with the following remarks on the possibility of applying our results to vortex filament motion in fluids, by regarding a moving vortex filament to be a non-stretching, moving space curve. In a fluid, as is well known, the induced velocity \mathbf{v} at a point is determined as a volume integral involving the vorticity \mathbf{w} , by using the Biot-Savart formula (see Appendix D). Firstly, it is to be noted that in this formula, if one expresses \mathbf{w} in terms of the vectors of the Frenet triad of the filament, then, in any realistic model of a fluid, \mathbf{v} is nonlocal in the curve variables. It becomes local only under certain approximations, such as the local induction model (see Appendix D for approximations used).

Secondly, it is worth noting that in an interesting experiment with a fluid in a rotating tank, Hopfinger and Browand [31] had observed *compact* distortions which twist and propagate along a vortex core like a soliton. In this experiment, the turbulent motion of a fluid, in a container rotating about its vertical axis, is studied. The fluid motion is made turbulent due to a horizontal grid at the bottom which oscillates in the vertical direction. The random field is opposed by the rotation of the container, which has an organizing influence on the fluid. It is noticed that in the resulting complex motion there are, however, regions of concentrated vorticity. The resulting vortices are found to have soliton-like distortions which propagate along the vortex core, in agreement with result obtained by Hasimoto [14], the only theoretical model available at that time. The curve velocity is \mathbf{v}_1 (see Eq. (3.85)).

In fact, Fig. (3.4) depicts the helical Hasimoto soliton propagation as snapshots at different instants of time. In Chapter 2, we have found two other formulations possible for an integrable equation. We have shown that these imply new geometric connections that link the curve velocities \mathbf{v}_2 and \mathbf{v}_3 (see Eqs. (3.86) and (3.87)) with the NLS and its soliton solutions. These may turn out to be of some relevance in actual fluids. In view of this, appropriate theoretical modeling of the vorticity, to go beyond the local induction approximation, would be worthwhile. Our results also suggest that it would indeed be of interest to carry out more experimental studies of the *detailed geometric structure* of moving vortex filaments, to look for any similarities with Figs. (3.5) and (3.6) which also depict propagation of compact distortions along the curve.

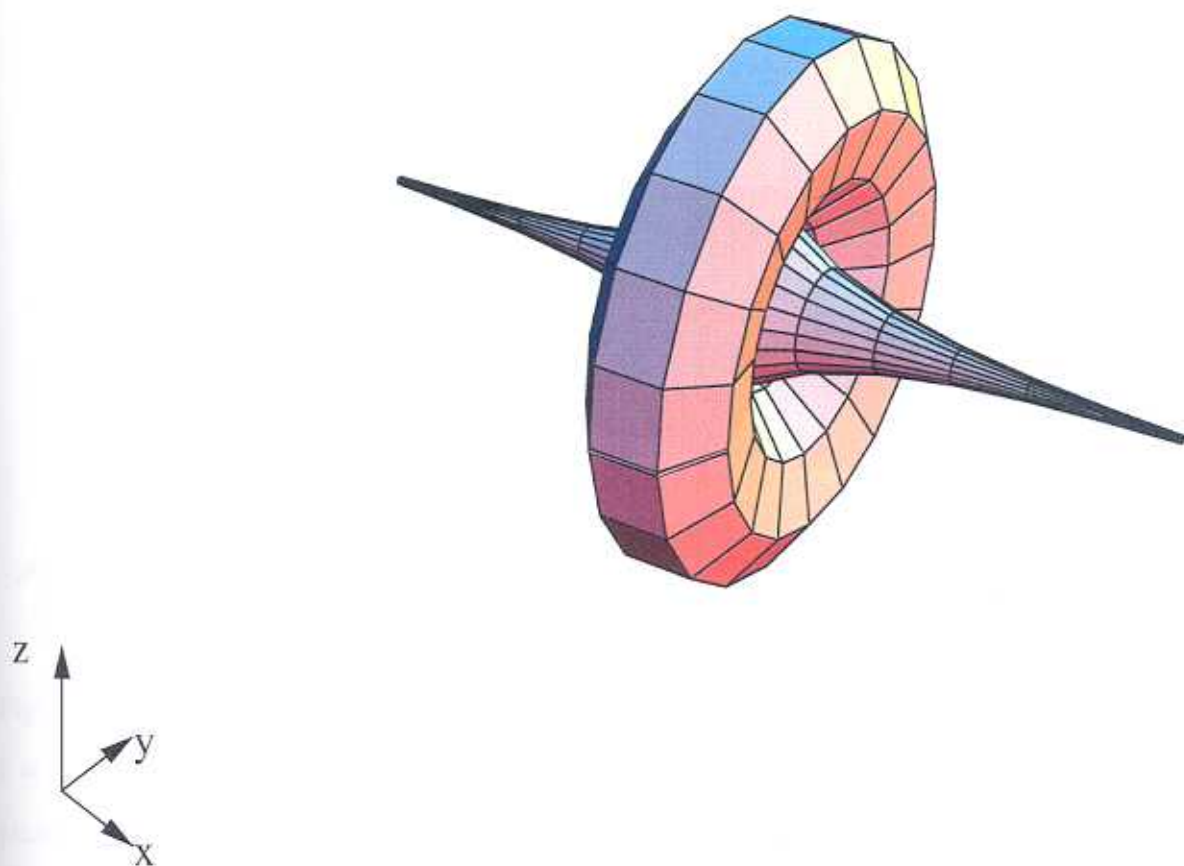


Figure 3.1: Surface swept-out by the moving space curve $\mathbf{r}_1(s, u)$ Eq. (3.58), for $\nu = 1, \lambda = 0$ and $0 \leq u \leq 6.3$. The surface is generated by a curve with a planar loop in the middle, rotating about the x -axis.

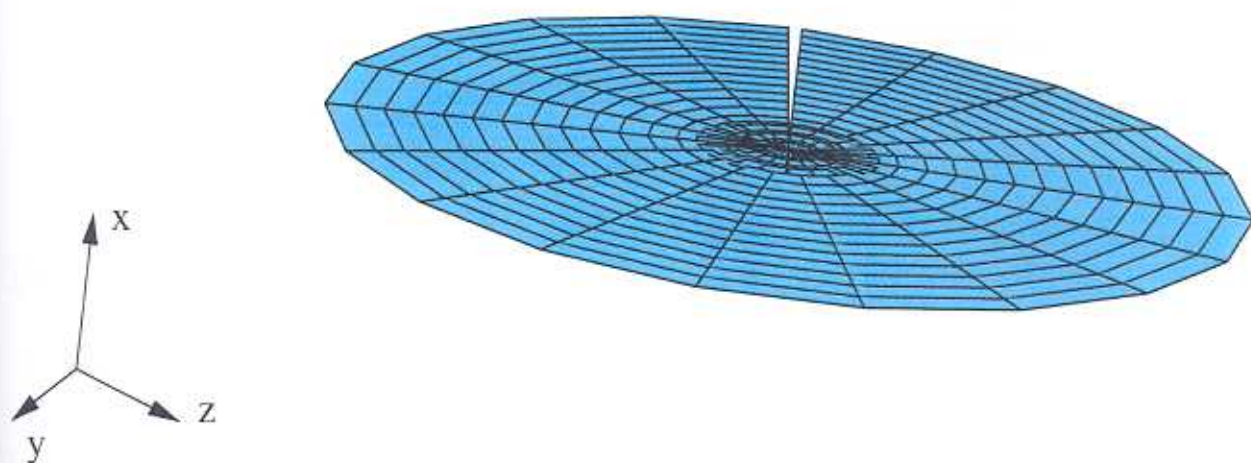


Figure 3.2: Surface swept-out by the moving space curve $\mathbf{r}_2(s, u)$ Eq. (3.61), for $\nu = 0.5, \lambda = 0$ and $0 \leq u \leq 25$. The curve at any time is a straight line in the $y - z$ plane. The surface is generated by the rotation of this straight line about the x axis.

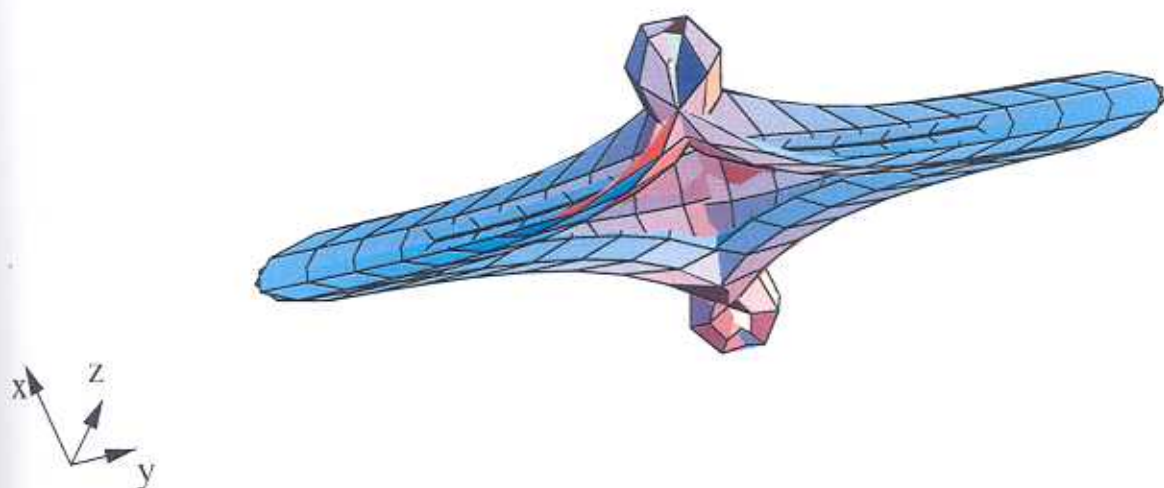


Figure 3.3: Surface swept-out by the moving space curve $\mathbf{r}_3(s, u)$ Eq. (3.63), for $\nu = 0.5, \lambda = 0$ and $0 \leq u \leq 25$. This surface is formed by an oscillating curve with a loop in the middle. As can be seen from the figure the surface is bounded in the x and z directions for all s and u . The wings in the $\pm y$ directions extend further as the length of the curve considered is increased. This matches the description given below Eq. (3.63).

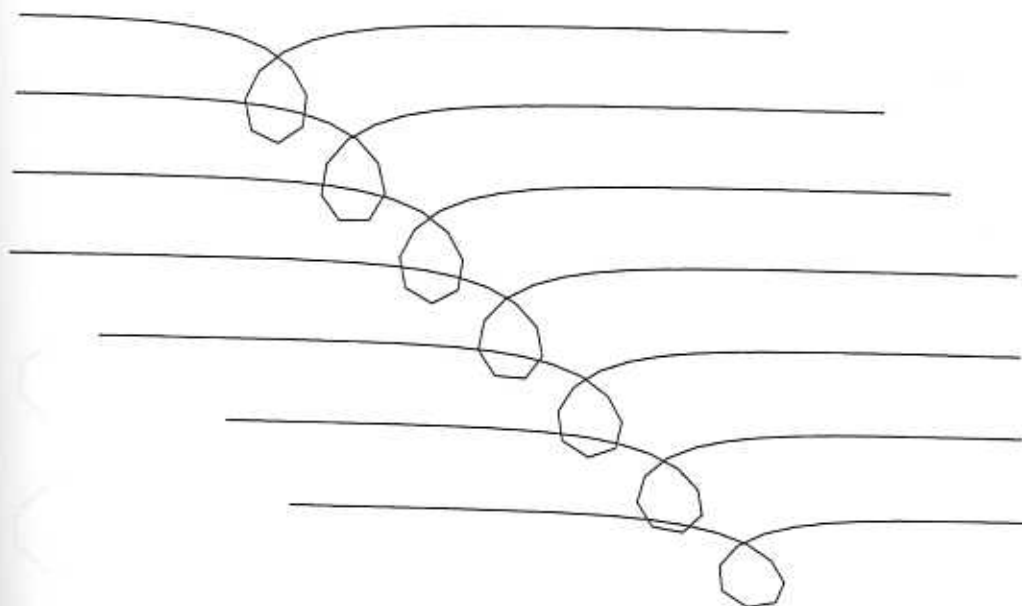


Figure 3.4: A stroboscopic plot of the evolving space curve $\mathbf{r}_1(s, u)$ Eq. (3.79), for $\nu = 1$ and $\lambda = 0.1$. The loop rotates as it moves along its axis with a regular period $T = 2\pi/(\nu^2 - \lambda^2)$. The various snapshots are shown separated for clarity.

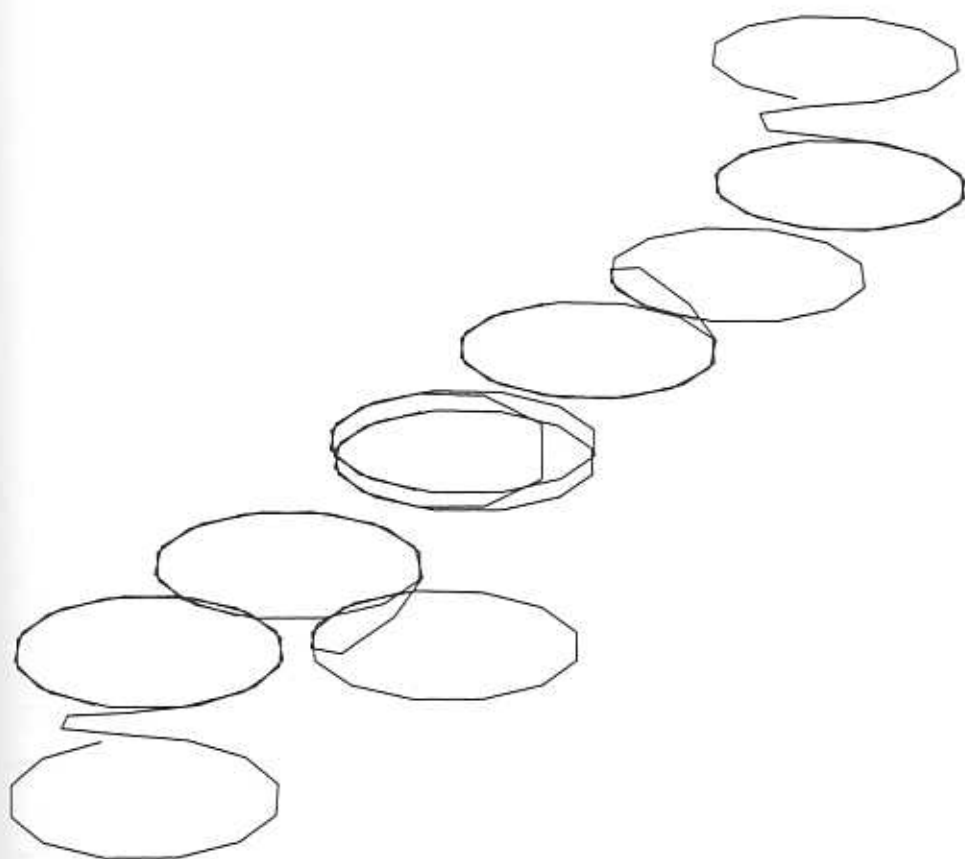


Figure 3.5: A stroboscopic plot of the evolving space curve $\mathbf{r}_2(s, u)$ Eq. (3.81), for $\nu = 0.3$ and $\lambda = 0.1$. As described in Section (3.6), the curve tends to a circle of radius $1/\lambda$ on either side. (The circles formed by the two arms lie in two different planes parallel to each other. The distance between the planes remains constant. The two circles are above each other (on different planes) at initial time $u = 0$ (centre). As time progresses, they move apart as well as rotate, still lying on their respective planes (right extreme). As earlier, the plots are shown separated for clarity.)

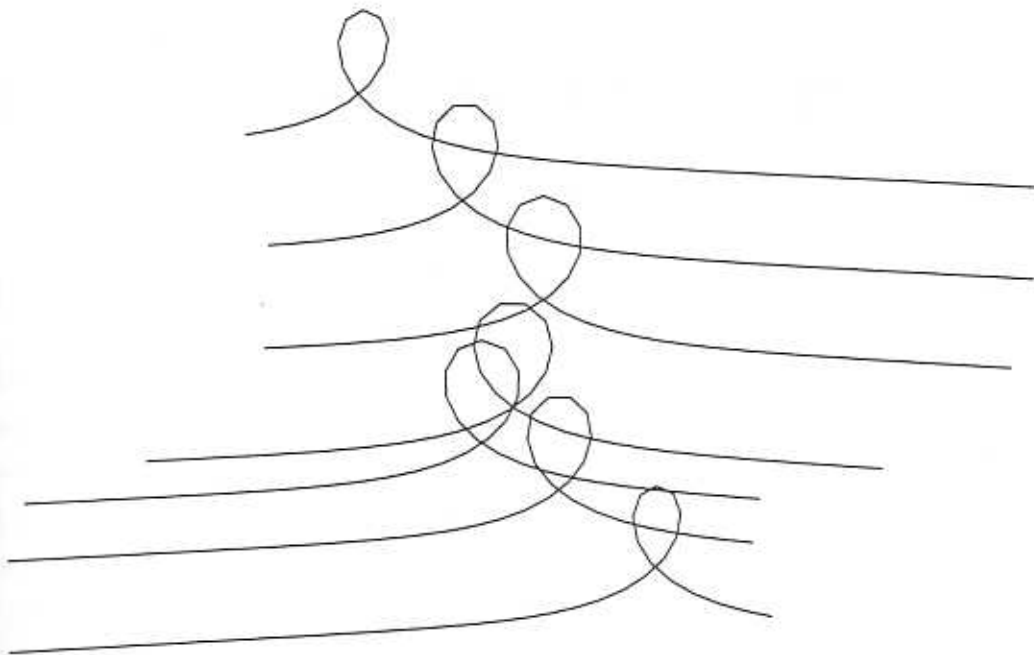


Figure 3.6: A stroboscopic plot of the evolving space curve $\mathbf{r}_3(s, u)$ Eq. (3.84), for $\nu = 1$ and $\lambda = 0.3$. As opposed to Fig. (3.4), here there is also an oscillation of the loop about its axis. Besides, the loop unwinds in the intermediate period, which are not shown however, since our interest here is only in noting the property of shape preservation. Here again, the plots are shown separated for clarity.

Chapter 4

Application to the Lamb equation

4.1 Introduction

In the last chapter, we had illustrated the three formulations developed in Chapter 2, using the NLS equation as an example, and explicitly constructed three moving curves and their swept out surfaces corresponding to its one soliton solution. The NLS is an example of an integrable NLPDE, that arose in the three formulations, by choosing the curve evolution parameters $\gamma_i, i = 1, 2, 3$, defined in Eqs. (2.15), (2.37) and (2.51), as in Eq. (3.2). As was pointed out below Eq. (2.27), for certain other specific choices of γ_i 's, in terms of ψ, Φ and χ respectively, it is possible to obtain not only integrable NLPDE, but also *integrable integro-differential equations*.

In this chapter, we consider one such example of the latter, namely the Lamb equation,

$$iq_u + q_s + q \int^s |q|^2 ds' = 0. \quad (4.1)$$

As mentioned in Chapter 1, this equation first appeared in [32] in connection to moving curves. We shall use the three formulations developed in Chapter 2, to associate three moving curves with a given solution of this equation. We parenthetically remark that by defining $\int^s |q|^2 ds' = \bar{Q}$, Eq. (4.1) takes the form of the following coupled NLPDE:

$$iq_u + q_s + \bar{Q}q = 0, \quad (4.2a)$$

$$\bar{Q}_s - |q|^2 = 0. \quad (4.2b)$$

Interestingly Eq. (4.1), is known to be related to the elliptic Liouville equation

[43]

$$f_{uu} + f_{ss} = -e^{2f}, \quad (4.3)$$

where $f(s, u)$ will be shown to be a real function of the curvature κ . Though this relation of a complex function $q(s, u)$ (and hence for *two* real functions) to a *single* real function $f(s, u)$ is surprising on first inspection, this indeed happens since f determines both $|q|$ and $\arg(q)$. Indeed, writing $q = \rho \exp[i\alpha]$, it can be shown that

$$\rho = |q| = \exp f; \quad \alpha = \arg(q) = - \int^s f_u ds'. \quad (4.4)$$

Thus given any exact solution f , the corresponding exact solution q can be written using Eq. (4.4) as

$$q = \exp[f - i \int^s f_u ds']. \quad (4.5)$$

The elliptic Liouville equation, (4.3), is of interest due to two reasons:

1) Although nonlinear, its *general* solution can be written in the form [60],

$$f(s, u) = \frac{1}{2} \ln \left(- \frac{A'(z^*)B'(z)}{[A(z^*) + B(z)]^2} \right), \quad (4.6)$$

where $z = s + iu$, $A'(z^*) = dA/dz^*$ and $B'(z) = dB/dz$, while A and B are arbitrary functions.

2) The equation holds importance in classical surface theory [24], and has been recognized by geometers for well over a century. Suppose $\mathbf{R}(s, u)$ is the position vector describing a surface in 3-D and let $\mathbf{X} \equiv (\mathbf{R}_s \times \mathbf{R}_u)/|\mathbf{R}_s \times \mathbf{R}_u|$ be the unit normal to the surface. Then the first and second fundamental forms are given by

$$d\mathbf{R}^2 = E ds^2 + 2F dsdu + Gdu^2, \quad (4.7)$$

$$-d\mathbf{R} \cdot d\mathbf{X} = Lds^2 + 2Mdsdu + Ndu^2. \quad (4.8)$$

The Gaussian curvature of such a surface is

$$K = (LN - M^2)/(EG - F^2). \quad (4.9)$$

For the specific choice $E = G$, and $F = 0$, as is well known, K is given by

$$K = -\frac{1}{2E} \left[\left(\frac{E_u}{E} \right)_u + \left(\frac{E_s}{E} \right)_s \right], \quad (4.10)$$

upon using the Gauss-Codazzi-Mainardi compatibility conditions, $\mathbf{R}_{ssu} = \mathbf{R}_{sus}$ and $\mathbf{R}_{suu} = \mathbf{R}_{uus}$. When K is a constant, defining $\tilde{E} = E/K$, Eq. (4.10) becomes

$$1 = -\frac{1}{2\tilde{E}} \left[\left(\frac{\tilde{E}_u}{\tilde{E}} \right)_u + \left(\frac{\tilde{E}_s}{\tilde{E}} \right)_s \right] \quad (4.11)$$

$$= -\frac{1}{2\tilde{E}}[(\log \tilde{E})_{uu} + (\log \tilde{E})_{ss}]. \quad (4.12)$$

Thus for constant K , it is seen that the elliptic Liouville equation, (4.3), is satisfied by $f = \frac{1}{2} \log \tilde{E}$. Hence, solutions of the elliptic Liouville equation, all correspond to surfaces of constant Gaussian curvature.

As demonstrated in the last chapter, the connection between the NLS and the LL equation proved very useful in obtaining the position vectors for the three moving curves associated with the NLS. In this chapter, a similar relationship of Eq. (4.1) to the Belavin-Polyakov (BP) equation

$$\mathbf{m}_u = \mathbf{m} \times \mathbf{m}_s ; \quad \mathbf{m}^2 = 1, \quad (4.13)$$

will be exploited in obtaining the explicit expressions for the position vectors for the three moving curves associated with the Lamb equation (4.1). The corresponding surfaces will be displayed pictorially, for some interesting solutions. All the figures pertaining to this chapter are given at the end of this chapter.

In the next section, we discuss the mapping of Eq. (4.1) to Eqs. (4.3) and (4.13), and show how they arise in the three formulations. We also find the corresponding time evolution parameters (see Eq. (2.5) g_i, h_i and τ_{oi} , ($i = 1, 2, 3$) for the three moving curves associated with Eq. (4.1).

4.2 Mapping of Lamb equation to the Belavin-Polyakov equation and the elliptic Liouville equation

To establish the equivalence of the Lamb equation (4.1) to the BP equation (4.13), we return to sections (2.3) and (2.4) of Chapter 2. It can be easily verified that with the choices

$$\gamma_1 = -i\psi ; \quad \gamma_2 = -i\Phi ; \quad \gamma_3 = -i\chi, \quad (4.14)$$

substituted into Eqs. (2.22), (2.41) and (2.55) immediately lead to Eq. (4.1), with ψ, Φ and χ replacing q . (Recall that ψ, Φ and χ are defined in Eqs. (2.1), (2.32) and (2.46), respectively).

Next, we list out the time evolution parameters g_i, h_i and τ_{oi} , in terms of κ_i and τ_i , $i = 1, 2, 3$, in the three cases.

(I) With the choice $\gamma_1 = -i\psi$ in Eq. (2.22), we have the Lamb equation:

$$i\psi_u + \psi_s + \psi \int^s |\psi|^2 ds' = 0. \quad (4.15)$$

Setting $\gamma_1 = i\psi$ in Eq. (2.15), we get

$$g_1 = 0; \quad h_1 = \kappa_1 \quad (4.16)$$

(subscript 1 has been used to indicate formulation (I)). Using these in the third compatibility condition Eq. (2.8), we find

$$\tau_{o1} = \kappa_{1s}/\kappa_1. \quad (4.17)$$

However, the same relation for the time evolution parameters g_1, h_1 , and τ_{o1} in terms of κ_1 and τ_1 , as in Eqs. (4.16) and (4.17), is obtained when \mathbf{t}_1 satisfies the BP equation (4.13). This is seen as follows:

$$\mathbf{t}_{1u} = \mathbf{t}_1 \times \mathbf{t}_{1s} \quad (4.18)$$

implies, from Eqs. (2.2) and (2.5),

$$g_1 \mathbf{n}_1 + h_1 \mathbf{b}_1 = \kappa_1 \mathbf{b}_1. \quad (4.19)$$

This directly gives Eq. (4.16), while τ_{o1} in Eq. (4.17) is obtained from Eq. (2.8). Hence Eq. (4.15) is seen to be associated with a moving curve *whose tangent \mathbf{t} satisfies the BP equation (4.13)*.

Next we show how the elliptic Liouville equation appears: Writing the real and imaginary parts of Eq. (4.15) separately, using the definition of ψ given in Eq. (2.1) (i.e., $\psi = \kappa_1 \exp(i \int^s \tau_1 ds')$ for formulation (I)), we have

$$\kappa_{1u} + \kappa_1 \tau_1 = 0 \quad (4.20)$$

and

$$-\kappa_1 \int^s \tau_{1u} ds' + \kappa_{1s} + \kappa_1 \int^s \kappa_1^2 ds' = 0. \quad (4.21)$$

Dividing Eq. (4.21) by κ_1 and differentiating with respect to s , we have

$$-\tau_{1u} + \left(\frac{\kappa_{1s}}{\kappa_1} \right)_s + \kappa_1^2 = 0. \quad (4.22)$$

On the other hand from Eq. (4.20), we have

$$\tau_1 = -(\kappa_{1u}/\kappa_1). \quad (4.23)$$

Using Eq. (4.23) in Eq. (4.22), we get

$$\left(\frac{\kappa_{1u}}{\kappa_1}\right)_u + \left(\frac{\kappa_{1s}}{\kappa_1}\right)_s + \kappa_1^2 = 0. \quad (4.24)$$

Defining

$$f_1(s, u) \equiv \log \kappa_1, \quad (4.25)$$

Eq. (4.24) yields the following elliptic Liouville equation for $f_1(s, u)$,

$$f_{1uu} + f_{1ss} = -e^{2f_1} \quad (4.26)$$

This establishes the connection between the Lamb equation Eq. (4.15) and the elliptic Liouville equation (4.26). Note that from Eq. (4.25)

$$\kappa_1 = \exp f_1. \quad (4.27)$$

But $\kappa_1 = |\psi|$. Hence $|\psi| = \exp f_1$. From Eq. (4.20),

$$\tau_1 = -(\log \kappa_1)_u = -f_{1u}. \quad (4.28)$$

Hence $\arg \psi = \int^s \tau_1 ds' = -\int^s f_{1u} ds'$. It must be noted that the function $f_1(s, u)$ in Eq. (4.25) is real and is a function of κ_1 only.

The equivalence of the Lamb equation to the BP equations satisfied by the binormal vector, \mathbf{b}_2 and the normal vector, \mathbf{n}_3 , in the other two formulations, (II) and (III), is established as given below:

(II) The choice $\gamma_2 = -i\Phi$, in Eq. (2.41), gives the Lamb equation:

$$i\Phi_u + \Phi_s + \Phi \int^s |\Phi|^2 ds' = 0. \quad (4.29)$$

Using the definition of γ_2 in Eq. (2.37) and writing Φ in Eq. (2.32), as $\Phi = \tau_2 \exp[i \int^s \kappa_2 ds']$ (where the subscript 2 stands for formulation (II)) the choice $\gamma_2 = -i\Phi$ implies

$$\tau_{o2} = 0; \quad h_2 = -\tau_2. \quad (4.30)$$

Substituting Eq. (4.30) in Eq. (2.8), we get

$$g_2 = \tau_{2s}/\tau_2. \quad (4.31)$$

We now show that the same relations (Eqs. (4.30) and (4.31)) are obtained when the BP equation is satisfied by the binormal vector \mathbf{b}_2 . This is because

$$\mathbf{b}_{2u} = \mathbf{b}_2 \times \mathbf{b}_{2s} \quad (4.32)$$

implies, from Eqs. (2.2) and (2.5),

$$-h_2 \mathbf{t}_2 - \tau_{o2} \mathbf{n}_2 = \tau_2 \mathbf{t}_2. \quad (4.33)$$

Eq. (4.30) is directly read off from Eq. (4.33), while Eq. (4.31) follows from Eq. (2.8), thus giving the equivalence of Eq. (4.29) and (4.32).

Writing Eq. (4.29) in terms of its real and imaginary parts, using the definition of Φ in Eq. (2.32), we obtain

$$\tau_{2u} + \kappa_2 \tau_2 = 0, \quad (4.34)$$

$$-\tau_2 \int^s \kappa_{2u} ds' + \tau_{2s} + \tau_2 \int^s \tau_2^2 ds' = 0. \quad (4.35)$$

A similar procedure as in (I), leads to the elliptic Liouville equation satisfied by $f_2(s, u)$ defined as

$$f_2(s, u) \equiv \log \tau_2, \quad (4.36)$$

$$f_{2uu} + f_{2ss} = -e^{2f_2}. \quad (4.37)$$

From Eq. (4.36)

$$\tau_2 = \exp f_2 \quad (4.38)$$

$$\kappa_2 = -(\log \tau_2)_u = -f_{2u}. \quad (4.39)$$

(III) Here, choosing $\gamma_3 = -i\chi$ in Eq. (2.55) leads to the Lamb equation:

$$i\chi_u + \chi_s + \chi \int^s |\chi|^2 ds' = 0. \quad (4.40)$$

With this choice, from the definitions of γ_3 and χ , Eqs. (2.37) and (2.46) respectively and writing $\chi = \kappa_3 + i\tau_3$, with the subscript 3 indicating formulation (III), we get

$$g_3 = -\tau_3; \quad \tau_{o3} = \kappa_3. \quad (4.41)$$

Substitution of Eq. (4.41) in Eq. (2.8) yields,

$$h_3 = \int^s (\kappa_3^2 + \tau_3^2) ds'. \quad (4.42)$$

Next, we show that these relations are equivalent to the BP equation *satisfied by the normal vector* \mathbf{n}_3 : It is seen that on using Eqs. (2.2) and (2.5), the equation

$$\mathbf{n}_{3u} = \mathbf{n}_3 \times \mathbf{n}_{3s} \quad (4.43)$$

gives

$$-g_3 \mathbf{t}_3 + \tau_{o3} \mathbf{b}_3 = \kappa_3 \mathbf{b}_3 + \tau_3 \mathbf{t}_3. \quad (4.44)$$

This is just Eq. (4.41), while Eq. (4.42) follows on using Eq. (2.8). Using $\chi_3 = \kappa_3 + i\tau_3$ and writing the real and imaginary parts of Eq. (4.40) separately, we get the coupled equations

$$\kappa_{3u} + \tau_{3s} + \tau_3 \int^s (\kappa_3^2 + \tau_3^2) ds' = 0, \quad (4.45)$$

$$-\tau_{3u} + \kappa_{3s} + \kappa_3 \int^s (\kappa_3^2 + \tau_3^2) ds' = 0. \quad (4.46)$$

From these two equations we can show that

$$\frac{\kappa_3 \kappa_{3u} + \tau_3 \tau_{3u}}{\kappa_3^2 + \tau_3^2} = -\frac{\partial}{\partial s} \tan^{-1}\left(\frac{\tau_3}{\kappa_3}\right) \quad (4.47)$$

and

$$\frac{\kappa_3 \kappa_{3s} + \tau_3 \tau_{3s}}{\kappa_3^2 + \tau_3^2} = \frac{\partial}{\partial u} \tan^{-1}\left(\frac{\tau_3}{\kappa_3}\right) - \int^s (\kappa_3^2 + \tau_3^2) ds'. \quad (4.48)$$

Thus, taking u -derivative of Eq. (4.47) and s -derivative of Eq. (4.48) and adding, we get

$$\left(\frac{\kappa_3 \kappa_{3u} + \tau_3 \tau_{3u}}{\kappa_3^2 + \tau_3^2}\right)_u + \left(\frac{\kappa_3 \kappa_{3s} + \tau_3 \tau_{3s}}{\kappa_3^2 + \tau_3^2}\right)_s = -(\kappa_3^2 + \tau_3^2). \quad (4.49)$$

In the above $(\tan^{-1}(\frac{\tau_3}{\kappa_3}))_{su} = (\tan^{-1}(\frac{\tau_3}{\kappa_3}))_{us}$ has been used. Defining

$$f_3(s, u) \equiv \frac{1}{2} \log(\kappa_3^2 + \tau_3^2) \quad (4.50)$$

we find that Eq. (4.49) becomes the elliptic Liouville equation for f_3 :

$$f_{3uu} + f_{3ss} = -e^{2f_3}. \quad (4.51)$$

Thus the Lamb equation Eq. (4.1), with $q = \psi$, Φ and χ respectively, can be mapped to the BP equation (4.13) satisfied by \mathbf{t}_1 , \mathbf{b}_2 and \mathbf{n}_3 respectively, as well as the elliptic Liouville equation for f_i , $i = 1, 2, 3$ (Eqs. (4.26), (4.37) and (4.51)).

Note that any real solution f presented in Eq. (4.6), will yield the general solution of the Lamb equation (4.1) on using Eq. (4.5). Thus, by setting $q = \psi, \Phi$ and χ given in Eqs. (2.1), (2.32) and (2.46) respectively, we obtain the curve parameters for the three curves to be

- (I) $\kappa_1 = e^f$; $\tau_1 = -f_u$,
- (II) $\kappa_2 = -f_u$; $\tau_2 = e^f$,
- (III) $\kappa_3 = e^f \cos \int^s f_u ds'$; $\tau_3 = -e^f \sin \int^s f_u ds'$.

The corresponding time evolution parameters g_i, h_i, τ_{oi} , $i = 1, 2, 3$, can be found in terms of f from Eqs. (4.16), (4.17); (4.30), (4.31); and (4.41), (4.42). We obtain

- (I) $g_1 = 0$; $h_1 = e^f$; $\tau_{o1} = f_s$,

$$(II) \quad g_2 = f_s; \quad h_2 = -e^f; \quad \tau_{02} = 0,$$

$$(III) \quad g_3 = e^f \sin \int^s f_u ds'; \quad h_3 = \int^s e^{2f} ds'; \quad \tau_{03} = e^f \cos \int^s f_u ds',$$

Thus we clearly see that the three moving space curves of the Lamb equation are indeed distinct.

In the next section we shall discuss some physical contexts in which the BP equation (4.13) arises.

4.3 Appearance of the BP equation in Low dimensional Heisenberg ferromagnets and anti-ferromagnets

Here we list three different contexts in which the BP equation (4.13) arises in the study of low-dimensional systems. The first two are spin systems and the third is a field theoretic model.

Two-dimensional ferromagnets

The dynamics of the isotropic Heisenberg ferromagnet in two dimensions is governed by the Hamiltonian

$$H = -J \sum_{\langle i,j \rangle} \mathbf{S}_i \cdot \mathbf{S}_j, \quad J > 0; \quad \mathbf{S}_i^2 = S^2, \quad (4.52)$$

\mathbf{S}_i being the spin vector at site i and $\langle i, j \rangle$ denoting nearest neighbors. The time evolution of these spin vectors is found by using essentially the same procedure as outlined for the 1D case in Section (3.3) (see discussion below Eq. (3.30)) to be,

$$\mathbf{S}_{iu} = J \mathbf{S}_i \times (\mathbf{S}_{i+l} + \mathbf{S}_{i-l}), \quad (4.53)$$

where now, the index l runs over the nearest neighbors. Taking the continuum limit of Eq. (4.53) as employed in Section (3.3), we get the equation for the Heisenberg ferromagnet in two dimensions in the continuum limit as

$$\mathbf{S}_u = \mathbf{S} \times (\mathbf{S}_{xx} + \mathbf{S}_{yy}); \quad \mathbf{S}^2 = 1. \quad (4.54)$$

(Note that in Eq. (4.54), the magnitude of the spin vector has been normalized to unity without loss of generality). The *static* configurations of the two dimensional

ferromagnet are thus given by

$$\mathbf{S} \times (\mathbf{S}_{xx} + \mathbf{S}_{yy}) = 0 ; \quad \mathbf{S}^2 = 1. \quad (4.55)$$

It is seen that, solutions of the first order equation

$$\mathbf{S}_x = \mathbf{S} \times \mathbf{S}_y, \quad (4.56)$$

are particular solutions for the static configuration as given by the second order equation (4.55), while the converse is not true [44]. This can be verified as follows: Firstly, Eq. (4.56) implies

$$\mathbf{S}_y = \mathbf{S}_x \times \mathbf{S}, \quad (4.57)$$

since \mathbf{S} is a unit vector. From Eqs. (4.56) and (4.57), we find

$$\mathbf{S}_{yy} + \mathbf{S}_{xx} = 2\mathbf{S}_x \times \mathbf{S}_y. \quad (4.58)$$

Taking vector product with \mathbf{S} , we get Eq. (4.55)

$$\mathbf{S} \times (\mathbf{S}_{yy} + \mathbf{S}_{xx}) = 2\mathbf{S} \times (\mathbf{S}_x \times \mathbf{S}_y) = 0, \quad (4.59)$$

since, $\mathbf{S} \cdot \mathbf{S}_x = \mathbf{S} \cdot \mathbf{S}_y = 0$.

Now, Eq. (4.56) resembles the BP equation Eq. (4.13), except that both parameters x and y are now spatial in nature. Thus the solutions of the BP equation directly yield a *subclass* of static configurations for the two dimensional Heisenberg ferromagnet.

One-dimensional antiferromagnets

The Hamiltonian for the one dimensional Heisenberg antiferromagnet is given by

$$H = -J \sum_i \mathbf{S}_i \cdot \mathbf{S}_{i+1}, \quad J < 0 ; \quad \mathbf{S}_i^2 = S^2. \quad (4.60)$$

Here adjacent spins tend to remain antiparallel for low energies, as seen from the Hamiltonian. Consequently, alternate spin vectors remain nearly parallel. Hence it becomes more convenient in this case, to describe the spin evolution by dividing the lattice into 'odd' and 'even' sublattices, depending on whether i is odd or even on the chain. For low energies, this allows us to go to the continuum limit, since the neighboring spins in a *sublattice* differ only by a small angle.

From the above Hamiltonian, the equation of motion for the spin vector \mathbf{S}_n , at site n , is found to be

$$\mathbf{S}_{nu} = J\mathbf{S}_n \times (\mathbf{S}_{n+1} + \mathbf{S}_{n-1}), \quad (4.61)$$

where, as earlier, the subscript u represents differentiation with respect to time. The spins interact only with their nearest neighbors. The dynamical equation can be written separately for spins at odd and even 'sublattices' as

$$\mathbf{S}_{nu}^o = J\mathbf{S}_n^o \times (\mathbf{S}_{n+1}^e + \mathbf{S}_{n-1}^e) \quad (4.62)$$

and

$$\mathbf{S}_{n-1u}^e = J\mathbf{S}_{n-1}^e \times (\mathbf{S}_n^o + \mathbf{S}_{n-2}^o), \quad (4.63)$$

where extra superscripts o and e have been added to indicate spins at the odd and even sublattices. As noted earlier, the nearest-neighbor spin vectors within the same sublattice differ only by a small angle, allowing us to go to the continuum limit in each sublattice. Thus we write [45],

$$\mathbf{S}_{n+1}^e + \mathbf{S}_{n-1}^e \rightarrow 2\mathbf{S}^e(x-a) + 2a\frac{\partial}{\partial x}\mathbf{S}^e, \quad (4.64)$$

$$\mathbf{S}_n^o + \mathbf{S}_{n-2}^o \rightarrow 2\mathbf{S}^o(x) - 2a\frac{\partial}{\partial x}\mathbf{S}^o. \quad (4.65)$$

Here, a is the lattice spacing between two adjacent spins and x , as is clear, is the (continuous) spatial parameter. Using Eqs. (4.64) and (4.65) in Eqs. (4.62) and (4.63) respectively, the evolution equations for spin vectors in the odd and even sublattice, become

$$\mathbf{S}_u^o(x) = 2J\mathbf{S}^o(x) \times \left(\mathbf{S}^e(x-a) + a\frac{\partial}{\partial x}\mathbf{S}^e(x-a) \right) \quad (4.66)$$

and

$$\mathbf{S}_u^e(x-a) = 2J\mathbf{S}^e(x-a) \times \left(\mathbf{S}^o(x) - a\frac{\partial}{\partial x}\mathbf{S}^o(x) \right). \quad (4.67)$$

Define two new unit vectors \mathbf{l} and \mathbf{m} as

$$\mathbf{l}(x) \equiv (\mathbf{S}^o(x) + \mathbf{S}^e(x-a))/(2S\epsilon), \quad (4.68)$$

$$\mathbf{m}(x) \equiv (\mathbf{S}^o(x) - \mathbf{S}^e(x-a))/2S\sqrt{1-\epsilon^2}. \quad (4.69)$$

Here, S is the magnitude of the spin vector and $\epsilon^2 = \frac{1}{2}(1 + \mathbf{S}^o \cdot \mathbf{S}^e/S^2)$. The dynamics of the spin vector in the continuum limit can equally well be described in terms of these two vectors. Combining the continuum equations, Eqs. (4.66), and (4.67) appropriately, the equations of motion for the two new vectors \mathbf{m} and \mathbf{l} are given by [45, 47],

$$\mathbf{l}_u = 2JaS\sqrt{1-\epsilon^2}\frac{\partial}{\partial x}(\mathbf{m} \times \mathbf{l}), \quad (4.70)$$

$$\begin{aligned} \mathbf{m}_u = & 4JS\epsilon(\mathbf{m} \times \mathbf{l}) + 2JaS \frac{\epsilon^2}{\sqrt{1-\epsilon^2}} \left(\mathbf{l} \times \frac{\partial}{\partial x} \mathbf{l} \right) \\ & - 2JaS \sqrt{1-\epsilon^2} \left(\mathbf{m} \times \frac{\partial}{\partial x} \mathbf{m} \right). \end{aligned} \quad (4.71)$$

The advantage in using the new vectors is seen by noting that for low energies, since adjacent spins remain almost antiparallel, $|\mathbf{l}| \simeq 0$ and $\epsilon \ll 1$. Therefore the dynamics is entirely dominated by \mathbf{m} , and Eq. (4.71) yields,

$$\mathbf{m}_u = -2JaS \left(\mathbf{m} \times \frac{\partial}{\partial x} \mathbf{m} \right). \quad (4.72)$$

On absorbing an appropriate normalization constant into time and space variables, this equation is seen to be of the form of the BP equation (4.13).

The $O(3)$ nonlinear σ model

The BP equation (4.13), first arose in the study of the static (2+1)-dimensional $O(3)$ nonlinear sigma model field theory [11, 12]. The following results are well known in field theory. We briefly summarize some of the results for the sake of completeness. The energy associated with the unit vector field $\mathbf{m}(x, y)$ is given by

$$H = \frac{1}{2} \int \int (\mathbf{m}_x^2 + \mathbf{m}_y^2) dx dy; \quad \mathbf{m}^2 = 1 \quad (4.73)$$

and the local energy minima found using $\delta H = 0$ are configurations that can be shown to satisfy the static field equation:

$$\mathbf{m}_{xx} + \mathbf{m}_{yy} - [\mathbf{m} \cdot (\mathbf{m}_{xx} + \mathbf{m}_{yy})] \mathbf{m} = 0. \quad (4.74)$$

This equation can be seen to be equivalent to Eq. (4.55), with \mathbf{S} replaced by \mathbf{m} ; showing the relation to the 2D ferromagnet. This is because Eq. (4.74) implies

$$\mathbf{m} \times (\mathbf{m}_{xx} + \mathbf{m}_{yy}) = 0, \quad (4.75)$$

$$\mathbf{m}_{xx} + \mathbf{m}_{yy} = c\mathbf{m}, \quad (4.76)$$

where c is a scalar. Using the constraint $\mathbf{m}^2 = 1$, to replace c in Eq. (4.76), we obtain Eq. (4.74). Thus, here again the BP equation for \mathbf{m} arises, whose solutions form a subclass of the solutions of equation (4.74).

Consider the identity [44]

$$\int \int (\partial_i \mathbf{m} \pm \varepsilon_{ij} \mathbf{m} \times \partial_j \mathbf{m}) \cdot (\partial_i \mathbf{m} \pm \varepsilon_{ik} \mathbf{m} \times \partial_k \mathbf{m}) dx dy \geq 0, \quad (4.77)$$

with i, j, k , running over x, y and summation over repeated indices assumed. This is an identity since, the integrand is just the scalar product of a vector with itself. Expanding the integrand and using the constraint $\mathbf{m}^2 = 1$, it can be shown that

$$\int \int (\partial_i \mathbf{m} \cdot \partial_i \mathbf{m}) \, dx dy \geq \int \int \varepsilon_{ij} \mathbf{m} \cdot (\partial_i \mathbf{m} \times \partial_j \mathbf{m}) \, dx dy. \quad (4.78)$$

By comparing Eq. (4.78) and Eq. (4.77), it can be seen that the equality in Eq. (4.78) is satisfied when \mathbf{m} satisfies the BP equation (4.13). Now, for field configurations with boundary conditions such that \mathbf{m} takes on the *same* value at the boundary, it can be shown that the quantity on the right hand side of Eq. (4.78) is

$$\frac{1}{8\pi} \int \int \varepsilon_{ij} \mathbf{m} \cdot (\partial_i \mathbf{m} \times \partial_j \mathbf{m}) \, dx dy = 8\pi Q, \quad (4.79)$$

where Q is an integer, the topological charge [11]. Q labels a topological sector. Since \mathbf{m} lives on a unit sphere $S_2^{(m)}$, and for the special boundary conditions, the coordinate space (x, y) can be compactified into a sphere S_2 , Q gives the number of times $S_2^{(m)}$ is covered, as we span the coordinate space. Thus, using Eq. (4.79) in Eq. (4.78) and recognizing that the left hand side of Eq. (4.78) is just H given in Eq. (4.73), we get

$$H \geq 4\pi Q; \quad Q = \text{integer}. \quad (4.80)$$

Eq. (4.80) is the Bogomol'nyi inequality [61]. We see that for the *special boundary conditions*, the configurations that satisfy BP equation correspond to the lower bound $4\pi Q$ of the energy.

In the next section we consider two types of solutions namely the instanton and twist solutions of the BP equation (The former has integer charge but not the latter, due to the boundary conditions). In particular we concentrate on the solutions q of the Lamb equation corresponding to the one-instanton and twist solutions and determine the three moving curves obtained in the three formulations, with each of these solutions.

4.4 Construction of the three moving curves for the Lamb equation

In this section we shall discuss the construction of the three moving curves associated with a general solution q of the Lamb equation.

In Section (4.2) we showed how the Lamb equation could be mapped to the BP equation. Note that we *also* have the *converse* of this result. That is, starting with the BP equation (4.13), we can obtain the Lamb equation as follows: Using the FS equations, we have

$$\mathbf{t}_{1u} = \mathbf{t}_1 \times \mathbf{t}_{1s} = \mathbf{t}_1 \times \kappa_1 \mathbf{n} = \kappa_1 \mathbf{b}_1. \quad (4.81)$$

Since $\mathbf{t}_{1u} = g_1 \mathbf{n}_1 + h_1 \mathbf{b}$ (from Eq. (2.5)), we read off from Eq. (4.81), $g_1 = 0$, $h_1 = \kappa_1$. From the compatibility condition Eq. (2.8), $\tau_{o1} = \kappa_{1s}/\kappa_1$. Thus, from Eq. (2.37)

$$\gamma_1 = -(g_1 + ih_1) \exp \left[i \int^s \tau_1 ds' \right] = -i\kappa_1 \exp \left[i \int^s \tau_1 ds' \right] = -i\psi. \quad (4.82)$$

Substituting Eq. (4.82) in Eq. (2.21), we get

$$R_1 = \int^s |\psi|^2 ds'. \quad (4.83)$$

Thus using Eq. (4.83) in Eq. (2.22), we see that the BP equation for the tangent \mathbf{t}_1 leads to the Lamb equation for the Hasimoto function ψ .

$$i\psi_u + \psi_s + \frac{1}{2} \int^s |\psi|^2 \psi ds' = 0. \quad (4.84)$$

The equation for the curve is obtained by integrating $\mathbf{t}_1 = \mathbf{m}$.

$$\mathbf{r}_1(s, u) = \int^s \mathbf{t}_1 ds' = \int^s \mathbf{m} ds'. \quad (4.85)$$

Likewise, in the other two formulations, starting with the BP equation for \mathbf{b}_2 and \mathbf{n}_3 respectively, the time evolution parameters are seen to be

$$g_2 = \tau_{2s}/\tau_2 ; \quad \tau_{o2} = 0 ; \quad h_2 = -\tau_2 \quad (4.86)$$

and

$$g_3 = -\tau_3 ; \quad \tau_{o3} = \kappa_3 ; \quad h_3 = \int^s (\kappa_3^2 + \tau_3^2), \quad (4.87)$$

respectively. These lead to $g_1 = -i\Phi$ and $\gamma_3 = -i\chi$, which when substituted into Eqs. (2.40) and (2.54) respectively, yield $R_2 = \int^s |\Phi|^2 ds'$ and $R_3 = \int^s |\chi|^2 ds'$. Substituting these in Eqs. (2.39) and (2.53) respectively, the Lamb equation (4.1) for Φ and χ are obtained.

Proceeding like one did for the NLS in Section (3.3), we have the analogs of Eq. (3.39) and (3.50), i.e.,

$$\mathbf{r}_2(s, u) = \int^s \mathbf{t}_2 ds' = \int^s \mathbf{m} \times \frac{\mathbf{m}_s}{|\mathbf{m}_s|} ds', \quad (4.88)$$

and

$$\mathbf{r}_3(s, u) = \int^s \mathbf{t}_3 ds = \int^s \frac{[(\mathbf{m} \times \mathbf{m}_s) \sin \alpha - \mathbf{m}_s \cos \alpha]}{\kappa_1} ds', \quad (4.89)$$

where $\alpha = \int^s \tau_1 ds' + C_2(u)$ and $C_2(u)$ an arbitrary function of time u . The function $C_2(u)$ will be determined in Appendix C. The results in this section are valid for any general solution \mathbf{m} , and hence for any general solution q of the Lamb equation. Below, we discuss the surfaces for the three different cases, by taking certain typical solutions for \mathbf{m} .

4.5 Instantons, Twists and associated geometries of the Lamb equation

On first inspection, a couple of observations can be made about the kind of solutions supported by the BP equation Eq. (4.13). Since \mathbf{m} is a unit vector, it follows from Eq. (4.13) that

$$\mathbf{m}_s = \mathbf{m}_u \times \mathbf{m}, \quad \mathbf{m}^2 = 1. \quad (4.90)$$

- (i) From Eqs. (4.13) and (4.90), it is easily seen that the above equation cannot support any nontrivial solution that is either purely static or purely time dependent.
- (ii) The solution cannot be a *pure* traveling wave, since assuming $\mathbf{m} = \mathbf{m}(\xi)$, $\xi = s - vu$, implies, from Eq. (4.13), $-v\mathbf{m}_\xi = \mathbf{m}_\xi \times \mathbf{m}$, which is inconsistent.

In this section, we shall first obtain the twist and one-instanton solutions of the BP equation. Parameterizing $\mathbf{m}(s, u)$ in spherical polar coordinates as

$$\mathbf{m}(s, u) = (\sin \theta \cos \phi, \sin \theta \sin \phi, \cos \theta), \quad (4.91)$$

Eq. (4.13) can be written as

$$\theta_u = -\phi_s \sin \theta, \quad (4.92)$$

$$\phi_u \sin \theta = -\theta_s. \quad (4.93)$$

(a) Twist solutions

From Eqs. (4.92) and (4.93), the compatibility condition $\theta_{su} = \theta_{us}$ gives,

$$\phi_{uu} + \phi_{ss} = 0. \quad (4.94)$$

This is the Laplace equation, for which the simplest nontrivial solution [45] is

$$\phi = (k_o s + \omega_o u), \quad (4.95)$$

where ω_o and k_o are arbitrary constants. Substituting this in Eqs. (4.92) and (4.93) gives

$$\theta_u = -k_o \sin \theta, \quad (4.96)$$

$$\theta_s = \omega_o \sin \theta. \quad (4.97)$$

Upon integration, this gives (on using $\int^s (d\theta/\sin \theta) = \log(\tan(\theta/2))$)

$$\cos \theta = -\tanh(\omega_o s - k_o u) \quad (4.98)$$

and

$$\sin \theta = \text{sech}(\omega_o s - k_o u). \quad (4.99)$$

Using Eqs. (4.98), (4.99) and (4.95), we get

$$\mathbf{m} = \text{sech}(\omega_o s - k_o u) \left(\cos(k_o s + \omega_o u) \hat{\mathbf{i}} + \sin(k_o s + \omega_o u) \hat{\mathbf{j}} \right) - \tanh(\omega_o s - k_o u) \hat{\mathbf{k}}. \quad (4.100)$$

This is the twist solution for the BP equation. From Eq. (4.100), it is clear that the $\hat{\mathbf{z}}$ component $m_z \rightarrow \mp 1$ as $s \rightarrow \pm\infty$. This is like a domain wall. In the interim region, the spin precesses. Since $\phi = (k_o s + \omega_o u)$, the precession velocity is $v_\phi = -\omega_o/k_o$ (see Eq. (4.95)). On the other hand, the domain wall moves with velocity $v_\theta = k_o/\omega_o = -1/v_\phi$ (see Eq. (4.98)). This behavior is clearly in agreement with (i) and (ii) stated in the beginning of this section. From its definition Eq. (4.69), $m_z = 1$ corresponds to $\hat{\mathbf{z}}$ component of spins in the 'odd' sublattice being up and spins in the 'even' sub lattice being down, at $s \rightarrow -\infty$. This situation is reversed for $m_z = -1$, at $s \rightarrow \infty$. The twist depicts a 'spin wave' within a domain wall.

Starting from the twist solution for the BP equation given in Eq. (4.100), we get

$$\begin{aligned} \mathbf{m}_s = \text{sech} \tilde{\eta} [& (-\omega_o \tanh \tilde{\eta} \cos \tilde{\xi} - k_o \sin \tilde{\xi}) \hat{\mathbf{i}} \\ & + (-\omega_o \tanh \tilde{\eta} \sin \tilde{\xi} + k_o \cos \tilde{\xi}) \hat{\mathbf{j}} - \omega_o \text{sech} \tilde{\eta} \hat{\mathbf{k}}] \end{aligned} \quad (4.101)$$

and

$$\begin{aligned} \mathbf{m} \times \mathbf{m}_s = \text{sech} \tilde{\eta} [& (k_o \tanh \tilde{\eta} \cos \tilde{\xi} - \omega_o \sin \tilde{\xi}) \hat{\mathbf{i}} \\ & + (k_o \tanh \tilde{\eta} \sin \tilde{\xi} + \omega_o \cos \tilde{\xi}) \hat{\mathbf{j}} + k_o \text{sech} \tilde{\eta} \hat{\mathbf{k}}], \end{aligned} \quad (4.102)$$

where

$$\tilde{\eta} = \omega_o s - k_o u ; \quad \tilde{\xi} = k_o s + \omega_o u. \quad (4.103)$$

Clearly, the corresponding solution for the Lamb equation (4.1) is

$$q = |\mathbf{m}_s| \exp[i \int^s \frac{\mathbf{m} \cdot (\mathbf{m}_s \times \mathbf{m}_{ss})}{|\mathbf{m}_s|^2} ds'], \quad (4.104)$$

yielding

$$q^{(S)} = \sqrt{(\omega_o^2 + k_o^2)} \operatorname{sech} \tilde{\eta} \exp[i \frac{k_o}{\omega_o} \log \operatorname{sech} \tilde{\eta}]. \quad (4.105)$$

The *envelope* of this solution is soliton-like. It is a localized function and is a traveling wave. We shall therefore refer to this solution given in Eq. (4.105), as an 'envelope-soliton' solution $q^{(S)}$ of the Lamb equation. We proceed to find the three moving curves corresponding to this solution, using the results of Section(4.4).

(I) Here $\mathbf{t}_1 = \mathbf{m}$, given in Eq. (4.100). Analogous to Eqs. (3.33) and (3.34), we find the curvature and torsion here as

$$\kappa_1^2 = \mathbf{m}_s^2 = (\omega_o^2 + k_o^2) \operatorname{sech}^2 \tilde{\eta}; \quad \tau_1 = \frac{\mathbf{m} \cdot \mathbf{m}_s \times \mathbf{m}_{ss}}{\kappa_1^2} = -k_o \tanh \tilde{\eta}. \quad (4.106)$$

The corresponding solution of the elliptic Liouville equation (4.26) is given by

$$f_1 = \log(\sqrt{(\omega_o^2 + k_o^2)} \operatorname{sech} \tilde{\eta}). \quad (4.107)$$

By substituting the twist solution Eq. (4.100) in Eq. (4.85), an exact closed form expression for the curve \mathbf{r}_1 can be found for two particular cases, $k_o = 0, \omega_o \neq 0$ and $k_o \neq 0, \omega_o = 0$. We discuss these cases before going to the more general case.

(i) Taking $k_o = 0$ in Eq. (4.106), we have

$$\kappa_1 = \omega_o \operatorname{sech}(k_o s); \quad \tau_1 = 0. \quad (4.108)$$

This is evidently a planar curve. The expression for the position vector of the curve \mathbf{r}_1 is found by substituting Eq. (4.100) in Eq. (4.85) to be

$$\begin{aligned} \mathbf{r}_1(s, u) = \int^s \mathbf{m}(k_o = 0) ds' &= \frac{1}{\omega_o} 2 \tan^{-1}(\exp(\omega_o s)) \left(\cos(\omega_o u) \hat{\mathbf{i}} + \sin(\omega_o u) \hat{\mathbf{j}} \right) \\ &\quad - \frac{1}{\omega_o} \log(\cosh(\omega_o s)) \hat{\mathbf{k}} \end{aligned} \quad (4.109)$$

A stroboscopic plot of the moving curve Eq. (4.109), as well as the swept-out surface are shown in Fig. (4.1). The curve is an inverted 'U' at any time and rotating about the z axis.

(ii) Taking $\omega_o = 0$ in Eq. (4.100), we get

$$\mathbf{r}_1(s, u) = \int^s \mathbf{m}(\omega_o = 0) ds' = \frac{1}{k_o} \operatorname{sech}(k_o u) \left(\sin(k_o s) \hat{\mathbf{i}} - \cos(k_o s) \hat{\mathbf{j}} \right) + \hat{\mathbf{k}} s \tanh(k_o u), \quad (4.110)$$

and from Eq. (4.106)

$$\kappa_1 = k_o \operatorname{sech}(k_o u) ; \quad \tau_1 = k_o \tanh(k_o u). \quad (4.111)$$

At $u = 0$, Eq. (4.110) is a circle in the $x - y$ plane. As time progresses, the two arms of the curve about the point $s = 0$, stretch out to become a straight line along the z axis, as $u \rightarrow \infty$. Fig. (4.2) shows a plot of the swept-out surface generated due to Eq. (4.110), along with a stroboscopic plot.

The swept out surface for a more general case, with parameter values $k_o = 0.5$ and $\omega_o = 1$ is shown in Fig. (4.3). This is found from

$$\mathbf{r}_1(s, u) = \int^s \mathbf{t}_1 ds' = \int^s \mathbf{m} ds', \quad (4.112)$$

where \mathbf{m} is given in Eq. (4.100).

(II) The BP equation is now obeyed by the unit binormal \mathbf{b}_2 , i.e., $\mathbf{b}_{2u} = \mathbf{b}_2 \times \mathbf{b}_{2s}$. Thus $\mathbf{b}_2 = \mathbf{m}$. The unit tangent vector in this case is given by

$$\mathbf{t}_2 = \frac{\mathbf{b}_2 \times \mathbf{b}_{2s}}{|\mathbf{b}_{2s}|} = \frac{\mathbf{m} \times \mathbf{m}_s}{|\mathbf{m}_s|}, \quad (4.113)$$

where \mathbf{m} is given in Eq. (4.100). Thus using Eqs. (4.102) and (4.106) in Eq. (4.113), we get

$$\mathbf{t}_2 = \frac{1}{\sqrt{\omega_o^2 + k_o^2}} \left\{ \omega_o (\cos \tilde{\xi} \hat{\mathbf{j}} - \sin \tilde{\xi} \hat{\mathbf{i}}) + k_o \tanh \tilde{\eta} (\cos \tilde{\xi} \hat{\mathbf{i}} + \sin \tilde{\xi} \hat{\mathbf{j}}) + \hat{\mathbf{k}} k_o \operatorname{sech} \tilde{\eta} \right\} \quad (4.114)$$

This yields

$$\mathbf{r}_2(s, u) = \int^s \mathbf{t}_2 ds'. \quad (4.115)$$

The curvature and torsion are given by

$$\kappa_2 = -k_o \tanh \tilde{\eta} ; \quad \tau_2 = \sqrt{(\omega_o^2 + k_o^2)} \operatorname{sech} \tilde{\eta}. \quad (4.116)$$

Here again, we consider first the special case $k_o = 0$. This implies a vanishing curvature, i.e., a straight line. This is a trivial case. For the other special case $\omega_o = 0$, Eq. (4.114) can be integrated exactly giving. We get

$$\mathbf{r}_2(s, u) = -\frac{1}{k_o} \tanh(k_o u) (\sin(k_o s) \hat{\mathbf{i}} + \cos(k_o s) \hat{\mathbf{j}}) + s \operatorname{sech}(k_o u) \hat{\mathbf{k}} \quad (4.117)$$

This is a helix rotating about its own axis generating a cylinder. For this case, the curvature and torsion are functions of time *only*, and are given by

$$\kappa_2 = k_o \tanh k_o u ; \quad \tau_2 = k_o \operatorname{sech} k_o u. \quad (4.118)$$



A plot of the surface generated for a more general case with $k_o = 0.5, \omega_o = 1$, is obtained by numerically integrating Eq. (4.114) using *Mathematica*. This is shown Fig. (4.4), which is indeed distinct from the surface in Fig. (4.3).

(III) Here $\mathbf{n}_{3u} = \mathbf{n}_3 \times \mathbf{n}_{3s}$. Thus $\mathbf{n}_3 = \mathbf{m}$. The corresponding tangent vector is given by (see Eq. (4.89) in Section (4.4))

$$\mathbf{t}_3 = \frac{\tau_3 \mathbf{n}_3 \times \mathbf{n}_{3s} - \kappa_3 \mathbf{n}_{3s}}{|\mathbf{n}_{3s}|^2} = \frac{\mathbf{m} \times \mathbf{m}_s \sin \alpha - \mathbf{m}_s \cos \alpha}{\kappa_1}. \quad (4.119)$$

where

$$\alpha = \int^s \tau_1 ds' + C_2(u) \quad (4.120)$$

and $C_2(u)$, an arbitrary function of time. Substituting for τ_1 from Eq. (4.106) and integrating we get

$$\alpha = -\frac{k_o}{\omega_o} \log \cosh \tilde{\eta} + C_2(u). \quad (4.121)$$

In Appendix C, we use the moving curve compatibility conditions to show that $C_2(u)$ is a constant which can be taken to be zero. The unit tangent vector is found by substitution of \mathbf{m} from Eq. (4.100) in Eq. (4.119), to yield

$$\mathbf{t}_3 = \frac{1}{\sqrt{\omega_o^2 + k_o^2}} \left[\left(\omega_o \cos \alpha + k_o \sin \alpha \right) \tanh \tilde{\eta} \hat{\mathbf{e}}_1 + \left(\omega_o \sin \alpha - k_o \cos \alpha \right) \hat{\mathbf{e}}_2 + \left(k_o \sin \alpha + \omega_o \cos \alpha \right) \text{sech} \tilde{\eta} \hat{\mathbf{k}} \right], \quad (4.122)$$

where, $\hat{\mathbf{e}}_1 = (\cos \tilde{\xi} \hat{\mathbf{i}} + \sin \tilde{\xi} \hat{\mathbf{j}})$ and $\hat{\mathbf{e}}_2 = (-\sin \tilde{\xi} \hat{\mathbf{i}} + \cos \tilde{\xi} \hat{\mathbf{j}})$. The curvature and torsion are given by

$$\kappa_3 = \sqrt{\omega_o^2 + k_o^2} \text{sech} \tilde{\eta} \cos \alpha; \quad \tau_3 = \sqrt{\omega_o^2 + k_o^2} \text{sech} \tilde{\eta} \sin \alpha. \quad (4.123)$$

For $k_o = 0$, Eq. (4.122), reduces to

$$\mathbf{t}_3 = \tanh(\omega_o s) (\cos(\omega_o u) \hat{\mathbf{i}} + \sin(\omega_o u) \hat{\mathbf{j}}) + \text{sech}(\omega_o s) \hat{\mathbf{k}}. \quad (4.124)$$

This can be exactly integrated to give the following moving curve:

$$\mathbf{r}_3(s, u) = \frac{1}{\omega_o} \left(\log(\cosh(\omega_o s)) (\cos(\omega_o u) \hat{\mathbf{i}} + \sin(\omega_o u) \hat{\mathbf{j}}) + 2 \tan^{-1}(\exp(\omega_o s)) \hat{\mathbf{k}} \right). \quad (4.125)$$

For $k_o = 0$, note that

$$\kappa_3 = \omega_o \text{sech} \omega_o s; \quad \tau_3 = 0. \quad (4.126)$$

This corresponds to a planar curve with curvature asymptotically vanishing as $s \rightarrow \pm\infty$. The surface for this special case (Eq. (4.125)) is shown in Fig. (4.5). Note that for the special case $\omega_o = 0, \alpha \rightarrow \infty$ and hence not considered unlike in (I) and (II). The surface for a more general case found by integrating Eq. (4.122) is depicted in Fig. (4.6).

(b) Instanton solutions

From the spherical polar decomposition for \mathbf{m} given in Eq. (4.91), consider the stereographic projection onto the complex plane defined through the complex function M by

$$M(s, u) = \cot \frac{1}{2} \theta(s, u) \exp i\phi(s, u) \quad (4.127)$$

$$= M_1 + iM_2. \quad (4.128)$$

Equations (4.92) and (4.93) (which arise from the BP equation), lead to the following Cauchy-Riemann conditions for the real and imaginary parts M_1 and M_2 of M .

$$\frac{\partial M_1}{\partial s} = \mp \frac{\partial M_2}{\partial u}; \quad \frac{\partial M_2}{\partial u} = \pm \frac{\partial M_1}{\partial s}. \quad (4.129)$$

On reparametrizing to complex coordinates $z = s + iu$ and $z^* = s - iu$, the above condition implies analyticity with respect to z or z^* , depending on the sign chosen. Thus the simplest solution for M (and hence the BP equation), is given by

$$M = \left(\frac{z - z_0}{\Lambda} \right)^n. \quad (4.130)$$

Here, n is an integer and Λ an arbitrary parameter, while z_0 is a arbitrary complex constant. For $n = 1$, from Eq. (4.127) and (4.129), we have the one-instanton solution given by,

$$\cot \left(\frac{1}{2} \theta \right) \exp i\phi = \frac{z - z_0}{\Lambda}. \quad (4.131)$$

This yields

$$\cos \theta = 1 - \frac{2\Lambda^2}{(s - s_0)^2 + (u - u_0)^2 + \Lambda^2}; \quad \phi = \tan^{-1} \frac{u - u_0}{s - s_0} \quad (4.132)$$

where $z_0 = s_0 + iu_0$. Using the above in Eq. (4.91), the instanton solution of the BP equation is given by

$$\mathbf{m} = \frac{\left(2\Lambda(s - s_0)\hat{\mathbf{i}} + 2\Lambda(u - u_0)\hat{\mathbf{j}} + ((s - s_0)^2 + (u - u_0)^2 - \Lambda^2)\hat{\mathbf{k}} \right)}{((s - s_0)^2 + (u - u_0)^2 + \Lambda^2)}. \quad (4.133)$$

As can be seen from Eq. (4.133), $\mathbf{m} \rightarrow \hat{\mathbf{k}}$ in the limit $|s|, |u| \rightarrow \infty$. At $s = s_0, u = u_0$, $\mathbf{m} \rightarrow -\hat{\mathbf{k}}$. Thus the unit vector \mathbf{m} starts in the $-\hat{\mathbf{k}}$ direction at (s_0, u_0) and goes to $\hat{\mathbf{k}}$ as we approach the boundary. The size of the instanton can thus be considered to be a radius Λ of a circle in the (s, u) plane, centered around (s_0, u_0) . This is because when $(s - s_0)^2 + (u - u_0)^2 = \Lambda^2$, the $\hat{\mathbf{k}}$ component of \mathbf{m} in Eq. (4.133) goes to zero.

From the instanton solution Eq. (4.133), we calculate

$$\mathbf{m}_s = \frac{2\Lambda}{((s-s_o)^2 + (u-u_o)^2 + \Lambda^2)^2} \left(((u-u_o)^2 - (s-s_o)^2 + \Lambda^2)\hat{\mathbf{i}} - 2(s-s_o)(u-u_o)\hat{\mathbf{j}} + 2\Lambda(s-s_o)\hat{\mathbf{k}} \right) \quad (4.134)$$

and

$$\mathbf{m} \times \mathbf{m}_s = \frac{2\Lambda}{((s-s_o)^2 + (u-u_o)^2 + \Lambda^2)^2} \left(2(s-s_o)(u-u_o)\hat{\mathbf{i}} + ((u-u_o)^2 - (s-s_o)^2 - \Lambda^2)\hat{\mathbf{j}} - 2\Lambda(u-u_o)\hat{\mathbf{k}} \right). \quad (4.135)$$

The curvature and torsion corresponding to the instanton solution Eq. (4.133) are

$$|\mathbf{m}_s| = \frac{2\Lambda}{((s-s_o)^2 + (u-u_o)^2 + \Lambda^2)} = \kappa_1, \quad (4.136a)$$

$$\frac{\mathbf{m} \cdot \mathbf{m}_s \times \mathbf{m}_{ss}}{|\mathbf{m}_s|^2} = -\frac{2(u-u_o)}{((s-s_o)^2 + (u-u_o)^2 + \Lambda^2)} = \tau_1. \quad (4.136b)$$

The solution for the Lamb equation (4.1) corresponding to the instanton solution Eq. (4.133) of \mathbf{m} can be found by substituting these two expressions in Eq. (4.104) to yield

$$q^{(I)} = \frac{2\Lambda}{((s-s_o)^2 + (u-u_o)^2 + \Lambda^2)} \exp\left[\frac{-2i(u-u_o)}{\sqrt{(u-u_o)^2 + \Lambda^2}} \tan^{-1}\left(\frac{(s-s_o)}{\sqrt{(u-u_o)^2 + \Lambda^2}}\right)\right]. \quad (4.137)$$

Note that this is *not* a traveling wave. The envelope of q is localized in both space and time. We shall refer to this as an "envelope-instanton" solution $q^{(I)}$ for the Lamb equation: The envelope takes on the maximum value $q^{(I)} = (2/\Lambda)$ when $s = s_o$ and $u = u_o$ and vanishes as $|s| \rightarrow \infty$ or $|u| \rightarrow \infty$. For $(s-s_o)^2 + (u-u_o)^2 = \Lambda^2$ (a circle of radius Λ), $q^{(I)} = (1/\Lambda)$. Thus the size of the instanton is Λ , as expected. Next, we obtain the three surfaces, swept-out by the moving curves, corresponding to this instanton, using the three formulations:

(I) The tangent vector $\mathbf{t}_1 = \mathbf{m}$ in this case, as given in Eq. (4.133). The expression for the corresponding moving curve is obtained by direct integration, *exactly*. We get

$$\mathbf{r}_1(s, u) = \int^s \mathbf{t}_1(s', u) ds', \quad (4.138)$$

yielding

$$\mathbf{r}_1(s, u) = 2\Lambda \log \sqrt{\frac{(s-s_o)^2 + (u-u_o)^2 + \Lambda^2}{(u-u_o)^2 + \Lambda^2}} \hat{\mathbf{i}}$$

$$\begin{aligned}
& + \frac{2\Lambda(u-u_o)}{\sqrt{(u-u_o)^2 + \Lambda^2}} \tan^{-1} \frac{(s-s_o)}{\sqrt{(u-u_o)^2 + \Lambda^2}} \hat{\mathbf{j}} \\
& + \left((s-s_o) - \frac{2\Lambda^2}{\sqrt{(u-u_o)^2 + \Lambda^2}} \tan^{-1} \frac{(s-s_o)}{\sqrt{(u-u_o)^2 + \Lambda^2}} \right) \hat{\mathbf{k}}. \quad (4.139)
\end{aligned}$$

The swept-out surface described by $\mathbf{r}_1(s, u)$ given in Eq. (4.139) for $\Lambda = 1$, $s_o = u_o = 0$, along with a stroboscopic plot is shown in Fig. (4.7). At $u = 0$, the curve is a planar loop in the $x-z$ plane. From Eq. (4.139) we find, as $u \rightarrow \infty$, the $\hat{\mathbf{i}}$ component tends to 0 while the $\hat{\mathbf{j}}$ and $\hat{\mathbf{k}}$ components obey the relation $z_1 \sim u \tan(y_1/2\Lambda)$. Thus, the two arms of the curve about $s = 0$ spread out, with the point $s = 0$ fixed and asymptotically in time become a curve described by a tangent function in the $y-z$ plane.

(II) The unit binormal vector obeys the BP equation and the tangent vector is given, as before, by

$$\mathbf{t}_2 = \frac{\mathbf{b}_2 \times \mathbf{b}_{2s}}{|\mathbf{b}_{2s}|} = \frac{\mathbf{m} \times \mathbf{m}_s}{|\mathbf{m}_s|}. \quad (4.140)$$

Substituting Eq. (4.135) in Eq. (4.140), we get

$$\begin{aligned}
\mathbf{t}_2 = & -\frac{2(s-s_o)(u-u_o)}{(s-s_o)^2 + (u-u_o)^2 + \Lambda^2} \hat{\mathbf{i}} \\
& + \frac{(s-s_o)^2 - (u-u_o) + \Lambda^2}{(s-s_o)^2 + (u-u_o)^2 + \Lambda^2} \hat{\mathbf{j}} + \frac{2\Lambda(u-u_o)}{(s-s_o)^2 + (u-u_o)^2 + \Lambda^2} \hat{\mathbf{k}}. \quad (4.141)
\end{aligned}$$

The curvature and torsion for this moving curve are

$$\kappa_2 = 2(u-u_o)/((s-s_o)^2 + (u-u_o)^2 + \Lambda^2); \quad \tau_2 = 2\Lambda/((s-s_o)^2 + (u-u_o)^2 + \Lambda^2). \quad (4.142)$$

Upon integration of Eq. (4.141) the expression \mathbf{r}_2 for the moving curve can be found *exactly* to be

$$\begin{aligned}
\mathbf{r}_2(s, u) = & \int^s \mathbf{t}_2 ds' = -2(u-u_o) \log \sqrt{\frac{(s-s_o)^2 + (u-u_o)^2 + \Lambda^2}{(u-u_o)^2 + \Lambda^2}} \hat{\mathbf{i}} \\
& + \left((s-s_o) - \frac{2(u-u_o)^2}{\sqrt{(u-u_o)^2 + \Lambda^2}} \tan^{-1} \frac{(s-s_o)}{\sqrt{(u-u_o)^2 + \Lambda^2}} \right) \hat{\mathbf{j}} \\
& + \frac{2\Lambda(u-u_o)}{\sqrt{(u-u_o)^2 + \Lambda^2}} \tan^{-1} \frac{(s-s_o)}{\sqrt{(u-u_o)^2 + \Lambda^2}} \hat{\mathbf{k}}. \quad (4.143)
\end{aligned}$$

The swept out surface due to $\mathbf{r}_2(s, u)$, is plotted in Fig. (4.8). At $u = u_o = 0$, the curve is a straight line along the $\hat{\mathbf{y}}$ axis, since the $\hat{\mathbf{x}}$ and $\hat{\mathbf{z}}$ components of \mathbf{r}_2 vanish. As time evolves, the surface formed is a shell-like structure: One arm of the straight line (at $u = 0$) corresponding to $s > 0$ bends and sweeps about $s = 0$ to form the

upper surface of the shell, while the other arm ($s < 0$) sweeps about $s = 0$ in the opposite direction to form the lower surface. Both for $u \rightarrow 0$ and $u \rightarrow \infty$, $\kappa_2 \rightarrow 0$ and the curve is a straight line. Fig. (4.9) depicts how the upper and lower surfaces are formed in the process of evolution.

(III) The tangent vector in this case is given by

$$\mathbf{t}_3 = \frac{-\kappa_3 \mathbf{n}_{3s} + \tau_3 \mathbf{n}_3 \times \mathbf{n}_{3s}}{|\mathbf{n}_{3s}|^2} = \frac{-\kappa_3 \mathbf{m}_s + \tau_3 \mathbf{m} \times \mathbf{m}_s}{|\mathbf{m}_s|^2}. \quad (4.144)$$

Again we write $\kappa_3 = \kappa_1 \cos \alpha$ and $\tau_3 = \kappa_3 \sin \alpha$ to find

$$\alpha = \int^s \tau_1(s', u) ds' + C_2(u). \quad (4.145)$$

Thus the curvature and torsion are

$$\kappa_3 = \frac{2\Lambda}{((s - s_o)^2 + (u - u_o)^2 + \Lambda^2)} \cos \alpha, \quad (4.146)$$

$$\tau_3 = \frac{2\Lambda}{((s - s_o)^2 + (u - u_o)^2 + \Lambda^2)} \sin \alpha, \quad (4.147)$$

$$\alpha = -\frac{2(u - u_o)}{\sqrt{(u - u_o)^2 + \Lambda^2}} \tan^{-1} \left(\frac{(s - s_o)}{\sqrt{(u - u_o)^2 + \Lambda^2}} \right). \quad (4.148)$$

In Appendix C, we have shown that $C_2(u) = 0$, by using the moving curve compatibility conditions Eqs. (2.6) to (2.8). Substituting Eqs. (4.146) and (4.147) in Eq. (4.144), we get

$$\begin{aligned} \mathbf{t}_3 = & \frac{1}{((s - s_o)^2 + (u - u_o)^2 + \Lambda^2)} \\ & \left(-\cos \alpha \left[(u - u_o)^2 - (s - s_o)^2 + \Lambda^2 \right] \hat{\mathbf{i}} \right. \\ & \left. - 2(s - s_o)(u - u_o) \hat{\mathbf{j}} + 2\Lambda(s - s_o) \hat{\mathbf{k}} \right] \\ & + \sin \alpha \left[2(s - s_o)(u - u_o) \hat{\mathbf{i}} \right. \\ & \left. + ((u - u_o)^2 - (s - s_o)^2 - \Lambda^2) \hat{\mathbf{j}} - 2\Lambda(u - u_o) \hat{\mathbf{k}} \right] \Big), \end{aligned} \quad (4.149)$$

where α is defined in Eq. (4.148). Unlike in (I) and (II), a closed form expression for the surface

$$\mathbf{r}_3 = \int^s \mathbf{t}_3 ds', \quad (4.150)$$

cannot be obtained in this case. A plot of this surface, for $\Lambda = 1$, ($s_o = 0, u_o = 0$), obtained by carrying out the integration using *Mathematica*, is shown in Fig. (4.10).

4.6 Summary and discussion

In this chapter, we have applied the three formulations described in Chapter 2 to obtain the three moving curves associated with the Lamb equation (4.1), by using its equivalence with the BP equation (4.13). The physical contexts in which the BP equation arises are also discussed. As illustrative examples, we have considered the one-instanton and the twist solutions of the BP equation. These solutions correspond to an "envelope-soliton" solution $q^{(S)}$ Eq. (4.105) and an "envelope-instanton" solution $q^{(I)}$ Eq. (4.137), of the Lamb equation (4.1). The three moving curves associated with each of these solutions, for various parameteric values of the solutions, are given at the end of this chapter, in Figs. (4.1) to (4.10). It should be clear that the Lamb equation is C-integrable (see Chapter 1), since it maps to the elliptic Liouville equation, whose general solution Eq. (4.6), is known.

We conclude by writing down the solutions of the elliptic Liouville equation (4.3) in the form given in Eq. (4.6), corresponding to the soliton and instanton solutions Eqs. (4.105) and (4.137) of the Lamb equation for completeness, although this form has not been used in our calculations.

(a) Twist

From Eqs. (4.4) and (4.105)

$$f = \log(\sqrt{(\omega_o^2 + k_o^2)} \operatorname{sech} \bar{\eta}). \quad (4.151)$$

In Eq. (4.6), this corresponds to the choice

$$A(z, z^*) = \frac{1}{B(z, z^*)} = e^{\bar{\eta}(z, z^*)}, \quad (4.152)$$

where, as can be verified from Eq. (4.103),

$$\bar{\eta}(z, z^*) = \frac{1}{2}\omega_o(z + z^*) + \frac{i}{2}k_o(z - z^*). \quad (4.153)$$

(b) Instanton

From Eqs. (4.4) and (4.137)

$$f = \log \left(\frac{2\Lambda}{((s - s_o)^2 + (u - u_o)^2 + \Lambda^2)} \right). \quad (4.154)$$

Particularly, comparing with the general solution in Eq. (4.6), this solution corresponds to the choice

$$B(z) = \frac{1}{A(z)} = \frac{z - z_o}{\Lambda}. \quad (4.155)$$

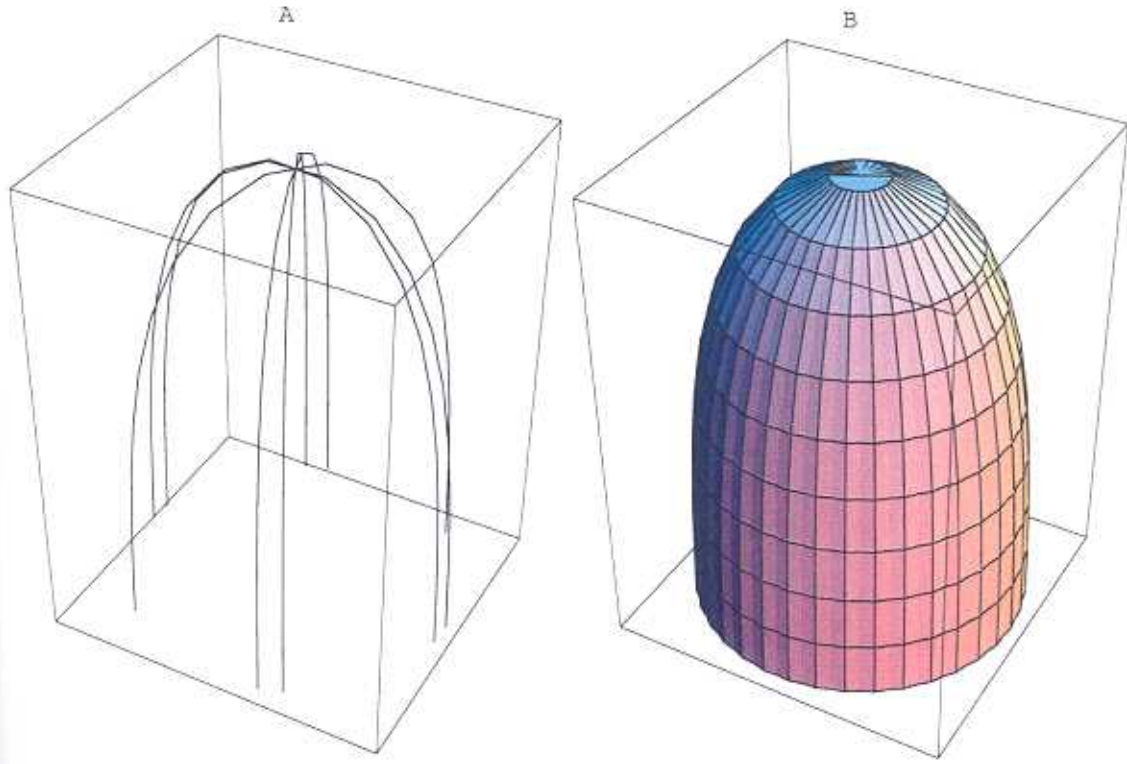


Figure 4.1: A twist surface $\mathbf{r}_1(s, u)$, Eq. (4.109): (a) A stroboscopic plot of the curve evolution and (b) the complete surface swept out in a period ($0 < u < 2\pi/\omega_o$) for $k_o = 0$ and $\omega_o = 1$. The curve at any instant of time is planar with curvature given by $\kappa_1 = \omega_o \text{sech}(\omega_o s)$. This is the first moving curve associated with the corresponding envelope soliton solution $q^{(S)}$ (Eq. (4.105)) of the Lamb equation, for $\kappa_o = 0$ and $\omega_o = 1$.

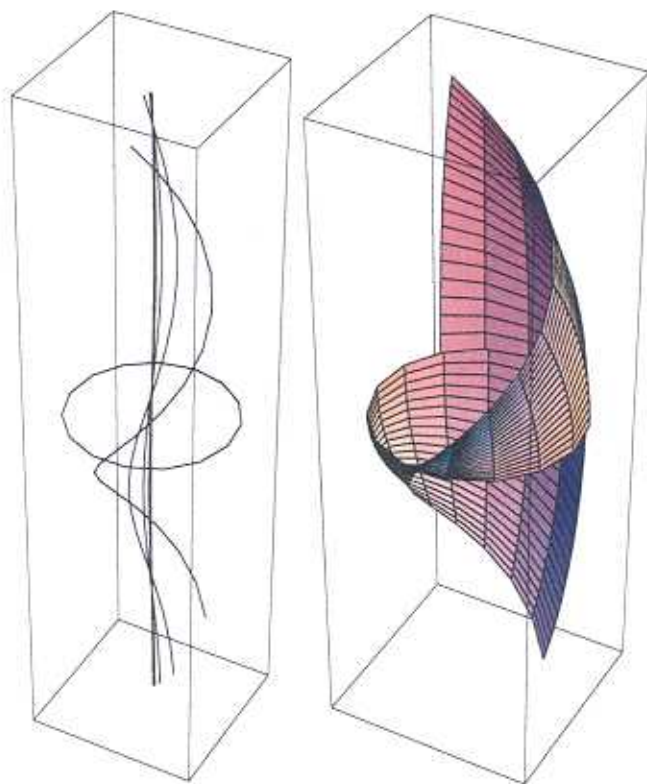


Figure 4.2: A twist surface $\mathbf{r}_1(s, u)$, Eq. (4.110): (a) A stroboscopic plot of the curve evolution and (b) the corresponding complete surface plot swept out over a time interval $0 < u < 1$, for $\omega_o = 0$ and $k_o = 1$. At $u = 0$, the curve forms a circle. As time progresses, the two arms about $s = 0$ stretch out in time, above and below the plane of the circle, to become a (vertical) straight line as $u \rightarrow \infty$. This is the first moving curve associated with the corresponding 'envelope-soliton' solution $q^{(S)}$ (Eq. (4.105)) of the Lamb equation, for $\kappa_o = 1$ and $\omega_o = 0$.

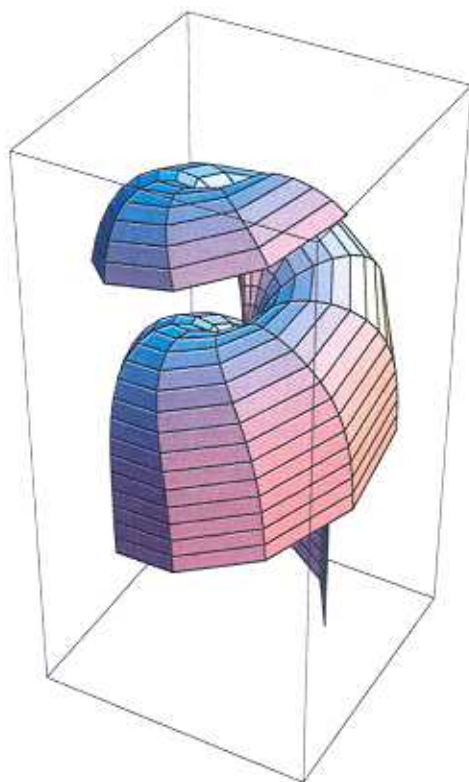


Figure 4.3: A twist surface $\mathbf{r}_1(s, u)$, Eq. (4.112): The surface swept out over the time interval $0 < u < 10$, for $k_o = 0.5$ and $\omega_o = 1$. The evolution is similar to Fig. (4.1), except for a translatory motion in the direction of the vertical axis, along with a rotation about this axis, leading to a twisting-out of the surface in Fig. (4.1). The curve at any instant, however, is not planar in this case. This is the first moving curve associated with the corresponding 'envelope-soliton' solution $q^{(S)}$ (Eq. (4.105)) of the Lamb equation, for $\kappa_o = 0.5$ and $\omega_o = 1$.

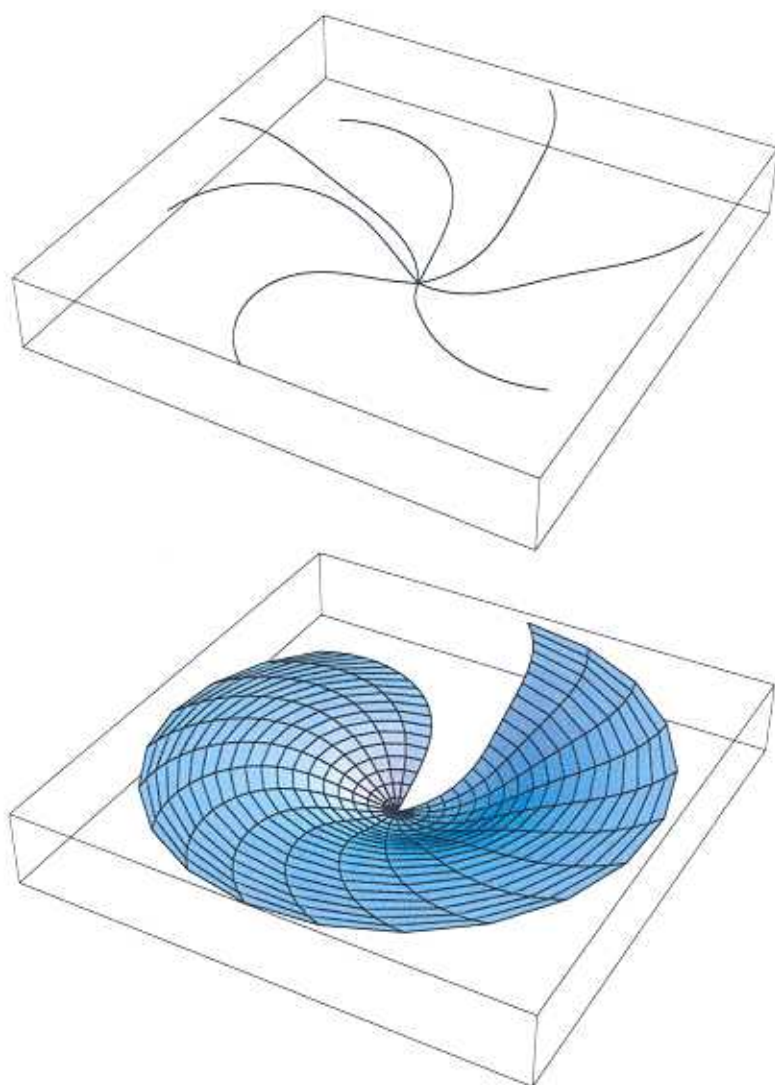


Figure 4.4: A twist surface $\mathbf{r}_2(s, u)$, Eq.(4.117): (a) A stroboscopic plot of the curve evolution and (b) the corresponding swept out surface over an interval $0 < u < 1$, for $k_o = 0.5$ and $\omega_o = 1$. As mentioned in Section (4.5) (see above Eq. (4.117)), for $k_o = 0$, the curvature κ_2 vanishes. As k_o assumes a nonzero value, both curvature and torsion assume nonzero values, as seen. This is the second moving curve associated with the corresponding 'envelope-soliton' solution $q^{(S)}$ (Eq. (4.105)) of the Lamb equation, for $\kappa_o = 0.5$ and $\omega_o = 1$.

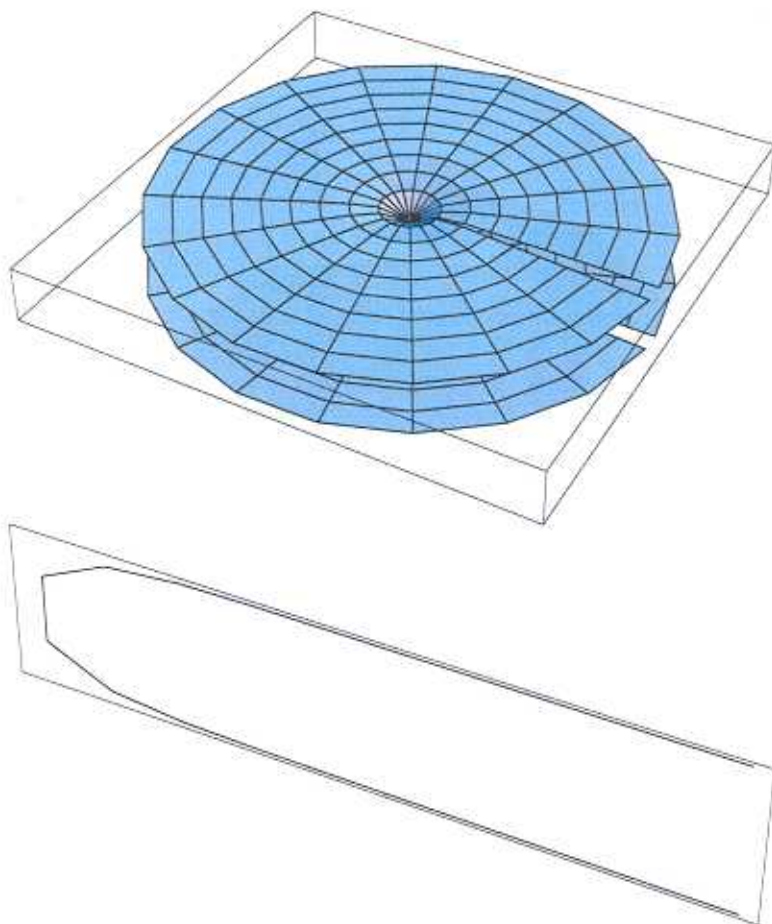


Figure 4.5: A twist surface $\mathbf{r}_3(s, u)$, Eq. (4.125): For $k_o = 0$ and $\omega_o = 1$, the curve is planar at any point in time as shown in the snapshot at $u = 0$ (b). The surface (a) is generated by the curve over an interval $0 < u < 6$, through a rotation about the vertical axis. This is the third moving curve associated with the corresponding 'envelope-soliton' solution $q^{(S)}$ (Eq. (4.105)) of the Lamb equation, for $\kappa_o = 0$ and $\omega_0 = 1$.

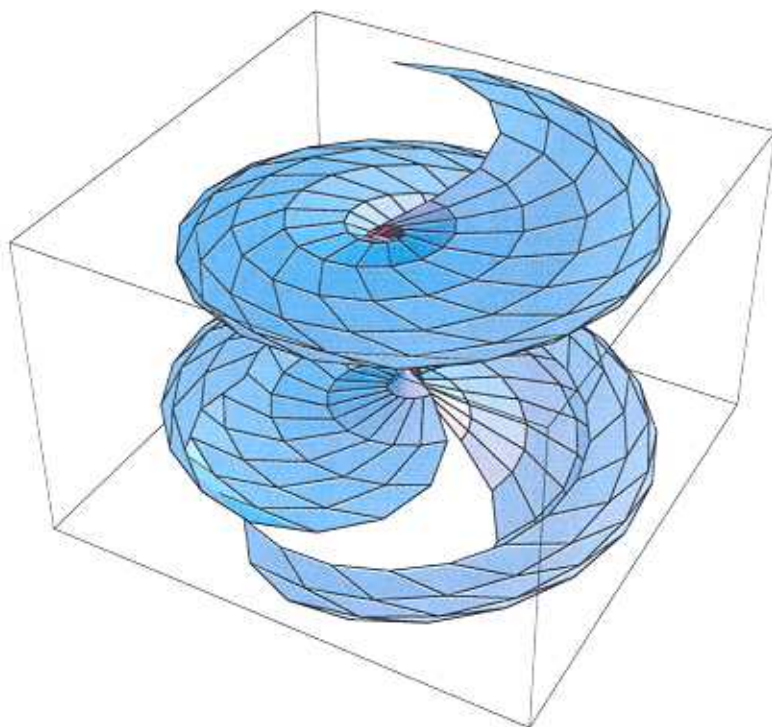


Figure 4.6: A twist surface $\mathbf{r}_3(s, u)$, Eq.(4.115): As k_o deviates from zero, however, the curve is no more planar (compare Fig. (4.5)) at any instant in time. The above surface is for $k_o = 0.3$ and $\omega_o = 1$ over the same period. This is the third moving curve associated with the corresponding 'envelope-soliton' solution (Eq. (4.105)) of the Lamb equation for $\kappa_o = 0.3$ and $\omega_0 = 1$.

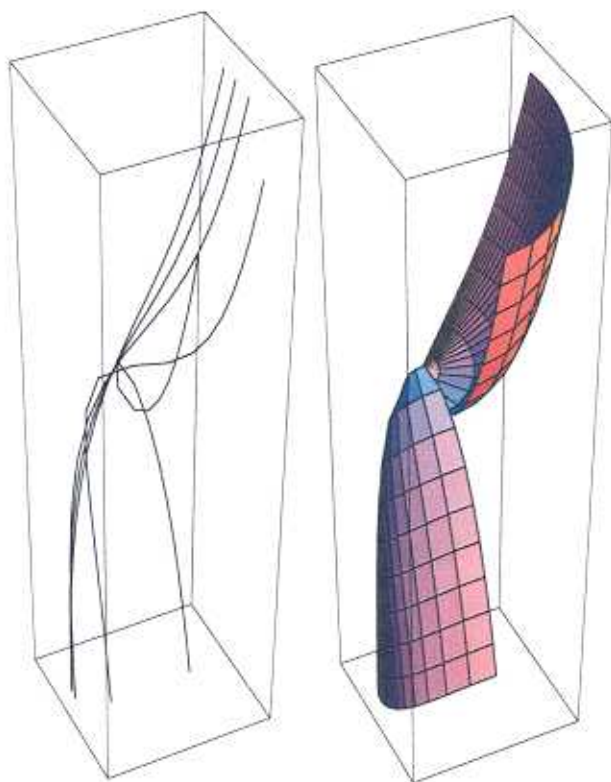


Figure 4.7: An instanton surface $\mathbf{r}_1(s, u)$, Eq. (4.139) with $\Lambda = 1$, $s_o = u_o = 0$: At $u = 0$, the curve is planar with an intersection in the middle, as seen in the stroboscopic plot (a). As time progresses, the two arms of the curve move on either sides to first become non planar. But asymptotically it approaches a tangent function (see discussion below Eq. (4.139)). The point $s = 0$ is however fixed. The snapshots are at unit intervals of time u . The surface formed (b) is over an interval $0 < u < 5$. This is the first moving curve associated with the corresponding 'envelope-instanton' solution $q^{(I)}$ (Eq. (4.137)) of the Lamb equation

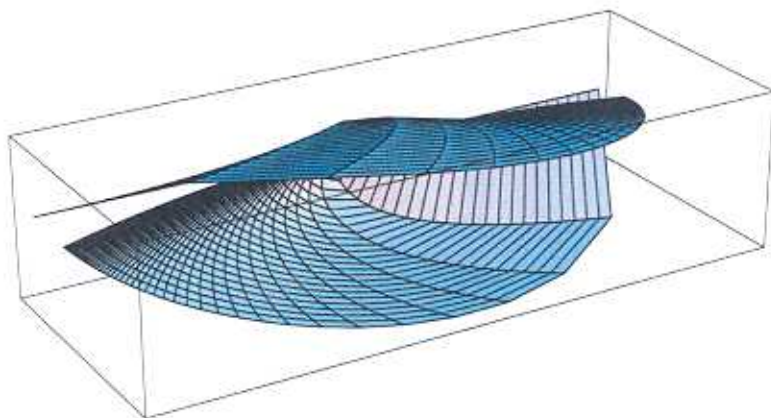


Figure 4.8: An instanton surface $\mathbf{r}_2(s, u)$, Eq.(4.143) with $\Lambda = 1$, $s_o = u_o = 0$: At $u = 0$, the curve is a straight line. With time, the two arms form the upper and lower covers of the shell like surface. The point $s = 0$ remains fixed at the center. This is the second moving curve associated with the 'envelope-instanton' solution $q^{(I)}$ (Eq. (4.137)) of the Lamb equation.

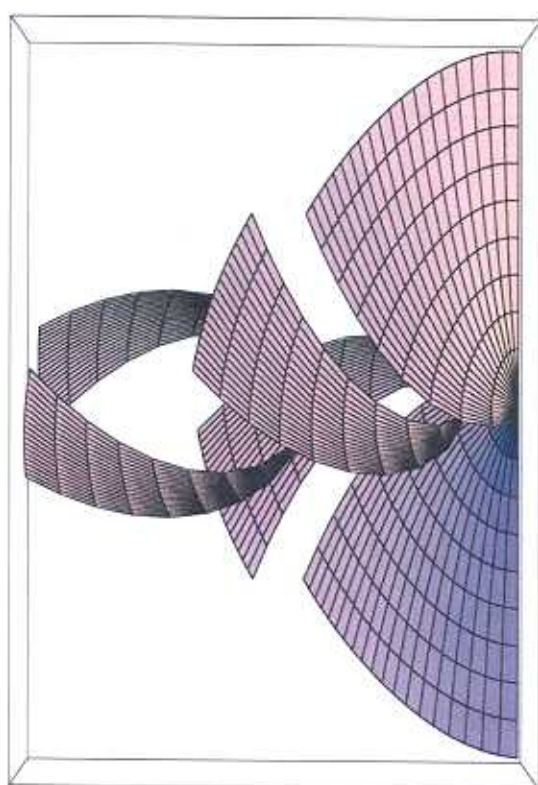


Figure 4.9: *Segments of the upper and lower surfaces that form the shell in Fig. (4.8). Surfaces swept out over different time-intervals are plotted. The segments are shown separated and from a different view point, for clarity .*

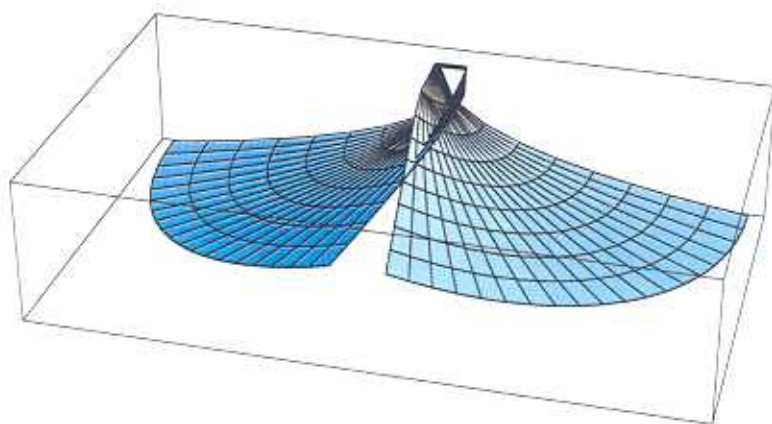


Figure 4.10: An instanton surface $\mathbf{r}_3(s, u)$, Eq. (4.150) with $\Lambda = 1, s_o = u_o = 0$: The surface swept-out by the moving curve over an interval $0 < u < 1$ is given. At $u = 0$, the curve is planar, with an intersection, with the point at $s = 0$ fixed. As time progresses, the curve becomes nonplanar. Asymptotically in time, the curve again becomes planar but in the plane perpendicular to the one it was on at $u = 0$. This is the third moving curve associated with the 'envelope-instanton' solution $q^{(I)}$ (Eq. (4.137)) of the Lamb equation.

Chapter 5

Summary of results and future directions

In a seminal paper in the late seventies, Lamb [32] presented a procedure to associate a fairly large class of completely integrable nonlinear evolution equations in $(1+1)$ dimensions with the evolution equation of a moving curve in three dimensional space. Thus a certain 'geometry' that gets associated with (an exact solution of) the integrable equation could be identified using his formulation. Nonlinear evolution equations such as the NLS, sine-Gordon equation, etc., were considered by him as examples.

In this thesis we have shown that while Lamb's formulation associates one specific moving curve to a solution of the nonlinear evolution equation, there are two other analogous formulations possible which lead to the association of two additional *distinct* moving curves with that *same* solution. Thus there are *three* moving curves (i.e., three 'geometries') that correspond to an integrable evolution equation. In other words, our new results unravel a much richer geometric structure of a given evolution equation. In order to understand this further, we have applied it to two examples: The first is the NLS Eq. (1.5), which is an S-integrable equation. The second, the Lamb equation (1.7), is a C-integrable equation. (The definitions of C-integrability and S-integrability are given in Chapter 1.) We have provided a method to obtain explicit analytic expressions for the three moving curves essentially by exploiting the mapping of the former to LL equation and the latter to the BP equation.

In Chapter 2, after presenting a basic description of a moving curve in terms

of the Frenet triad $(\mathbf{t}, \mathbf{n}, \mathbf{b})$ on a curve (see Eqs. (2.2) and (2.5) in Section (2.2)), we briefly reviewed Lamb's formulation (Formulation (I), Section (2.3)). We then extended it to present our two new formulations (Formulations (II) and (III), Section (2.4)). Association of a given integrable equation to three distinct curves was achieved by showing that the *same* evolution equation for a complex function q can be satisfied by the Hasimoto function $\psi = \kappa \exp[\int^s \tau ds']$ in the Lamb's formulation, as well as by $\Phi = \tau \exp[\int^s \kappa ds']$ and $\chi = \kappa + i\tau$ in Formulations (II) and (III) respectively. Thus given a solution q of the nonlinear evolution equation, of the form $q(s, u) = \rho(s, u) \exp(i\alpha(s, u))$, comparing with ψ , Lamb's formulation associates with it a moving curve with curvature $\kappa = \rho$ and torsion $\tau = \alpha_s$. On the other hand, equating q to Φ and χ lead to the other two moving curves with the sets $(\kappa_2 = \rho, \tau_2 = \alpha_s)$ and $(\kappa_3 = \rho \cos \alpha, \tau_3 = \rho \sin \alpha)$ associated with them respectively. Further, the temporal evolution parameters g, h and τ_0 can be identified using the curve compatibility conditions Eqs. (2.6) to (2.8). These are clearly three distinct moving curves associated with the same solution of the nonlinear evolution equation concerned. The analysis in this chapter was *general* without reference to any specific evolution equation.

In Chapter 3, we applied the methods developed in Chapter 2 to the particular case of the NLS (Eq. (3.1)). First, we considered the one-soliton solution of the NLS with vanishing carrier velocity as an example, and found the corresponding curve parameters $(\kappa, \tau, g, h, \tau_0)$ for each of the three curves that get associated with this solution. These are given in Tables (3.1) and (3.2). These parameters are distinct, and show that we do have three distinct curves for a given solution. In these tables, we observe the following symmetry: The geometric parameters of formulation (II) can be obtained from those of formulation (I) by simply making the interchanges

$$\kappa \longleftrightarrow \tau ; \quad g \longleftrightarrow \tau_0 ; \quad h \longleftrightarrow -h. \quad (5.1)$$

This symmetry can be understood as arising due to the fact that the basic curve evolution equations (Eqs. (2.2) and (2.5)) are invariant under the above interchanges, *along with* the interchange of the vectors

$$\mathbf{b} \longleftrightarrow \mathbf{t} ; \quad \mathbf{n} \longleftrightarrow -\mathbf{n}. \quad (5.2)$$

It is easily verified that these interchanges would in turn interchange the complex functions ψ and Φ , (Eqs. (2.1) and (2.32)) as well as the complex vectors \mathbf{N} and $-\mathbf{M}$ (Eqs. (2.10) and (2.30)) that appear in the first two formulations. (There seems to be no such obvious symmetry in either of the first two formulations with respect to

the third.) However, we remark that the presence of the above symmetry between Formulations (I) and (II) was not helpful in any way in the actual construction of the moving curves. This is not surprising because, as is clear, interchanging of curve parameters, e.g., $\kappa \rightarrow \tau$, etc., generically changes the very nature of the curve.

We remark that even if κ and τ are known (see Chapter 2) and hence the existence of the curve is guaranteed *in principle* due to the fundamental theorem of curves [46], finding these curves explicitly by integrating the FS equations (2.2) is a nontrivial task. To achieve this end, we exploited in an effective way, the relationship of the NLS to the LL equation (3.20), a dynamic equation for a unit vector, in Section (3.3). The LL equation is well known in the context of one dimensional Heisenberg ferromagnets in the continuum limit. It was shown that for the first curve, the tangent satisfies the LL equation, whereas for the second and third moving curves, the same equation is satisfied by the binormal and normal respectively. The procedure for determining the above three moving curves $\mathbf{r}_i, i = 1, 2, 3$, is presented in Section (3.3). While in Formulation (I), given the tangent \mathbf{t}_1 , a curve \mathbf{r}_1 is given by $\mathbf{r}_1 = \int^s \mathbf{t}_1 ds'$, in (II) and (III) we have a situation where, given the binormal \mathbf{b}_2 and the normal \mathbf{n}_3 , we must find \mathbf{r}_2 and \mathbf{r}_3 respectively. To our knowledge, this is the first time that such a situation has arisen in the literature. We have given a method and carried it out to explicitly find the corresponding geometries of the NLS. This section presents *general* results valid for *any* solution \mathbf{S} of the LL equation and hence a corresponding solution q of the NLS. Next, we obtain the explicit expression for the three moving curves, associated with the special case of a one-soliton of vanishing envelope velocity in Section (3.4). The corresponding three surfaces swept out by the respective moving curves are presented in Figs. (3.1) to (3.3).

The interesting connection of moving space curves and integrable evolution equations started with the work of Hasimoto [14], who showed that the local induction equation (see Appendix D) for the motion of a thin vortex filament in a fluid, is related to the NLS equation. It turns out that it leads to coupled equations for κ and τ , namely the DB equations, (3.64) and (3.65). For the two new formulations (II) and (III), we have found two analogs of the DB equations in Section (3.5). A stroboscopic plot of the three moving curves associated with the one-soliton solution with a moving envelope was presented in Section (3.6), along with the explicit expressions for the corresponding position vectors. The local induction equation $\mathbf{v}_1 = \kappa \mathbf{b}$ is a local expression of the velocity $\mathbf{v}_1(s, u)$ of a vortex filament in a fluid. However, the analogous velocities associated with the two new curves obtained were found to be

nonlocal in nature (see Eqs. (3.86) and (3.87)). The meaning and interpretation of this feature was discussed in Section (3.7). In the end, we also discussed some possible applications of the two new connections to actual fluids, where nonlocal velocities are of relevance.

In Chapter 4, we considered the Lamb equation (4.1), as a second example to illustrate the methods developed in Chapter 2. This equation is of interest, for it can be shown to be equivalent to the BP equation (4.13) (Section (4.2)). It can also be mapped to the elliptic Liouville equation. This in turn is of interest in surface theory since it describes surfaces of constant Gaussian curvature (see Section (4.1)). Further, though nonlinear, its *general* solution can be written down (Eq. (4.6)). Thus the Lamb equation (4.1) is C-integrable [43]. In addition, the BP equation (4.13) itself arises in a number of physical contexts, including static two dimensional Heisenberg ferromagnets, one dimensional Heisenberg antiferromagnets and the nonlinear sigma model. The BP equation supports twist and instanton solutions. These were briefly discussed in Section (4.3). In Section (4.4), we exploited the connection between the Lamb equation and the BP equation, to associate three moving curves with a given solution of the former. In particular, in Section (4.5) we considered solutions q of Lamb equation which correspond to the twist and instanton solutions of the BP equation. These were shown to have the form of an ‘envelope-soliton’ solution $q^{(S)}$ Eq. (4.105) and an ‘envelope-instanton’ solution $q^{(I)}$ Eq. (4.137), respectively, of the Lamb equation. We then obtained the explicit expression for the position vectors of the three moving curves that can be associated with each of these solutions. The swept out surfaces corresponding to each of these cases were derived and graphically illustrated using *Mathematica*.

We conclude with a discussion on future directions in which the methods developed here can be extended. As mentioned in the beginning, a number of integrable equations can be associated with moving curves. This include, apart from the NLS Eq. (3.1) and the Lamb equation (4.1), the mKdV, the sine-Gordon equation, etc.. These equations are well known and also arise in various contexts in physics as did the NLS and (as we have shown) the Lamb equation. Note that the moving curve formulation led to the association of distinct dynamical NLPDE for a unit vector for these two equations. Hence it would be of interest to find such connections to dynamical unit vector equations for other integrable equations as well. Once that is done, the connection can be exploited effectively in obtaining the explicit expression for the corresponding moving curves, as we have done in Chapters 3 and 4.

Let us see how this can be achieved, by considering an example [32]:

Complex mKdV equation: Consider the choice $\gamma_1 = \psi_{ss} + 1/2|\psi|^2\psi$ (and similar choices for γ_2 and γ_3 in terms of Φ and χ respectively). Upon substitution in Eqs. (2.22), (2.32) and (2.46), we get the complex mKdV equation

$$q_u + q_{sss} + \frac{3}{2}|q|^2q_s = 0, \quad (5.3)$$

with $q = \psi, \Phi$ and χ respectively. A short calculation shows that the corresponding curve velocity \mathbf{r}_u will be given by the following equation in formulation (I):

$$\mathbf{r}_u = -\frac{1}{2}\kappa^2\mathbf{t} - \kappa_s\mathbf{n} - \kappa\tau\mathbf{b}, \quad (5.4)$$

By writing down the equation for \mathbf{t}_u from Eq. (5.4) and by finding its exact solution, the explicit expressions for the three curves corresponding to the soliton solution of the cmKdV can be found using the method we gave in Section (3.3) for the NLS. Since the cmKdV equation is well studied in literature with known solutions and given their interests in various physical contexts [7, 8], it may be worthwhile finding these curves explicitly. This is an open problem.

It should be noted that while the moving curve formulation associates a number of integrable equations to specific evolutions of curves, the dynamic equation for the curve itself need not *always* an NLPDE. For instance, the equation of motion of the position vector of the first curve \mathbf{r}_1 corresponding to the NLS, is the one given by the local induction equation, (1.2), which can also be written as the following NLPDE for \mathbf{r}_1 :

$$\mathbf{r}_{1u} = \mathbf{r}_{1s} \times \mathbf{r}_{1ss}. \quad (5.5)$$

As discussed in Section (3.7), the velocities in the other two formulations however were nonlocal in nature. So while such an NLPDE cannot be written down for \mathbf{r}_2 and \mathbf{r}_3 in these formulations, nothing is lost since these can indeed be found exactly, by using the exact solution of \mathbf{b}_2 or \mathbf{n}_3 , since these unit vectors satisfy the integrable evolution equations as well. In the case of the Lamb equation, *none* of the three position vectors $\mathbf{r}_i, i = 1, 2, 3$ satisfied an NLPDE, but still they could all be found exactly from $\mathbf{t}_1, \mathbf{b}_2$ and \mathbf{n}_3 , as we showed in Chapter 4. This is an important point to be stressed.

We remark that the NLS equation, and the other equations in the hierarchy such as the complex modified Korteweg-de Vries(cmKdV) equation, etc., can also be obtained through the constrained motion of a non-stretching curve on the surface of a sphere, S^3 in 4-D [62]. It was further shown that the inverse of the radius of the sphere, is indeed the spectral parameter, while the curvature κ and torsion τ , play the role of the potential for the corresponding linear scattering problem. This leads

to the direct construction of the corresponding Lax pair for the nonlinear equation concerned, for nontrivial values of the spectral parameter. Besides, the real mKdV equation, sine-Gordon equation, etc., were shown to result from similar constrained motion of non-stretching curves on a sphere S^2 in 3-D. The corresponding linear problem in the case of S^2 , is indeed the ZS-AKNS spectral problem considered in [41]. It would be of interest to see if the other two formulations (II) and (III) can be applied here. This is another open problem.

Finally, extension of these formulations developed here to study connections between integrable evolution equations in $(2+1)$ dimensions and moving *surfaces*, is another possible subject of interest.

Appendix A

One-soliton solution for the nonlinear Schrödinger equation

Here we derive the one soliton, Eq. (3.19), of the NLS

$$i\psi_u + \psi_{ss} + \frac{1}{2}|\psi|^2\psi = 0. \quad (\text{A.1})$$

Let $\psi = \rho \exp(i\alpha)$. Substituting this in Eq. (A.1), the real equations for the amplitude(ρ) and phase(α) can be shown to be

$$\rho_u + 2\rho_s\alpha_s + \rho\alpha_{ss} = 0, \quad (\text{A.2})$$

$$-\rho\alpha_u + \frac{1}{2}\rho^3 + \rho_{ss} - \rho\alpha_s^2 = 0. \quad (\text{A.3})$$

We look for travelling wave solutions of the type

$$\rho(s, u) = \rho(s - V_e u); \quad \alpha(s, u) = \alpha(s - V_e u), \quad (\text{A.4})$$

where clearly, V_e and V_c denote the velocities of the respective travelling waves. Hence,

$$\rho_u(s, u) = -V_e\rho_s(s, u); \quad \alpha_u(s, u) = -V_e\alpha_s(s, u). \quad (\text{A.5})$$

Consequently, Eq. (A.2) becomes

$$-V_e\rho_s + 2\rho_s\alpha_s + \rho\alpha_{ss} = 0. \quad (\text{A.6})$$

Upon integration, after multiplying with r , we get

$$\left(\frac{-V_e}{2} + \alpha_s\right)\rho^2 = C_0. \quad (\text{A.7})$$

Choosing $C_o = 0$, we have,

$$\alpha_s = \frac{V_e}{2}. \quad (\text{A.8})$$

This yields

$$\alpha = \frac{V_e}{2}(s - V_c u), \quad (\text{A.9})$$

since α is a function of $(s - V_c u)$ as in Eq. (A.4). Substituting Eq. (A.9) in Eq. (A.3) gives

$$\frac{V_e}{2}(V_c - \frac{V_e}{2})\rho + \frac{1}{2}\rho^3 + \rho_{ss} = 0. \quad (\text{A.10})$$

Multiplying by ρ_s and integrating, we get

$$\rho_s^2 = \rho^2 \left(\frac{V_e}{2} \left(\frac{V_e}{2} - V_c \right) - \frac{\rho^2}{4} \right) + D_o. \quad (\text{A.11})$$

This has, in general, elliptic functions as solutions. Choosing the constant of integration $D_o = 0$ leads to the one-soliton solution. Also note that in order for the left hand side to be positive, the quantity in parenthesis in Eq. (A.11) on the right hand side must be positive. This in turn imposes a bound on the amplitude ρ . Besides, from Eq. (A.11), the first term in parenthesis itself must be positive, i.e.,

$$V_e(V_e - 2V_c) \geq 0. \quad (\text{A.12})$$

Upon integrating Eq. (A.11) we obtain

$$\rho = \sqrt{V_e(V_e - 2V_c)} \operatorname{sech}(\sqrt{V_e(V_e - 2V_c)}(s - V_e u - \zeta_0)), \quad (\text{A.13})$$

where ζ_0 is the constant of integration. From Eq. (A.13) and (A.9), setting $\zeta_o = 0$ for convenience, we get the one soliton solution

$$q = a_0 \operatorname{sech}\left(\frac{a_0}{2}\xi\right) \exp(iV_e(s - V_c u)/2), \quad (\text{A.14})$$

which is Eq. (3.19).

Setting $\sqrt{V_e(V_e - 2V_c)} = 2\nu$, $V_e = 2\lambda$ and $\xi = s - 2\lambda u$, Eq. (A.14) can be rewritten as

$$\psi = 2\nu \operatorname{sech}\nu\xi \exp(i\eta), \quad (\text{A.15})$$

where

$$\eta = \lambda s + (\nu^2 - \lambda^2)u. \quad (\text{A.16})$$

Eq. (A.15) is the one-soliton solution given in Eq. (3.53) in terms of parameters ν and λ .

Appendix B

One-soliton solution of the Landau-Lifshitz equation

The LL equation is given in Eq. (3.20)

$$\mathbf{S}_u = \mathbf{S} \times \mathbf{S}_{ss} \quad ; \quad \mathbf{S}^2 = 1. \quad (\text{B.1})$$

In what follows, we obtain the solution given in Eq. (3.51) of Chapter 3. Parameterizing the unit vector \mathbf{S} in terms of the polar angle θ and azimuthal angle ϕ ,

$$\mathbf{S}(s, u) = \{\sin \theta \cos \phi, \sin \theta \sin \phi, \cos \theta\}. \quad (\text{B.2})$$

Substituting Eq.(B.2) in Eq.(B.1) yields the coupled equations

$$\theta_u = -\phi_{ss} \sin \theta - 2\theta_s \phi_s \cos \theta, \quad (\text{B.3})$$

$$\sin \theta \phi_u = \theta_{ss} - \phi_s^2 \sin \theta \cos \theta. \quad (\text{B.4})$$

Looking for particular solutions for Eqs.(B.3) and (B.4) of the form

$$\theta(s, u) = \theta(\xi); \quad \phi(s, u) = \bar{\phi}(\xi) + \Omega u, \quad (\text{B.5})$$

where $\xi = (s - vu)$, we get,

$$-v\theta_\xi = -\bar{\phi}_{\xi\xi} \sin \theta - 2\theta_\xi \bar{\phi}_\xi \cos \theta, \quad (\text{B.6})$$

$$-v\bar{\phi}_\xi \sin \theta + \Omega \sin \theta = \theta_{\xi\xi} - \bar{\phi}_\xi^2 \sin \theta \cos \theta. \quad (\text{B.7})$$

Multiplying Eq.(B.6) by $\sin \theta$ and integrating w.r.t ξ , gives

$$v \cos \theta = -\bar{\phi}_\xi \sin^2 \theta + c_o, \quad (\text{B.8})$$

where c_o is an arbitrary constant. The condition at $\theta = 0$ in the above equation gives $c_o = v$. Hence ,

$$\bar{\phi}_\xi = v \left(\frac{1 - \cos \theta}{\sin^2 \theta} \right) \quad (\text{B.9})$$

$$= \frac{v}{1 + \cos \theta}. \quad (\text{B.10})$$

From Eq.(B.7)

$$\theta_{\xi\xi} = \bar{\phi}_\xi \sin \theta (-v + \bar{\phi}_\xi \cos \theta) + \Omega \sin \theta. \quad (\text{B.11})$$

From Eq.(B.6)

$$\theta_\xi (-v + \bar{\phi}_\xi \cos \theta) = -(\bar{\phi}_\xi \sin \theta)_\xi. \quad (\text{B.12})$$

Substituting Eq. (B.12) in Eq.(B.11), multiplying by θ_ξ and integrating, we get,

$$\theta_\xi^2 = -\bar{\phi}_\xi^2 \sin^2 \theta - 2\Omega \cos \theta + d_o. \quad (\text{B.13})$$

Imposing the condition of smoothness that as $|s| \rightarrow \infty$, $\theta \rightarrow 0$, and $\theta_\xi \rightarrow 0$, we obtain $d_o = 2\Omega$. Using this and Eq.(B.10), Eq. (B.13) can be written in the form,

$$\theta_\xi^2 = 4\Omega \left(\frac{1 - \cos \theta}{1 + \cos \theta} \right) \left(\frac{1 + \cos \theta}{2} - \frac{v^2}{4\Omega} \right). \quad (\text{B.14})$$

Defining $\beta = \theta/2$, we get,

$$\beta_\xi^2 \cos^2 \beta = \Omega \sin^2 \beta \left(\cos^2 \beta - \frac{v^2}{4\Omega} \right). \quad (\text{B.15})$$

Setting $Q = \sin \beta$, the above equation becomes

$$Q_\xi = \Omega^{1/2} Q \sqrt{b^2 - Q^2}; \quad b^2 = 1 - \left(\frac{v^2}{4\Omega} \right). \quad (\text{B.16})$$

Note that in defining b we have implied the condition $\Omega > v^2/4$. Upon integration, Eq. (B.16) gives

$$Q = \sin \frac{\theta}{2} = b \operatorname{sech}(b\sqrt{\Omega}(\xi - \xi_o)), \quad (\text{B.17})$$

Where ξ_o is a integration constant. Hence

$$\cos \theta = 1 - 2 \sin^2 \frac{\theta}{2} = 1 - 2b^2 \operatorname{sech}^2(b\sqrt{\Omega}(\xi - \xi_o)). \quad (\text{B.18})$$

Using the above result in Eq.(B.10) and integrating, we get (with $\xi_o = 0$),

$$\bar{\phi} - \bar{\phi}_0 = \frac{v}{2} \xi + \tan^{-1} \left(\sqrt{\frac{b^2}{1 - b^2}} \tanh(b\sqrt{\Omega}\xi) \right). \quad (\text{B.19})$$

Taking the constant $\bar{\phi}_0$ as $-\pi/2$ and using $\phi = \bar{\phi} + \Omega u$ (see Eq. (B.5)), a short calculation using Eq. (B.19) yields

$$\sin \phi = \frac{1}{\sqrt{1 - b^2 \text{sech}^2(b\sqrt{\Omega}\xi)}} \left(-\sqrt{1 - b^2} \cos\left(\frac{v}{2}\eta\right) + b \sin\left(\frac{v}{2}\eta\right) \tanh(b\sqrt{\Omega}\xi) \right) \quad (\text{B.20})$$

and

$$\cos \phi = \frac{1}{\sqrt{1 - b^2 \text{sech}^2(b\sqrt{\Omega}\xi)}} \left(\sqrt{1 - b^2} \sin\left(\frac{v}{2}\eta\right) + b \cos\left(\frac{v}{2}\eta\right) \tanh(b\sqrt{\Omega}\xi) \right), \quad (\text{B.21})$$

where

$$\eta = s - \left(v - \frac{2\Omega}{v}\right)u. \quad (\text{B.22})$$

Summing up, we have the solution to the LL equation given by Eq. (B.2), where

$$\sin \theta \cos \phi = 2b \left(\sqrt{1 - b^2} \sin\left(\frac{v}{2}\eta\right) + b \cos\left(\frac{v}{2}\eta\right) \tanh(b\sqrt{\Omega}\xi) \right) \text{sech}(b\sqrt{\Omega}\xi) \quad (\text{B.23})$$

$$\sin \theta \sin \phi = 2b \left(-\sqrt{1 - b^2} \cos\left(\frac{v}{2}\eta\right) + b \sin\left(\frac{v}{2}\eta\right) \tanh(b\sqrt{\Omega}\xi) \right) \text{sech}(b\sqrt{\Omega}\xi) \quad (\text{B.24})$$

and

$$\cos \theta = 1 - 2b^2 \text{sech}^2(b\sqrt{\Omega}\xi). \quad (\text{B.25})$$

In the above, note that $S^{(z)} = \cos \theta \rightarrow 1$ as $s \rightarrow \pm\infty$. Further Ω (see Eq. (B.5)) must be finite to support a solution of the LL equation.

An inspection of Eq. (B.5) shows that Eq. (B.25) implies that the soliton has a finite intrinsic precession or angular momentum Ω about the \hat{z} axis. In other words, physically a magnetic field in the \hat{z} direction to the ferromagnetic Hamiltonian automatically results in a precession of frequency Ω needed to support a soliton [63].

Denoting $b\sqrt{\Omega}$ as ν and v as 2λ , we get $\Omega = \nu^2 + \lambda^2$, and $b^2 = \nu^2/(\nu^2 + \lambda^2)$. With the parameters ν and λ , the unit vector \mathbf{S} given by Eqs. (B.23) to (B.25) becomes

$$\sin \theta \cos \phi = \mu \left(\lambda \sin \eta + \nu \cos \eta \tanh(\nu\xi) \right) \text{sech}(\nu\xi), \quad (\text{B.26})$$

$$\sin \theta \sin \phi = \mu \left(-\lambda \cos \eta + \nu \sin \eta \tanh(\nu\xi) \right) \text{sech}(\nu\xi) \quad (\text{B.27})$$

and

$$\cos \theta = 1 - \mu\nu \text{sech}^2(\nu\xi), \quad (\text{B.28})$$

where $\mu = 2\nu/(\nu^2 + \lambda^2)$, $\eta = \lambda s(\nu^2 - \lambda^2)u$ and $\xi = (s - 2\lambda u)$. The solution given in Eqs. (B.26) to (B.28) is just the soliton solution for the LL equation given in Eq. (3.51), Chapter 3.

Appendix C

Determination of functions $C_1(u)$ and $C_2(u)$

As noted in Chapters 3 and 4, in formulation (III), the unit normal vector \mathbf{n}_3 satisfied the LL and BP equations respectively (see Eqs. (3.29) and (4.43)).

In general, the expression for the position vector of a curve $\mathbf{r}(s, u)$ in terms of the unit normal vector is given by Eq. (3.50):

$$\mathbf{r}_3 = \int^s \frac{-\kappa_3 \mathbf{n}_{3s} + \tau_3 \mathbf{n}_3 \times \mathbf{n}_{3s}}{|\mathbf{n}_{3s}|^2} ds'. \quad (\text{C.1})$$

However, as noted in Eqs. (3.44) and (3.47),

$$\kappa_3^2 + \tau_3^2 = \kappa_1^2; \quad \frac{\partial}{\partial s} \tan^{-1}\left(\frac{\tau_3}{\kappa_3}\right) = \tau_1, \quad (\text{C.2})$$

where κ_1 is the curvature obtained in formulation (I). Without loss of generality, we choose the parameterization

$$\kappa_3 = \kappa_1 \cos \alpha; \quad \tau_3 = \kappa_1 \sin \alpha. \quad (\text{C.3})$$

Substituting this in the second equation in Eq. (C.2) yields

$$\alpha_s = \tau_1. \quad (\text{C.4})$$

Thus

$$\alpha = \int \tau_1 ds + C(u), \quad (\text{C.5})$$

where $C(u)$ is an arbitrary function of time at this stage.

To find $C(u)$ we proceed as follows: First, from Eq. (C.3) $\alpha = \tan^{-1} \frac{\tau_3}{\kappa_3}$. Hence,

$$\alpha_u = \frac{\kappa_3 \tau_{3u} - \kappa_{3u} \tau_3}{(\kappa_3^2 + \tau_3^2)}. \quad (C.6)$$

From the compatibility conditions (Eqs. (2.6) and (2.7) with the appropriate subscript 3), $\kappa_{3u} - g_{3s} = -\tau_3 h_3$ and $\tau_{3u} - \tau_{o3s} = \kappa_3 h_3$. Combining these two, we obtain

$$\kappa_3 \tau_{3u} - \kappa_{3u} \tau_3 = (\kappa_3^2 + \tau_3^2) h_3 + \kappa_3 \tau_{o3s} - g_{3s} \tau_3. \quad (C.7)$$

Hence, from Eqs. (C.6) and (C.7),

$$\alpha_u = \frac{\kappa_3 \tau_{3u} - \kappa_{3u} \tau_3}{(\kappa_3^2 + \tau_3^2)} = h_3 + \frac{\kappa_3 \tau_{o3s} - g_{3s} \tau_3}{\kappa_3^2 + \tau_3^2}. \quad (C.8)$$

But from Eq. (C.5),

$$\alpha_u = \frac{\partial}{\partial u} \int^s \tau_1 ds' + \frac{d}{du} C. \quad (C.9)$$

Hence from Eqs. (C.8) and (C.9),

$$\frac{d}{du} C(u) = -\frac{\partial}{\partial u} \int^s \tau_1 ds' + \alpha_u = -\frac{\partial}{\partial u} \int^s \tau_1 ds' + h_3 + \frac{\kappa_3 \tau_{o3s} - g_{3s} \tau_3}{\kappa_3^2 + \tau_3^2}. \quad (C.10)$$

Below, by using Eq. (C.10), we first find the constant of integration $C(u)$ in Eq. (C.5), for a *general* solution of the LL equation and the BP equation respectively. We then specialize to the one-soliton solution considered in Chapter 3 and the twist and instanton solutions obtained in Chapter 4. Note that Eq. (C.10) is the *general* expression for $C(u)$ in terms of the time evolution parameters κ_3, τ_3, g_3 and τ_{o3} . If \mathbf{n}_3 satisfies an NLPDE, we will see that all these can be expressed in terms of κ_1 and τ_1 . Thus dC/du is determined in terms of κ_1 and τ_1 which are *known* functions for unit vector equations like LL and BP equations and hence can be found. We now show how this happens for the LL and BP equations respectively.

The LL equation (Ch. 3, Sec. (3.3)): $C(u) = C_1(u)$

Here, the normal vector \mathbf{n}_3 satisfies the LL equation

$$\mathbf{n}_{3u} = \mathbf{n}_3 \times \mathbf{n}_{3ss}. \quad (C.11)$$

From the second equation of the set (2.5), $\mathbf{n}_{3u} = -g_3 \mathbf{t}_3 + \tau_{o3} \mathbf{b}_3$. From the second equation of the set (2.2), we find $\mathbf{n}_3 \times \mathbf{n}_{3ss} = \tau_{3s} \mathbf{t}_3 + \kappa_{3s} \mathbf{b}_3$. Thus Eq. (C.11) yields, for the LL equation

$$g_3 = -\tau_{3s}; \quad \tau_{o3} = \kappa_{3s}; \quad h_3 = \frac{1}{2}(\kappa_3^2 + \tau_3^2). \quad (C.12)$$

(see also Eqs. (3.17) and (3.18).) Substituting (C.12) in Eq. (C.10) and setting $C(u) = C_1(u)$ for the LL case, we get

$$\frac{d}{du}C_1 = -\frac{\partial}{\partial u} \int^s \tau_1 ds' + \frac{1}{2}(\kappa_3^2 + \tau_3^2) + \frac{\kappa_3\kappa_{3ss} + \tau_{3ss}\tau_3}{\kappa_3^2 + \tau_3^2}. \quad (C.13)$$

Upon using Eqs. (C.3) and (C.4), a short calculation yields

$$\kappa_3\kappa_{3ss} + \tau_{3ss}\tau_3 = \kappa_1\kappa_{1ss} - \kappa_1^2\tau_1^2. \quad (C.14)$$

Using Eqs. (C.14) and (C.2) in (C.13),

$$\frac{d}{du}C_1 = -\frac{\partial}{\partial u} \int^s \tau_1 ds' + \frac{1}{2}\kappa_1^2 + \frac{\kappa_{1ss}}{\kappa_1} - \tau_1^2. \quad (C.15)$$

Note that Eq. (C.15) yields $C_1(u)$ for *any* solution \mathbf{S} of the LL equation, with $\kappa_1 = |\mathbf{n}_{3s}| = |\mathbf{S}_s|$ and $\tau_1 = \mathbf{S} \times \mathbf{S}_s \times \mathbf{S}_{ss}/\kappa_1^2$.

Example: Specializing to the one soliton solution Eq. (3.51), we have from Eq. (3.78),

$$\kappa_1 = 2\nu \operatorname{sech}(\nu\xi); \quad \tau_1 = \lambda. \quad (C.16)$$

Using Eq. (C.16), after some algebra we can show that $(\frac{1}{2}\kappa_1^2 + \kappa_{1ss}/\kappa_1) \equiv \nu^2$. Substituting this in Eq. (C.15) yields

$$\frac{d}{du}C_1 = (\nu^2 - \lambda^2). \quad (C.17)$$

Hence

$$C_1(u) = (\nu^2 - \lambda^2)u. \quad (C.18)$$

Thus from Eq. (C.5), $\alpha = \int^s \tau_1 ds' + C_1(u) = (\lambda s + (\nu^2 - \lambda^2)u) \equiv \eta$ (see Eq. (3.52)). This expression has been used in our analysis (see Eq. (3.83)).

It is clear that $C_1(u)$ will depend on the form of the solution of the NLS (and hence the corresponding solution of the LL equation).

The BP equation (Ch. 4, Sec. (4.5)): $C(u) = C_2(u)$

Here, the normal vector \mathbf{n}_3 satisfies the BP equation

$$\mathbf{n}_{3u} = \mathbf{n}_3 \times \mathbf{n}_{3s} \quad (C.19)$$

Using the second equation in the set (2.2) and the second equation of the set (2.5), Eq. (C.19) implies $\tau_3\mathbf{t}_3 + \kappa_3\mathbf{b}_3 = -g_3\mathbf{t}_3 + \tau_{o3}\mathbf{b}_3$. Hence (as also noted in Eqs. (4.41) and (4.42)) we have

$$g_3 = -\tau_3; \quad \tau_{o3} = \kappa_3; \quad h_3 = \int^s (\kappa_3^2 + \tau_3^2) ds'. \quad (C.20)$$

Substituting Eq. (C.20) in Eq. (C.10) and setting $C(u) = C_1(u)$ for the BP case,

$$\frac{d}{du}C_2 = -\frac{\partial}{\partial u} \int^s \tau_1 ds' + \int^s (\kappa_3^2 + \tau_3^2) ds' + \frac{\kappa_3\kappa_{3s} + \tau_3\tau_{3s}}{\kappa_3^2 + \tau_3^2}. \quad (C.21)$$

Using Eqs. (C.3) and (C.4), $\kappa_3\kappa_{3s} + \tau_3\tau_{3s} = \kappa_1\kappa_{1s}$. Substituting this in Eq. (C.21),

$$\frac{d}{du}C_2 = -\frac{\partial}{\partial u} \int^s \tau_1 ds' + \int^s \kappa_1^2 ds' + \frac{\kappa_{1s}}{\kappa_1}. \quad (C.22)$$

Note that Eq. (C.22) is a general expression for $C_2(u)$ valid for *any* solution \mathbf{m} of the BP equation, with $\kappa_1 = |\mathbf{n}_{3s}| = |\mathbf{m}_s|$ and $\tau_1 = \mathbf{n}_3 \cdot \mathbf{n}_{3s} \times \mathbf{n}_{3ss} / |\mathbf{n}_{3s}|^2 = \mathbf{m} \cdot \mathbf{m}_s \times \mathbf{m}_{ss} / |\mathbf{m}_s|^2$. We now specialize to the twist and an instanton as examples.

(a) Twist

For this case, using the twist solution \mathbf{m} of the BP equation given in Eq. (4.100), we obtain Eq. (4.106),

$$\kappa_1 = \sqrt{(\omega_o^2 + k_o^2)} \text{sech } \bar{\eta}; \quad \tau_1 = -k_o \tanh \bar{\eta}, \quad (C.23)$$

where $\bar{\eta} = \omega_o s - k_o u$. Substituting Eq. (C.23) in Eq. (C.22), we see that all integrals can be exactly evaluated and after some algebra we get

$$\frac{d}{du}C_2(u) = 0 \quad (C.24)$$

for the twist. Thus C_2 is a constant which can be set to zero without loss of generality.

(b) Instanton

Here, using the instanton solution \mathbf{m} for the BP equation given in Eq. (4.133), we get Eq. (4.136),

$$\kappa_1 = 2\Lambda / ((s - s_o)^2 + (u - u_o)^2 + \Lambda^2); \quad \tau_1 = -2(u - u_o) / ((s - s_o)^2 + (u - u_o)^2 + \Lambda^2). \quad (C.25)$$

Substituting Eq. (C.25) in Eq. (C.22), we see again that all integrations can be carried out exactly and a short calculation yields

$$\frac{d}{du}C_2(u) = 0 \quad (C.26)$$

for the instanton. Therefore, C_2 is a constant which can be chosen to be zero.

Thus from Eq. (C.5), $\alpha = \int^s \tau_1 ds'$ for both the twist as well as the instanton solution, where τ_1 is given in Eq. (C.23) and (C.25) respectively.

Appendix D

The local induction approximation

The interesting connection between curve motion and solitons started with Hasimoto's work on fluid mechanics [14]. We briefly describe here the 'local induction approximation' for a thin vortex filament [27] and end with the mapping to NLS due to Hasimoto.

Consider a thin vortex filament moving in an incompressible, in-viscid fluid. Its vorticity is given by

$$\mathbf{w}(\mathbf{r}) = \nabla \times \mathbf{V}(\mathbf{r}), \quad (\text{D.1})$$

where $\mathbf{V}(\mathbf{r})$ is the fluid velocity at a point with position vector \mathbf{r} . The fluid being incompressible ($\nabla \cdot \mathbf{V} = 0$), the velocity \mathbf{V} is given from (Eq. (D.1)), by the Biot-Savart integral:

$$\mathbf{V}(\mathbf{r}) = \int d^3r' \frac{\mathbf{w}(\mathbf{r}') \times (\mathbf{r} - \mathbf{r}')}{|\mathbf{r} - \mathbf{r}'|^3}. \quad (\text{D.2})$$

This expression gives the velocity at any point in a fluid, in terms of the vorticity \mathbf{w} . For a thin filament the vorticity is concentrated entirely on the filament core. Consequently the volume integral in Eq. (D.2) becomes a line integral over the filament. Besides, if we assume the vorticity to be entirely in the tangential direction to the axis of the filament, then the velocity of the filament itself, *induced* by its own vorticity, is given by the line integral

$$\mathbf{V}_I(\mathbf{r}) \sim \int k \mathbf{t}(\mathbf{r}') \times (\mathbf{r} - \mathbf{r}') / |\mathbf{r} - \mathbf{r}'|^3 ds', \quad (\text{D.3})$$

where now the integral runs over the filament whose position vector is given by $\mathbf{r}(s, u)$ and k is the magnitude of vorticity. Local contributions dominates the Biot-Savart integral, as seen from the integrand in Eq. (D.3). Expanding \mathbf{r}' in a Taylor

series around $\mathbf{r}(s, u)$, we have,

$$\mathbf{r}'(s', u) = \mathbf{r}(s, u) + (s' - s)\mathbf{r}_s + \frac{1}{2}(s' - s)^2\mathbf{r}_{ss} + O(s' - s)^3. \quad (\text{D.4})$$

Since $\mathbf{r}_s = \mathbf{t}$ and $\mathbf{r}_{ss} = \mathbf{t}_s = \kappa\mathbf{n}$ from Eq. (2.2), substituting Eq. (D.4) in Eq. (D.3) yields, after rescaling,

$$\mathbf{V}_I \sim \kappa(\mathbf{t} \times \mathbf{n}) = \kappa\mathbf{b}. \quad (\text{D.5})$$

Eq. (D.5) gives the velocity of a vortex filament, i.e.,

$$\mathbf{r}_u = \mathbf{V}_I, \quad (\text{D.6})$$

obtained with the various approximations mentioned above. As a result of these approximations, it is to be noted that the expression for $\mathbf{V}_I(s, u)$ is *local*, that is, the velocity depends only on the curvature κ and is along the direction of the binormal \mathbf{b} at the point s and at time u .

It must be noted that Eq. (D.5) has no tangential and normal components but only a component along the binormal. This is indeed an indication of the non stretching nature of the filament to the order of approximation considered. Now, differentiating Eq. (D.5) with respect to time, we have,

$$\mathbf{t}_u = \kappa_s\mathbf{b} - \kappa\tau\mathbf{n}, \quad (\text{D.7})$$

where Eqs. (2.2) has been used. Comparing with Eqs. (2.5), the corresponding equations for the curve parameters κ and τ are found using Eq. (2.6) and (2.7) as,

$$\kappa_u = -(\kappa\tau)_s - \kappa_s\tau, \quad (\text{D.8})$$

$$\tau_u = [(\kappa_{ss}/\kappa) - \tau^2]_s + \kappa\kappa_s. \quad (\text{D.9})$$

Which are indeed the DB equations (3.65) and (3.64). These two can be combined into a single equation for the complex Hasimoto function ψ , Eq. (2.1), to yield the nonlinear Schrödinger equation, Eq. (3.1), with q replaced by ψ . For a given soliton solution, the curvature and torsion of the filament can be read off using Eq. (2.1). Thus, the local induction expression for the velocity is seen to lead to a shape- and velocity-preserving motion of a vortex filament in the fluid.

Bibliography

- [1] See, for instance, M. J. Ablowitz and H. Segur, *Solitons and the Inverse Scattering Transform* (SIAM, Philadelphia, 1981).
- [2] See, for e.g., A. J. Lichtenberg and M. A. Lieberman, *Regular and Chaotic Motion* (Springer, Berlin, 1994).
- [3] P. D. Lax, *Comm. Pure Appl. Math.* **21**, 467 (1968).
- [4] C. S. Gardner, J. M. Greene, M. D. Kruskal and R. M. Miura, *Phys. Rev. Lett.* **19**, 1095 (1967).
- [5] L. D. Faddeev and L. A. Takhtajan, *Hamiltonian Methods in the Theory of Solitons* (Springer-Verlag, 1987).
- [6] N.J. Zabusky and M. D. Kruskal, *Phys. Rev. Lett.* **15**, 240 (1965).
- [7] E. A. Jackson, *Perspectives of Nonlinear Dynamics* (Cambridge University Press, 1990).
- [8] R. K Dodd et al., *Solitons and Nonlinear Wave Equations* (Academic Press, New York, 1982).
- [9] G. P. Agarwal, *Nonlinear Fiber Optics* (Academic, San Diego, 1989).
- [10] A. Hasegawa, *Optical Solitons in Fibers* (Springer-Verlag, 1990).
- [11] R. Rajaraman, *Solitons and Instantons* (North-Holland, Amsterdam, 1989).
- [12] W. J. Zakrzewski, *Low Dimensional Sigma Models* (Adam Hilger, Bristol and Philadelphia, 1989).
- [13] See, for instance, F. Lund and T. Regge, *Phys. Rev. D* **14**, 1524 (1976).
- [14] H. Hasimoto, *J. Fluid. Mech.* **51**, 477 (1972).

- [15] K. W. Schwarz, *Phys. Rev. B* **38**, 2398 (1998).
- [16] R. E. Goldstein and D. M. Petrich, *Phys. Rev. Lett.* **67**, 3203 (1991).
- [17] M. C. Cross and P. C. Hohenberg, *Rev. Mod. Phys.* **65**, 851 (1993).
- [18] A. T. Winfree, *SIAM Rev.* **32**, 1 (1990); J. P. Keener and J. J. Tyson, *SIAM Rev.* **34**, 1 (1992).
- [19] J. P. Keener, *Physica D* **31**, 269 (1998) and references therein.
- [20] R. A. Harris and J. E. Hearst, *J. Chem. Phys.* **44**, 2595 (1996); For a review, see R. B. Bird, O. Hassager, R. C. Armstrong and C. F. Curtiss, *Dynamics of Polymeric Liquids* (Wiley, New York, 1977).
- [21] T. Schlick and W. K. Olson, *J. Mol. Biol.* **223**, 1089 (1992).
- [22] M. Lakshmanan, Th. W. Ruijgrok and C. J. Thomson, *Physica* **84 A**, 597 (1976).
- [23] Radha Balakrishnan, *J. Phys. C* **15**, L1305 (1982).
- [24] See, for instance, D. J. Struik, *Lectures on Classical Differential Geometry* (Addison-Wesley, Reading, MA 1961).
- [25] R. L. Ricca, *Nature* **352**, 561 (1991).
- [26] L. S. Da Rios, *Rend. Circ. Mat. Palermo* **22**, 117 (1906).
- [27] See, for e.g., G. K. Batchelor, *An Introduction to Fluid Dynamics* (Cambridge University Press, Cambridge, 1967).
- [28] R. Betchov, *J. Fluid Mech.* **22**, 471 (1965).
- [29] S. P. Novikov, S. V. Manakov, L. P. Pitaevskii and V. E. Zakharov, *Theory of Solitons* (Consultants Bureau, Plenum Publishing, 1984); M. J. Ablowitz and P. A. Clarkson, *Solitons, Nonlinear Evolution Equations and Inverse Scattering* (London Mathematical Society Lecture Notes Series 149, Cambridge University Press, 1991).
- [30] V. E. Zakharov and A. B. Shabat, *Zh. Eksp. I Teor. Fiz.* **61**, 118 (1971) [*Soviet Phys. -JETP* **34**, 62 (1973)].
- [31] E. J. Hopfinger and F. K. Browand, *Nature* **295**, 393 (1982).

- [32] G. L. Lamb, *J. Math. Phys.* **18**, 1654 (1977).
- [33] G. L. Lamb, *Phys. Rev. Lett.* **37**, 235 (1976).
- [34] See, e.g., I. Klapper and M. Tabor, *J. Phys. A* **27**, 4919 (1994); K. Nakayama, H. Segur and M. Wadati, *Phys. Rev. Lett.* **69**, 260 (1992); R. E. Goldstein and S.A. Langer, *Phys. Rev. Lett.* **75**, 1094 (1995) and references therein.
- [35] F. Calogero and W. Eckhaus, *Inverse Probl.* **3**, 229 (1982); L27.
- [36] S. Murugesh and Radha Balakrishnan, *Phys. Lett. A* **290**, 81 (2001); nlin. PS/0104066.
- [37] S. Murugesh and Radha Balakrishnan, *Euro. Phys. Jour. B* (to appear (2002)); nlin. PS/0111052.
- [38] L.A. Takhtajan, *Phys. Lett. A* **64**, 235 (1977).
- [39] J. Tjon and J. Wright, *Phys. Rev. B* **15**, 3470 (1977).
- [40] Radha Balakrishnan and S. Murugesh, *Theor. Math. Phys.* (to appear (2002)); nlin. SI/0111048.
- [41] M. J. Ablowitz, D. J. Kaup, A. C. Newell and H. Segur, *Stud. Appl. Math.* **53**, 249 (1974).
- [42] G. Calogero and A. Degasperis, *Nuovo. Cimento* **32**, 201 (1976).
- [43] Radha Balakrishnan, *Phys. Lett. A* **204**, 243 (1995).
- [44] A. Belavin and A. M. Polyakov, *Pis. Zh. Eksp. Teor. Fiz.* **22**, 503 (1975) [*JETP Lett.* **22**, 245 (1975)].
- [45] Radha Balakrishnan, A. R. Bishop and R. Dandoloff, *Phys. Rev. B* **47**, 3108 (1993).
- [46] L.P. Eisenhart, *A Treatise on the Differential Geometry of Curves and Surfaces* (Dover, New York, 1960).
- [47] Radha Balakrishnan, A. R. Bishop and R. Dandoloff, *Phys. Rev. Lett.* **64**, 2107 (1990); Radha Balakrishnan and R. Blumenfeld, *J. Math. Phys.* **38**, 5878 (1997).

- [48] We caution that the cases $\alpha = 1, 2, 3$ (see below Eq.(2.28)) should not be confused with the formulations (I), (II) and (III).
- [49] G. L. Lamb, *Elements of Soliton Theory* (Wiley, New York 1980).
- [50] M. Lakshmanan, *Phys. Lett. A* **61**, 53 (1977).
- [51] L.D. Landau and E. M. Lifshitz, *Phys. Z Sowjet* **8**, 153 (1935).
- [52] R. Hirota, *J. Phys. Soc. Jpn.* **51**, 323 (1982).
- [53] The Hamiltonians for these three evolutions are just the respective invariants I_1 given in Eqs.(3.67), (3.71) and (3.74). These can be written in the form $H = \int (\mathbf{S}_s)^2 ds$, with the spin vector \mathbf{S} identified with \mathbf{t}_1 , \mathbf{b}_2 and \mathbf{n}_3 , respectively. Thus the components of each of these three vectors satisfy the usual angular momentum Poisson brackets.
- [54] V. E. Zakharov and L. A. Takhtajan, *Theor. Math. Phys.* **38**, 26 (1979).
- [55] A. Sym, *Lett. Nuovo Cimento* **22**, 420 (1978) .
- [56] S. Wolfram, *The Mathematica Book*, 3rd Edition (Wolfram Media/Cambridge University Press, 1996).
- [57] Here, I_3 is the Hamiltonian which gives rise to (3.1), on using the Poisson brackets $\{F, G\} = i \int [(\delta F/\delta q)(\delta G/\delta q^*) - (\delta G/\delta q)(\delta F/\delta q^*)] ds$.
- [58] J. Langer and R. Perline, *J. Math. Phys.* **35**, 1732 (1993).
- [59] D. Levi, A. Sym and S. Wojciechowski, *Phys. Lett. A* **94**, 408 (1983).
- [60] A. R. Forsyth, *Theory of Differential Equations* (Dover Publishing Inc. 1959).
- [61] E. B. Bogomol'nyi, *Sov. J. Nucl. Phys* **24**, 449 (1976).
- [62] A. Doliwa and P. M. Santini, *Phys. Lett A* **185**, 373 (1994).
- [63] H. J. Mikeska and M. Steiner, *Adv. Phys.* **40**, 191 (1991).